Master's thesis

NTNU
Norwegian University of Science and Technology
Faculty of Engineering
Department of Energy and Process Engineering

Trygve H. Stuen

Influence of Hydrogen Use As a Fuel on Aeroderivative Gas Turbine Performance

Master's thesis in Energy and Environmental Engineering
Supervisor: Lars O. Nord
Co-supervisor: Marcin Pilarczyk
June 2021

NTNU
Norwegian University of Science and Technology

Trygve H. Stuen

Influence of Hydrogen Use As a Fuel on Aeroderivative Gas Turbine Performance

Master's thesis in Energy and Environmental Engineering
Supervisor: Lars O. Nord
Co-supervisor: Marcin Pilarczyk
June 2021

Norwegian University of Science and Technology
Faculty of Engineering
Department of Energy and Process Engineering

NTNU
Norwegian University of
Science and Technology

Abstract

The energy associated with hydrogen combustion is several times that of natural gas on an energy per mass basis. Currently, conventional gas turbines are using natural gas as fuel. In the offshore sector a large quantity of the emissions are related to the operation of gas turbines, here aeroderivative gas turbines are preferred due to their flexibility and compact size. Due to global warming and the depletion of natural gas and oil, the power sector looks toward new and environmentally friendly energy carriers. To reduce emissions the influence of hydrogen as fuel in an aeroderivative gas turbine will be investigated with regards to the overall performance change.

The GasTurb software was used to model and evaluate the change in performance output for a GE LM2500+G4. The model was found to match external data for natural gas at on-design and off-design. Generally, the power output and thermal efficiency increased when switching to hydrogen, while the exhaust gas temperature was lowered. When changing to hydrogen with ambient temperature change the power output and thermal efficiency increased by 7.8% and 4% respectively, while the exhaust gas temperature decreased by 1.4%. For hydrogen at part-load the exhaust gas temperature decreased by 1.4% and the thermal efficiency increased by 4.2%. When operating at part-load variable IGV's was implemented. The implementation of variable IGV's showed that different angle settings needed to be used for the different fuels.

The results imply that different settings and operating conditions need to be selected when changing the fuel to hydrogen.

Sammendrag

Den spesifikke energien til hydrogen er flere ganger høyere enn den spesifikke energien til naturgass. I dag bruker generelle gassturbiner naturgass som brensel. Dette fører til at en stor prosentandel av utslippene assosiert med offshoresektoren er knyttet til gassturbiner. Fleksibilitet og størrelse gjør at aeroderivatturbiner foretrekkes offshore. På grunn av global oppvarming og reduksjon i olje og naturgass kilder ser energisektoren mot nye og miljøvennlige energibærere. For å redusere utslipp vil påvirkning av hydrogen som drivstoff i en aeroderivatturbin bli undersøkt med tanke på endring i ytelse.

Programvaren GasTurb ble brukt til å modellere og evaluere endringen i ytelse for en GE LM2500+G4. Modellen samsvarte med eksterne data for naturgass som brensel ved on-design og off-design. Generelt sett økte effekten og den termiske virkningsgraden når man bruker hydrogen, men eksostemperaturen ble redusert. Ved endring av omgivelsestemperatur økte effekten og den termiske virkningsgraden med henholdsvis 7.8% og 4% for hydrogen, mens eksostemperaturen sank med 1.4%. Ved varierende effekt sank eksostemperaturen med 1.4% for hydrogen og den termiske virkningsgraden økte med 4.2%. Variasjon av vinklene på gassturbinens inngangsfoiler ble brukt til å kontrollere gassturbinen ved endring i effekt. Implementeringen av variable vinkler for inngangsfoilene viste at forskjellige vinkelinnstillinger måtte brukes for de forskjellige drivstoffene.

Resultatene viser til at ulike kontrollinnstillinger i forhold til drift må brukes når en bruker hydrogen i gassturbiner.

Acknowledgements

First and foremost, I want to thank my supervisor Lars Nord for giving me the freedom and opportunity to write this thesis. To be able to write on such a relevant topic for the future has been a great encouragement. With such a broad research topic it can be difficult to know where to start, I would therefore like to express my sincere gratitude towards my co-supervisor Marcin Pilarczyk for his continuous support and guidance throughout my master thesis and project work. You've helped me a great deal with structuring and focusing the scope of this thesis. A special thanks should also be given to Mohammad Ali Motamed for helping me with much of the theory and software needed for this work and for being available for discussions. This wouldn't have been possible without you guys.

This last year at NTNU has been very different. Due to COVID-19 many of my day-to-day interactions and social arenas have become digital. I would therefore like to address my family and close friends that have been there when I need someone to talk to, thank you.

Contents

List of Figures

List of Tables

Nomenclature

Symbols

A	Area	$[m^2]$
c_θ	Tangential component of absolute velocity	$[\frac{m}{s}]$
C_p	Heat capacity	$[\frac{kJ}{K}]$
c_p	Specific heat capacity at constant pressure	$[\frac{kJ}{kgK}]$
c_v	Specific heat capacity at constant volume	$[\frac{kJ}{kgK}]$
H	Enthalpy	$[kJ]$
h	Specific enthalpy	$[\frac{kJ}{kg}]$
k	Specific heat ratio	$[-]$
M	Mach number	$[-]$
N	Rotational speed	$[rpm]/[\frac{rev}{s}]$
n	Amount of moles	$[mol]$
n_T	Polytropic temperature exponent	$[-]$
n_v	Polytropic volume exponent	$[-]$
P	Power output	$[kW]$
p	Pressure	$[kPa]$
Q	Heat	$[kJ]$
s	Specific entropy	$[\frac{kJ}{kgK}]$
S_{NO_x}	NO_x severity parameter	$[-]$
T	Temperature	$[K]$
U	Turbine blade speed	$[\frac{m}{s}]$
$\dot{V}$	Volumetric flow rate	$[\frac{m^3}{s}]$
V	Velocity	$[\frac{m}{s}]$
W	Work	$[kJ]$
w	Mass flow rate	$[\frac{kg}{s}]$
X	Compressibility factor	$[-]$
Y	Compressibility factor	$[-]$
α	Blade heat transfer coefficient	$[\frac{kW}{m^2K}]$
η_p	Polytropic efficiency	$[-]$

η_s	Isentropic efficiency	$[-]$
κ	Thermal conductivity	$[\frac{W}{mK}]$
μ	Viscosity	$[Pas]$
ρ	Density	$[\frac{kg}{m^3}]$
ψ	Entropy function	$[-]$

Constants

R_0	Universal gas constant	$8.413[\frac{kJ}{kgK}]$

Abbreviations

DLE	Dry low emission
FAR	Fuel to air ratio
FHV	Fuel heating value
HPT	High pressure turbine
HRSG	Heat recovery steam generator
IGV	Inlet guide vanes
ISO	International organization for standardization
LHV	Lower heating value
MAPE	Mean average percentage error
NGV	Nozzle guide vanes
OTSG	Once-through heat recovery steam generator
PR	Pressure ratio
PT	Power turbine
PWSD	Shaft power delivered
RH	Relative humidity
RMSE	Root mean square error
rpm	Rounds per minute
SAE	Society of automotive engineers
SM	Surge margin
TIT	Turbine inlet temperature
WF	Fuel flow rate

1 Introduction

In 1791 the inventor John Barber came up with a design to use compressed air to exert mechanical energy. The motivation behind this idea was to replace the horse and carriage in what was befittingly named the "horseless carriage". Sadly for John Barber, this project never flourished but it stands as the first patented gas turbine that consists of a compressor, a combustion chamber and a turbine [1]. Gas turbines are now widely used to provide heat and power, from turbojets used in aeroplanes to large industrial turbines used in the power industry. Currently, the most used fuel for gas turbines operating on the ground is natural gas. Because of the excessive emission of carbon dioxide, a change towards hydrogen fuel is anticipated. Some of the state-of-the-art gas turbines can run on pure hydrogen while other gas turbines can use a mixture of hydrogen and natural gas.

This master thesis aims to present how the influence of hydrogen as fuel will affect the performance of an aeroderivative gas turbine. This will be done by answering the following objectives:

- Determination of the two spool gas turbine performance in the GasTurb software.
- Gas turbine performance benchmarking for natural gas and hydrogen fuel.
- Linking analyses to a specific gas turbine model (preferably the GE LM2500+G4 or the LM6000 PF).

These objectives will be answered by constructing a scope that defines the term *gas turbine performance*. Theory regarding general two-spool gas turbines and parameters significant to performance determination and turbine operation will be presented. A specific aeroderivative gas turbine will be modelled in the GasTurb software [2] for on- and off-design with regards to flexible operation and the usage of hydrogen as a fuel. The GasTurb model will then be used to benchmark the performance parameters when switching fuel from natural gas to hydrogen. Results from the GasTurb simulations will be presented and discussed with regards to the model accuracy, operation conditions and the change of fuel. In-house scripts will be used to analyse and present the simulation results. Additional theory will be added in the discussion to validate and explain the result from the GasTurb simulations.

1.1 Motivation and contribution

The HES-OFF project is currently working on an optimized energy system with cleaner hybrid energy. This project is planning on using a gas turbine offshore that is running on part load hydrogen. An aeroderivative gas turbine will be used, because of its flexibility and size. The physical specifications of an aeroderivative gas turbine make it a common choice for offshore applications [3]. The work presented can therefore be used as a reference for further work in determining the performance of the aeroderivative turbine used in the HES-OFF project [4]. The Norwegian petroleum sector is one of the leading advocates for reducing greenhouse gas emissions by implementing new technologies and solutions to the offshore industry. Several policies like the CO2 Tax Act no 21 on Petroleum Activities, The Pollution Control Act and the Petroleum Act are used to regulate emissions.

With the energy demand in the world increasing, combined with the eminent uncertainty and threat of global warming one need to look towards other environmentally friendly sources of energy. The development of renewable energy technology has come a long way, with the emissions related to the operation of solar panels, wind turbines and hydropower stations being close to zero. But the

production of renewable energy technology is often associated with emissions and a high initial cost. Of course, the initiative and rapid evolution surrounding renewable energy will increase the general lifespan of the components and reduce the production costs and corresponding emission, but by using already existing technology and components in a new way one skips many steps in the development process. By altering existing technology to reduce emissions one will increase the availability, reduce the implementation time, reduce the initial costs and reduce emissions associated with the production of the components. This is one of the advantages of hydrogen fueled gas turbines as gas turbines are used in a wide variety of sectors. In 2019 85.06% of the CO_2 emissions related to offshore activity in Norway was connected to turbines [5]. By cutting the CO_2 emissions related to the gas turbine operation one will have a large scale impact in reducing emission over a wide variety of sectors. Focusing on adapting hydrogen fuel in gas turbines would therefore be a promising near term option to reduce emissions.

Even though the knowledge surrounding turbomachinery is well established and the alteration of components and operation conditions for eventual hydrogen use might be attainable in the near future, there are some problems that present themselves when using hydrogen. One of the first challenges related to hydrogen use is the production cost. A study from Iskenderun Technical University and Siemens Energy presents the cost per kWh of a simple gas turbine cycle running at 20 bar to be 0.322 $ for hydrogen versus 0.071 $ for natural gas [6]. There are different methods associated with hydrogen production. The hydrogen produced is often categorized as either blue hydrogen or green hydrogen. Blue hydrogen is produced from fossil fuels, while green hydrogen is not produced from fossil sources. The two main methods of producing blue and green hydrogen are methane-steam reforming and electrolysis of water respectively [7]. The HES-OFF project is planning on using green hydrogen. The hydrogen produced in the HES-OFF project will come from electrolysers that will be powered by wind turbines, but for a general offshore system blue hydrogen can also be used because of the access to methane directly from the well. Methane-steam reforming is currently the least expensive method of producing hydrogen, it is done by separating the hydrogen from the carbon found in methane by making it react with high temperature steam. The steam and methane combined with a catalyst will produce hydrogen, CO and CO_2. By combining the methane-steam reforming with carbon-capture and storage the CO_2 emissions would be lowered. As for green hydrogen, the electrolysis separates hydrogen from water by using electricity. In the electrolysis of water the other product produced aside from hydrogen is oxygen (O_2). By using electrolysis the cost of producing hydrogen is directly linked to the cost of electricity. The electricity can come from different sources for example renewable energy sources such as in the HES-OFF project. There has also been done work on producing hydrogen from the excess heat from a gas turbine cycle by using a $CuCl$-hydrogen cycle. The conclusion made was that the $CuCl$-hydrogen system had a higher conversion efficiency than that of the water electrolysis system [8].

Due to its high energy per unit mass, the interest in hydrogen as a fuel has existed for a long time. In 1915 a report was made by the National Advisory Committee for Aeronautics about the combustion properties of hydrogen [9]. Hydrogen along with ammonia have been studied in comparison to natural gas with regards to varying air-fuel mixtures and flame stability. It showed that mixtures with methane-ammonia and ammonia-hydrogen could be burned with a stable flame by implementing strong swirling flows for mixing [10]. A CFD-model (Computational fluid dynamics model) of the combustion chamber of a medium sized gas turbine has been developed and studied for hydrogen combustion [11]. Research into carrying out DLE (dry low emission) combustion for hydrogen is presented by Tekin, Ashikaga, Horikawa and Funke with positive results. By using a Micro-Mix DLE test burner, the NO_x formation is reduced as well as the chance of flash back [12]. Further comparisons between hydrogen combustion with different burners have also been carried out [13]. Physical testing of hydrogen combustion has been performed in a test

chamber by General Electric and Norsk Hydro with regards to variation in load [14]. The reliability and safety of hydrogen use along with combustion strategy and aerothermal effects are presented in [15], with optimistic results regarding further hydrogen use in gas turbines. Mixtures of natural gas and hydrogen have been tested in variable proportions, where the composition of the mixture is weighted against load output, NO_x formation and carbon emission. It was concluded that the optimal solution for fuel composition should be dependant on the load [16]. NCCS Annual report from 2019 presents the challenges with hydrogen as fuel in relation to the high chance of flashback, auto-ignition, combustion dynamics and NO_x formation. The challenges presented in the NCCS report can be met by new and innovate fuel injection systems, combustion control systems and combustion chamber designs. The report also puts forward a reduced fuel cost for hydrogen because of the higher efficiency and lower emission tax associated with the fuel [17]. General Electric (GE) has developed gas turbines that can run on a wide variety of different fuel compositions. GE gas turbines with a hydrogen concentration ranging from 5% to 95% (volume percent) have been successfully implemented commercially, but the change in fuel causes additional considerations with regards to safety and the overall structure of operation. Burning hydrogen efficiently and safely with regards to the gas turbine operation is what currently is being worked towards [18].

All these articles along with several others present and discuss the challenges and possibilities related to hydrogen combustion in gas turbines. The challenges that occur when switching to hydrogen are mainly related to the reactions in the combustion chamber as the previous cited articles suggest. This paper takes a step back and looks at the overall effects of hydrogen combustion instead of the technical challenges related to the implementation of the fuel. When looking at the change in performance when using hydrogen one gains a general understanding of how the fuel affects the entire gas turbine. A similar article regarding the overall effects of hydrogen use in gas turbines have been presented and discussed by Paolo Chiesa, Giovanni Lozza and Luigi Mazzocchi [19]. In the article three different scenarios for hydrogen combustion is presented and compared against natural gas. The present thesis correlates well with what has been done by Chiesa, Giovanni and Mazzocchi, but the basis for comparison between natural gas and hydrogen is different. Instead of constructing three possible scenarios for hydrogen combustion, GasTurb will be used to benchmark the difference between hydrogen fuel and natural gas for the exact same model and the exact same operating conditions. By keeping the reference system constant one will be able to see the differences when changing fuel more clearly. The current thesis will also study a more particular gas turbine model with focus on operation related to the HES-OFF project. Another article that is directly relevant to what is presented in the current thesis is the *Design of Aero Gas Turbines Using Hydrogen* by F. Haglind and R. Singh [20]. Haglind and Singh presents the general use of hydrogen in an aeroderivative gas turbine from a technical point of view, the article also presents design choices when switching fuels and compares it to kerosene fuel. This differs from the thesis at hand which looks at an aeroderivative gas turbine meant to be used offshore and with the reference fuel being natural gas.

Furthermore the present thesis gives a good insight into the limitations and use of the GasTurb software for modelling a GE LM2500+G4. In the project work leading up to the current thesis the GasTurb software was verified against general thermodynamic equations. Different methods for determining performance and efficiencies for a single-spool gas turbine was investigated and compared to the results given by GasTurb. The simulations from GasTurb was evaluated against known data and theory for different scenarios. In general the simulation results from GasTurb corresponded with the presented theory for natural gas. The results from GasTurb presented in this thesis will therefore not be evaluated against thermodynamic performance calculations, but rather specific performance data. This is done to evaluate the accuracy of the model.

1.2 Scope of project

As mentioned in the preface of the introduction, the term *gas turbine performance* will be defined for this thesis. A gas turbine is a complex system with many components and auxiliaries designed towards robust operation and high performance. To cover all parameters influencing the performance would be virtually impossible given the time and simulation tool for this thesis. By including all these parameters the thesis becomes very model dependent. Meaning that if there does not exist any external reference data, the simulation data would need to be evaluated by itself. Due to the lack of data surrounding commercial gas turbine models this approach would not be beneficial. Therefore, the parameters studied will be chosen based on available data, this is done to be able to verify the GasTurb model. These parameters include the power output, thermal efficiency, exhaust mass flow and exhaust gas temperature. Added to the main performance outputs of the cycle is the individual efficiencies of the turbomachinery (compressor, high pressure turbine and power turbine), this is to give an impression on how the change of fuel will affect the main components of the gas turbine. Parameters that will be detrimental to the operation of the gas turbine will also be included, this will predominantly be the surge margin (the chance of the surge phenomenon occurring in the compressor). One of the main reasons for gradually phasing out natural gas with hydrogen is the CO_2 emissions associated with the combustion of natural gas. It will therefore be reasonable to include some of the challenges associated with hydrogen combustion. This includes some of the chemical properties of hydrogen combustion and the combustion products associated with hydrogen.

Much of the thesis will focus on modelling the selected gas turbine, this will include how the gas turbine is operated and controlled at part-load and with ambient temperature change. The reason for introducing the model to ambient temperature change and part-load operation is to present how flexible operation will affect the gas turbine when changing fuel. The general control of the gas turbine at off-design will be decided by general assumptions regarding how the gas turbine is operated. The entirety of Section 2 will present the general theory associated with the performance parameters discussed above as well as a brief overview of the correlations between the components of a two-spool gas turbine. Section 3 will introduce the chosen gas turbine and the modelling process in GasTurb as well as the operating conditions for the model. The data gained from the GasTurb model will be verified against available data for natural gas in Section 4. The results from the GasTurb model using hydrogen fuel will be presented and discussed in Section 5. The discussion will consist of additional theory supporting the results from GasTurb and eventual sources of errors caused by the GasTurb model or the assumptions made.

2 General background

As a starting point, the core functions and parameters of a gas turbine will be explained. This section will start off by giving an overview of a general two-spool gas turbine cycle and the different components involved. The information provided in this section will give a physical context to the theory presented later on. Specific notations, correlations and phenomenons regarding turbomachinery will be presented along with some additional combustion characteristics for hydrogen and natural gas.

2.1 The two-spool gas turbine

The general gas turbine is composed of three main parts. The compressor, the combustion chamber and the turbine itself. The gas turbine works such that a fluid (most often air) is drawn in to the compressor where the fluid's pressure and temperature is increased by impellers (stage 1-2 in Figure 1). In the combustion chamber the fluid is mixed with fuel (stage 2-3 in Figure 1). The fuel can consist of different types of hydrocarbons and/or hydrogen. When igniting the fuel/air mixture the temperature is increased and the energy of the mix is released. After the combustion, the exhaust gas mixture is passed through the turbine where it expands (stage 3-4 in Figure 1). The turbine works as an expander. By expanding the high pressure and high temperature working fluid that comes from the compressor and combustion chamber, one can extract work in terms of mechanical energy. The mechanical energy is produced from rotor blades in the turbine that spins freely when fluid passes through them.

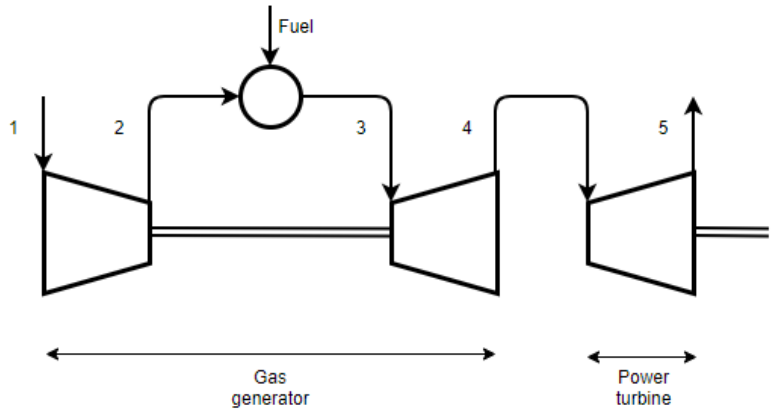

Figure 1: Sketch of a general two-spool gas turbine

A two-spool gas turbine consists of a compressor, combustion chamber and two separate turbines. The first turbine in the two-spool configuration drives the compressor, this is called the gas generator. The gas generator supplies high temperature and pressure to a separate turbine called a power turbine or free turbine. The power turbine is responsible for supplying the net power output of the system. Gas turbines have many appliances, for heat and power generation there are mainly two options: Aeroderivative gas turbines and heavy duty gas turbines. Aeroderivative gas turbines are developed from aircraft engine technology. Generally, the heavy duty gas turbines have a lower overall efficiency than aeroderivative gas turbines, but heavy duty gas turbines tend to have a higher total power output due to their increased mass flow of air. By connecting the shaft of the power turbine to a generator one could convert the mechanical energy into electricity. The exhaust gas from a given gas turbine can be used to heat up water that can further be used

in an external steam turbine or be used for heating appliances. Connecting a gas turbine system to a steam cycle is called a combined cycle. In a combined cycle the exhaust gas temperature from the gas turbine is of great significance, this will be considered later in Section 5.3.4.

2.2 Isentropic efficiency

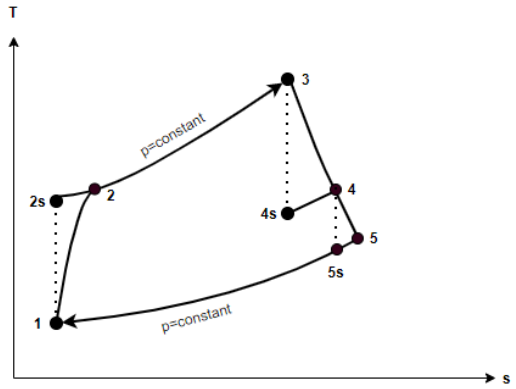

Figure 2: Temperature-entropy diagram for a general two-spool gas turbine with isentropic compression and expansion.

When working with general turbomachinery one usually regard the compression and expansion processes as isentropic and the combustion process as isobaric, this is shown in Figure 2. By defining the compression and expansion processes as isentropic and the specific heat as constant one can find the isentropic efficiency for the compressor and high pressure turbine (HPT) from Equations (1) and (2) respectively [21]. The power turbine's isentropic efficiency is found by replacing stage 3 and 4 in Equation (2) with stage 4 and 5.

$$\eta_{c,s} = \frac{c_p(T_{2s} - T_1)}{c_p(T_2 - T_1)} \tag{1}$$

$$\eta_{t,s} = \frac{c_p(T_3 - T_4)}{c_p(T_3 - T_{4s})} \tag{2}$$

Instead of expressing the isentropic efficiency as a function of temperature it can be written in terms of the pressure ratio for both the compressor and turbine [22] [23]. The pressure ratio for the compressor is given as $PR_c = (\frac{T_{out,s}}{T_{in}})^{\frac{k}{k-1}}$ and similarly for the turbine as $PR_t = (\frac{T_{in}}{T_{out,s}})^{\frac{k}{k-1}}$ [24].

$$\eta_{c,s} = \frac{(PR_c)^{\frac{k-1}{k}} - 1}{\frac{T_2}{T_1} - 1} \tag{3}$$

$$\eta_{t,s} = \frac{1 - \frac{T_4}{T_3}}{1 - (\frac{1}{PR_t})^{\frac{k-1}{k}}} \tag{4}$$

Both Equations (3) and (4) show that the isentropic efficiency is largely dependant on the pressure ratio (PR). Through thermodynamic correlations Equations (3) and (4) can be written as a

function of the polytropic efficiency ($\eta_{t,p}$) as shown by Equations (5) and (6) respectively.

$$\eta_{c,s} = \frac{(PR_c)^{\frac{k-1}{k}} - 1}{PR_c^{\frac{k-1}{k}\frac{1}{\eta_{c,p}}} - 1} \tag{5}$$

$$\eta_{t,s} = \frac{1 - (\frac{1}{PR_t})^{\frac{k-1}{k}\eta_{t,p}}}{1 - (\frac{1}{PR_t})^{\frac{k-1}{k}}} \tag{6}$$

2.3 Polytropic efficiency

For turbomachinery isentropic and isobaric processes are not feasible to implement physically, this is shown in Figure 3. A slight pressure drop in the combustion chamber (stage 3 to stage 4) is caused by skin friction, mixing and turbulence [25]. Isentropic compression and expansion is not attainable to implement physically, this is because of an increase in entropy due to various losses(skin friction losses, turbulence and separation) [26]. Instead of looking at the expansion and compression processes as isentropic one can look at it polytropically. The polytropic efficiency accounts for the real gas applications of the working fluid. This includes compressibility factors and polytropic temperature exponents and polytropic volume exponents. Polytropic calculations are done by tracing infinte small steps along the physical compression path. The polytropic efficiency is given by Equation (7), where Y and X are the compressibility factors introduced by Schultz [27]. The compressibility factors accounts for the variation of working fluid density throughout the compression and expansion processes. n_T and n_v are the polytropic temperature and volume exponents, which are relations between change in temperature, pressure and specific volume. The symbol k is used to represent the relation between the specific heat capacity for constant pressure and volume respectively [28].

$$\eta_p = \frac{Y}{\frac{n_T-1}{n_T}\frac{k}{k-1}(1+X)^2 - XY} \tag{7}$$

In GasTurb the polytropic efficiency for both the compressor and turbine is calculated using Equation (8).

$$\eta_p = \frac{ln(\frac{p_{out}}{p_{in}})}{ln(\frac{p_{out.is}}{p_{in}})} \tag{8}$$

As shown by Equations (5) and (6) in Section 2.2 the polytropic efficiency can also be used to represent the isentropic efficiency.

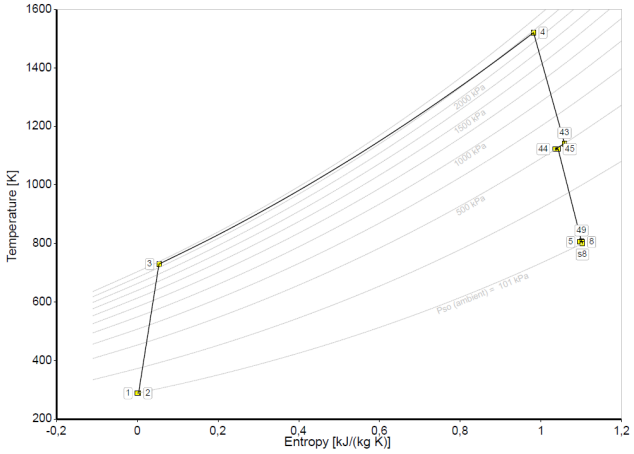

Figure 3: Temperature-entropy diagram for a general two-spool gas turbine extracted from the software GasTurb.

2.4 GasTurb stage notations

The following subsection will lay a foundation for how the GasTurb software refers to the different stages of a gas turbine. The notations found in the GasTurb user manual [29] are described in Table 1. The influence and distribution of cooling air is not the focus of this thesis and the stages that will be presented and referred to are the compressor inlet and outlet (stage 2 and 3), the burner outlet (stage 4), HPT inlet and outlet (stage 41 and 44) and the power turbine (PT) inlet and exhaust outlet (stage 45 and 5 respectively). It is worth noting that Figure 3 does not include all of the stages presented in Table 1, this is most likely due to the some of the stage points overlapping due to the short intervals described in Table 1.

Stage notation for GasTurb	
Stage notation	**Description**
2	Compressor inlet
3	Compressor exit
31	Burner inlet
4	Burner exit
41	First turbine stator exit
43	HPT exit before adding cooling air
44	HPT exit after adding cooling air
45	PT inlet
49	PT exit before adding cooling air
5	PT exit after adding cooling air

Table 1: GasTurb stage notation.

2.5 Component map notations

The component maps i.e. compressor, HPT and PT maps presented by GasTurb uses some parameters and notations that should be explained. These notations are used to explain component relations in Section 2.6 and to give context to the operating lines in Section 5.3.6. The first parameter that needs to be introduced is the *standard day corrected mass flow* (w_{2RStd}). The standard

corrected mass flow is the mass flow delivered by the compressor under standard conditions. From Joachim Kurzke and Ian Halliwell [30] the standard corrected mass flow is given as

$$w_{2RStd} = \frac{\sqrt{\Theta_2} w_2}{\delta_2} \tag{9}$$

where $\delta_2 = \frac{p_2}{p_{std}}$ and $\Theta_2 = \frac{T_2}{T_{std}}$ are used to scale the actual flow against the standard conditions. The standard corrected mass flow is used to quantify the Mach number at the entry area of the compressor. The Mach number is defined as the relation between the actual flow velocity and the sonic velocity. By using the relation between Mach number and mass flow one can eventually get an expression for the Mach number that can be linked to the standard day corrected mass flow as shown in Equation (10). The subscript s denotes the static conditions.

$$M = \frac{w\sqrt{\frac{R}{k}T}\sqrt{\frac{T_s}{T}}}{A \cdot p\frac{p_s}{p}} \tag{10}$$

By assuming the gas constant R to be constant one observes from Equation (10) that the standard corrected mass flow is given as a function of the Mach number and k. The same can be done for the tip speed on the rotors of the compressor, but now from the radial direction instead of the axial direction as shown by Equation (11).

$$M_{rot} = c_\theta \frac{N}{\sqrt{kRT}} \cdot \frac{T}{T_s} \tag{11}$$

By neglecting the gas constant Equation (11) shows that the corrected spool speed $\frac{N}{\sqrt{T}}$ is a function of the Mach number and k.

Therefore the compressor map shows the corrected mass flow against the pressure ratio related to the corrected speed. These corrected parameters are connected to the Mach number in the flow and at the spool, which can be connected to the losses and overall performance.

The parameter on the x-axis for the turbine maps in Section 5.3.6 is $N/\sqrt{\Theta}w \cdot \sqrt{\Theta}/\delta$ which is the corrected speed $N/\sqrt{\Theta}$ multiplied by the corrected mass flow. This is to get better looking maps since it would be hard to distinguish the speed lines corresponding to the different mass flow rates.

2.6 Matching relations

To better understand the behaviour of a gas turbine working at off-design, some of the relations between the parameters involved will be presented. The theory presented will use the notations presented in Table 1 to match the notations from the GasTurb simulation results in Section 3.

2.6.1 Conservation of flow in-between compressor and turbine

The first relation will be between the compressor and turbine. The system is simplified by the following assumptions and conditions:

- Considering high power output.
- The mass fraction of fuel injected is small compared to the total mass flow of air (for natural gas it normally ranges between $3\% - 6\%$ [31]).

- In the combustion chamber the losses in pressure are small compared to the overall pressure.
- The use of bleeding and cooling air are constant and are fractions of the compressor inlet mass flow.

Due to the assumptions and conditions above the following relation is presented by Equation (12).

$$\frac{w_{41}}{w_2} = constant \tag{12}$$

Equation (12) can be expanded such that it includes corrected flows, area, pressures and temperatures [30].

$$\frac{w_2\sqrt{T_2}}{A_2 p_2} = \frac{w_{41}\sqrt{T_{41}}}{A_{41}p_4}\frac{A_{41}}{A_2}\frac{p_4}{p_3}\frac{w_2}{w_{41}}\frac{p_3}{p_2}\sqrt{\frac{T_2}{T_{41}}} \tag{13}$$

By looking at Equation (13) one can deduce that:

- $\frac{w_{41}\sqrt{T_{41}}}{A_{41}p_4}$ is constant since the flow is choked or close to choked at turbine inlet (close to sonic speed).
- $\frac{p_4}{p_3}$ is a constant since by neglecting the pressure losses in the combustion chamber.
- $\frac{w_2}{w_{41}}$ is constant because of the assumption done on the bleeding and cooling air.

By rearranging Equation (13) an expression for the compressor ratio is presented by (14).

$$\frac{p_3}{p_2} = \frac{1}{\frac{w_{41}\sqrt{T_{41}}}{A_{41}p_{41}}\frac{A_{41}}{A_2}\frac{p_4}{p_3}\frac{w_2}{w_{41}}}\sqrt{\frac{T_{41}}{T_2}}\frac{w_2\sqrt{T_2}}{p_2} \tag{14}$$

This gives the relationship:

$$\frac{p_3}{p_2} = constant \cdot \sqrt{\frac{T_{41}}{T_2}}\frac{w_2\sqrt{T_2}}{p_2} \tag{15}$$

Equation (15) shows that the corrected flow entering the compressor and the pressure ratio through the compressor are linearly connected with a gradient that depends on the ratio $\frac{T_{41}}{T_2}$. From Equation (15) one can deduce the following:

- The efficiency will not affect $\frac{T_{41}}{T_2}$ since no efficiency parameter is included in Equation (15).
- The gradient of the $\frac{T_{41}}{T_2}$ lines decrease when bleed air is removed from the compressor, which will increase the mass ratio $\frac{w_2}{w_{41}}$. Figure 4 shows an example of the temperature ratio lines in the compressor map.

It is worth noting that assuming $\frac{w_{41}\sqrt{T_{41}}}{A_{41}p_4} = constant$ is only valid when the flow is choked or close to choked. At a low power output the speed is decreasing and the assumption does not hold. When lowering the power output a decrease in $\frac{w_{41}\sqrt{T_{41}}}{A_{41}p_4}$ will occur, which will, according to Equation (15), increase $\frac{p_3}{p_2}$. (This implies that the temperature ratio lines should not pass through the origin but rather (0.1)).

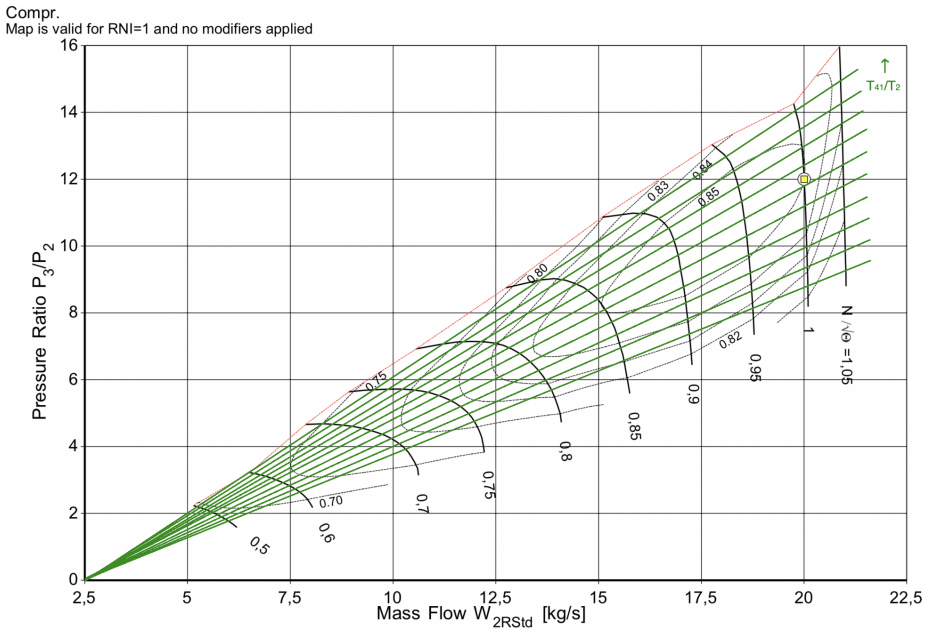

Figure 4: Correlation between turbine inlet temperature, $\frac{T_{41}}{T_2}$, and the compressor map.

2.6.2 Conservation of flow in between the compressor exit and the turbine inlet

The mass balance in the combustion chamber is given by Equation (16) [30]:

$$\frac{w_3\sqrt{T_3}}{p_3} = \frac{w_{41}\sqrt{T_{41}}}{p_4}\frac{p_4}{p_3}\frac{w_3}{w_3+w_F}\sqrt{\frac{T_{41}}{T_3}} \tag{16}$$

As stated above the pressure loss in the combustion chamber is small compared to the pressure entering, therefore $\frac{p_2}{p_3}$ can be regarded as a constant. The assumptions of choked flow and a small mass fraction of fuel compared to air still holds, and the following relations can be applied:

$$\frac{w_3\sqrt{T_3}}{p_3}\sqrt{\frac{T_{41}}{T_3}} = const \tag{17}$$

the corrected mass flow $\frac{w_3\sqrt{T_3}}{p_3}$ can be found separately from:

$$\frac{w_3\sqrt{T_3}}{p_3} = \frac{w_2\sqrt{T_2}}{p_2}\frac{w_3}{w_2}\frac{p_2}{p_3}\sqrt{\frac{T_3}{T_2}} \tag{18}$$

this shows that the corrected mass flow from the compressor outlet follows the temperature relation line $\frac{T_{41}}{T_3}$.

The turbine and the compressor forming the gas generator are directly coupled together by a shaft. The following relationship for the rotational speed of the turbine and compressor are presented by H.I.H Saravanamutto et al. [22]:

$$\frac{N}{\sqrt{T_4}} = \frac{N}{\sqrt{T_2}}\cdot\sqrt{\frac{T_2}{T_3}} \tag{19}$$

2.6.3 Conservation of energy in between the turbine and compressor

The general energy balance for the gas turbine comes from the fact that the turbine drives the compressor. This relation is presented in Equation (20).

$$P_T = P_C + P_X \tag{20}$$

The term P_X is the power the gas turbine generates for external use [30].

By implementing enthalpy change in Equation (20) with the correlating isentropic efficiencies for both turbine and compressor the following relation is acquired in Equation (21).

$$\frac{w_2 \Delta h_{is,C}}{\eta_C} = w_{41} \Delta h_{is,T} \eta_T - P_x \tag{21}$$

The relation between work and pressure ratio for the compressor and turbine is given by Equation (22) and Equation (23) respectively.

$$\frac{\Delta h_{is,C}}{T_2} = c_{p,C}[(\frac{p_3}{p_2})^{\frac{R}{c_{p,C}}} - 1] \tag{22}$$

$$\frac{\Delta h_{is,T}}{T_{41}} = c_{p,T}[1 - (\frac{p_{44}}{p_4})^{\frac{R}{c_{p,T}}}] \tag{23}$$

Combining Equations (22), (23) and (21) gives:

$$c_{p,C}[(\frac{p_3}{p_2})^{\frac{R}{C_{p,C}}} - 1] = \frac{T_{41}}{T_2}\eta_C\eta_T\frac{w_{41}}{w_2}C_{p,T}[1 - (\frac{p_{44}}{p_4})^{\frac{R}{c_{p,T}}}] - \frac{\eta_C PW_X}{T_2 w_2} \tag{24}$$

The turbine pressure ratio $\frac{p_{44}}{p_4}$ correlates directly to the pressure ratio of the turbine [22]:

$$\frac{p_4}{p_{44}} = \frac{p_3}{p_2}\frac{p_4}{p_3}\frac{p_2}{p_{44}} \tag{25}$$

where $\frac{p_4}{p_3}$ and $\frac{p_2}{p_5}$ is approximately equal to one, which means that the pressure ratio of the compressor ($\frac{p_3}{p_2}$) is related to $\frac{T_{41}}{T_2}$, which is the ratio of the turbine inlet temperature and the temperature at the compressor inlet. Equations (24) and (22) are the equations that determine the operating line.

2.6.4 Power turbine considerations

When adding a free turbine or power turbine (PT) to a gas generator one gets a two-spool gas turbine, the following relations are found in the book *Gas Turbine Theory* by Saravanamuttoo et al. [22]. The power output for the free turbine is presented in Equation (26).

$$PowerOutput = w \cdot c_p \Delta T_{45-5} \tag{26}$$

The difference between the exhaust gas temperature and the PT inlet temperature is given by Equation (27).

$$\Delta T_{45-5} = \eta_{PT} T_4 [1 - (\frac{1}{p_4/p_a})^{\frac{(\gamma-1)}{\gamma}}] \tag{27}$$

Equations (26) and (27) will be used to explain the correlation when changing the gas turbine operating fuel.

2.7 Surge margin

One parameter that needs to be explained when looking at the general operation of a gas turbine is the surge margin. Because it is a percentage based value it will not have any significance to the reader without the theoretical explanation behind it. Surge occurs when the operating point of a compressor crosses the surge line (shown in red in Figure 4). To briefly present the surge phenomenon one can refer to Figure 5, which shows the general operation of a compressor in terms of pressure ratio and mass flow. By decreasing the mass flow from point A, one would get a decrease in the pressure entering the compressor due to the positive slope of the pressure ratio. If the pressure downstream of the delivery pressure does not fall rapidly enough one would experience a positive pressure gradient across the compressor which would result in back flow. The back flow caused by surge can damage the compressor blades and cause violent aerodynamic pulsations. On the contrary, if one were to decrease the mass flow on the right side of point A, one would get an increase in inlet pressure due to the negative slope in pressure ratio. The change in mass flow will not induce surge since the pressure at entry will be higher than the exit pressure, regardless of how quickly the exit pressure reacts to the change in mass flow [32].

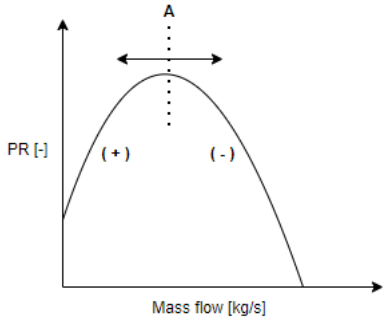

Figure 5: Sketch of the correlation between the compressor pressure ratio (PR) and mass flow.

The surge margin is commonly defined as the distance from the current operating point to the surge line for a constant mass flow, this is shown by Equation (28) which is the standard SAE (society of automotive engineers) definition. The definition that is employed by GasTurb is shown in Equation (29). The equation used by GasTurb is justified by the assumption that the operating pressure of the gas turbine usually doesn't drop below one. Another definition of the surge margin is the distance from the surge line to the operation point but following the line of constant compressor speed as shown in Equation (30). The surge margin is a good indicator of the safety and stability when operating a gas turbine. The surge margin is presented in terms of a certain percentage which usually lies around 25% [29]. From the GasTurb user manual the surge margin is given as:

$$SM_{p/p} = 100\frac{(p/p)_{surgeline}}{(p/p)_{operatingline}}@constflow \tag{28}$$

$$SM_{p/p-1} = 100\frac{(p/p)_{surgeline} - (p/p)_{operatingline}}{(p/p)_{operatingline} - 1}@constflow \tag{29}$$

$$SM_{speed} = 100\frac{w_{operatingline}[(p/p)_{surgeline} - 1]}{w_{surgeline}[(p/p)_{operatingline} - 1]}@conspeed \tag{30}$$

In GasTurb the surge line is predefined by the type of gas turbine that is selected. Equation (29) gives surge at 0% surge margin ($(p/p)_{surgeline} = (p/p)_{operatingline}$). The SAE definition in

Equation (28) seems to imply surge at 100% surge margin ($(p/p)_{surgeline} = (p/p)_{operatingline}$). One can tie the chance of surge occurring to the initiation of blade stalls in the compressor [33]. Blade stalls occur when the angle of attack is high [34]. As a general rule of thumb one can refer to increased blade loading as increasing the chance of surge. Due to the uncertainty regarding the occurrence of surge it should be noted that the phenomenons presented should not be a clear indication of surge, but rather phenomenons that might increase the chance of surge. There are other conditions that might cause surge and the general uncertainty around the topic leaves the question regarding causes of surge open. This thesis will not try to answer this question but rather present some situations that might increase the probability of surge, and how the change of gas turbine fuel might cause a change in surge margin.

2.8 Hydrogen combustion characteristics

Since one of the main objectives of this thesis is to investigate the influence of hydrogen in an aeroderivative gas turbine, it would be sensible to present some of the main characteristics related to hydrogen combustion and how it differs from natural gas. To simplify, the natural gas will be assumed to only contain methane (CH_4). The fuel heating value will be evaluated as the lower heating value of the fuel, this is due to the assumption that no condenser will be used in the combustion process. The parameters in Table 2 are presented at $298.15K$ and $101.325kPa$:

Characteristics for hydrogen and natural gas			
Parameter	**Unit**	**Natural gas**	**Hydrogen**
Density, ρ	$\frac{kg}{m^3}$	0.67	0.09
FHV per mass (LHV)	$\frac{kJ}{kg}$	55500	142081
FHV per volume (LHV)	$\frac{kJ}{m^3}$	37074	12109

Table 2: Different properties for hydrogen and natural gas [35].

The fuel heating value is one of the core parameters in the combustion process as it determines the amount of energy released when burning a fuel. The amount of fuel needed to produce a certain quantity of energy directly correlates with the FHV and the density of the fuel. The higher FHV per mass for hydrogen than for natural gas (Table 2) would mean that less hydrogen per unit mass is needed to produce the same amount of energy compared to the amount of natural gas needed. The lesser density for hydrogen than for natural gas gives a lower energy per volume. A lower energy density for hydrogen would imply that even though one would require a lower amount of hydrogen, one would need to increase the volume flow rate of fuel due to the lower quantity of hydrogen per cubic metre. The relation between volume flow and turbine specific speed N_S is presented in Equation (31) [36].

$$N_S = \frac{2\pi\sqrt{\dot{V}_{inlet}}}{\Delta h_s^{0.75}} \tag{31}$$

Equation (31) shows that a higher volumetric flow will increase the individual stage speed of a turbine, this will be discussed in more detail in Section 5.

The combustion characteristics are important when evaluating the different fuels, but the exhaust gas composition associated with the fuels affects the components downstream of the combustion chamber and should also be accounted for. Quantifying the exhaust gas composition is a difficult task due to the uncertainty regarding the formation of CO, CO_2 and NO_x. Since there is no carbon present in the reaction (assuming the gas turbine is running on pure hydrogen) there will be no CO_2 or CO associated with the fuel in the exhaust gas.

Below is the chemical reaction for H_2 and CH_4 reacting with air.

$$H_2 + \frac{1}{2}(O_2 + 3.76N_2) \rightarrow H_2O + \frac{1}{2} \cdot 3.76N_2 \tag{32}$$

$$CH_4 + 2(O_2 + 3.76N_2) \rightarrow CO_2 + 2H_2O + 2 \cdot 3.76N_2 \tag{33}$$

In both reactions H_2O and N_2 is present, but Equation (33) also produces CO_2. It should be noted that both reactions assume complete combustion and that the composition of air is reduced to nitrogen and oxygen. In a physical reaction one would get bi-products such as CO and NO_x in the exhaust gas, and the air reacting with the fuel would have traces of CO_2, SO_2, H_2O, Ar as well as other elements [37]. The quantity of air is also higher for an actual combustion due to the amount of excess air drawn by the compressor. Equations (32) and (33) are not meant to represent an actual combustion but rather give an insight into some of the main constituents that gets produced in the combustion chamber. This paper will not delve into many of the chemical processes that occurs in the combustion chamber, but rather the effects it might have on the performance. The thermodynamic characteristics of the exhaust gas products plays an important role in determining the effects caused by changing fuel. The thermodynamic properties of the exhaust gas at varying temperatures will be presented in Section 5 to justify the results from the simulation in GasTurb. Either way, the importance of the exhaust gas composition should be addressed due to its influence on the operation of the turbine.

3 Modelling in GasTurb

3.1 Choosing gas turbine

When choosing a gas turbine the GE LM2500+G4 or the LM6000 PF is preferred. These aero-derivative gas turbines correlates with the HES-OFF project and the objectives set for the thesis. The LM6000 PF is referred to as the best compromise for simultaneously dealing with the storage size of hydrogen and reducing the emissions of operation [4], but the LM2500+G4 is the gas turbine that is currently being used. The current thesis will therefore present a model for the LM2500+G4 due to it being the current aeroderivative gas turbine used offshore. The LM2500+G4 is an aeroderivative gas turbine fitted with dry low emission (DLE) technology. DLE technology aims to mainly reduce the formation of NO_x from the combustion process. State-of-the-art DLE combustors are called catalytic combustors and allows for more air to be mixed with the fuel, this is done by premixing some of the fuel with air before the combustion [38]. The gas turbine has been implemented in military frigates and advertises itself as easy to repair. The LM2500+G4 has split compressor casting, external fuel nozzles, in-place hot-section maintenance and in-place blade and vane replacement. The general LM2500+G4 weights $5237kg$ and has a length of $6.7m$ and a height of $2.04m$ [39]. This makes it small in size compared to industrial gas turbines which makes it more flexible in terms of location of operation. Figure 6 shows one of the models from the LM2500 family of gas turbines. From observing Figure 6 one can work out the amount of HPT (high pressure turbine) and PT (power turbine) stages for the LM2500 family of gas turbines.

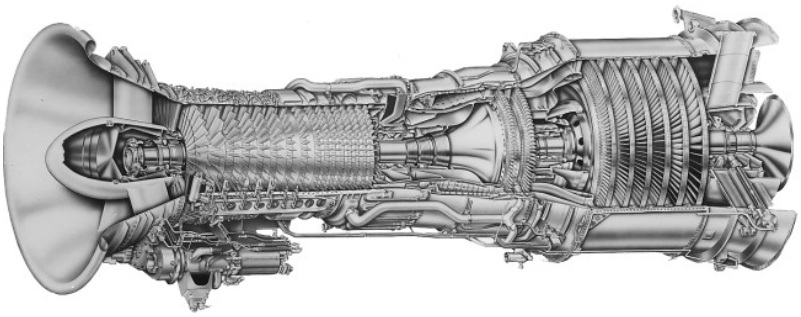

Figure 6: Illustration of a LM2500 PH gas turbine adapted from source [40].

3.2 On-design simulation in GasTurb

Because of the set mechanical parameters such as flow diameter, impeller angles and diffusor design the gas turbine will be designed to operate at certain nominal conditions i.e. inlet temperature, pressure and operating load. This is called the on-design point. Because of the competition between different gas turbine manufacturers, gas turbine data are rarely published publicly. This means that the component efficiencies, thermodynamic stage data and component maps for a gas turbine are usually unknown. By modifying one of the existing generic gas turbine models in GasTurb one can try to replicate the known outputs of a LM2500+G4. The data for the LM2500+G4(RD) are extracted from a licensed version of the commercial software GT MASTER (GT MASTER 29) [41]. The LM2500+G4(RD) is a specific version of the LM2500+G4 where the LM2500+G4 is the fourth generation in the LM2500 line. GT MASTER includes performance data for many different gas turbine models. The performance data for different ambient temperatures are given in Table 3. The complete information regarding the conditions in which the gas turbine performance data is provided from GT MASTER is found in Appendix A.

GE LM2500+G4(RD) ambient temperature change				
GT Inlet Temperature $[C^{\circ}]$	Power Output $[MW]$	Exhaust Temperature $[C^{\circ}]$	Exhaust mass flow rate $[\frac{kg}{s}]$	Thermal Efficiency LHV
15	32.939	532	90	38.59%
20	31.898	535	88	38.33%
25	30.714	540	86	38.01%
30	29.326	545	83	37.55%
35	27.877	551	80	37.03%
40	26.465	557	77	36.48%
45	25.108	564	75	35.86%

Table 3: Change in performance parameters of a GE LM2500+G4(RD) with ambient temperature change.

The information in Table 3 can be combined with the gas turbine parameters of a LM2500+G4 [42]. Some of the notable parameters of a LM2500+G4 is presented in Table 4.

Gas Turbine Parameters for LM2500+G4	
Compression Pressure Ratio	23.6
Number of Turbine Stages	8
Power Turbine Speed $[rpm]$	3600

Table 4: Physical gas turbine parameters for the LM2500+G4.

The data provided can be used to model a LM2500+G4 in GasTurb. This is done by matching the on-design output of the model against the given performance output for ISO conditions ($T_{ambient} = 288.15K$, $p_{ambient} = 101,325kPa$, $RH = 60\%$) in Table 3 along with the gas turbine parameters in Table 4. The model for the LM2500+G4 will be created from one of the existing predefined models from the GasTurb software. For simplicity's sake a generic two-spool turbine model is chosen.

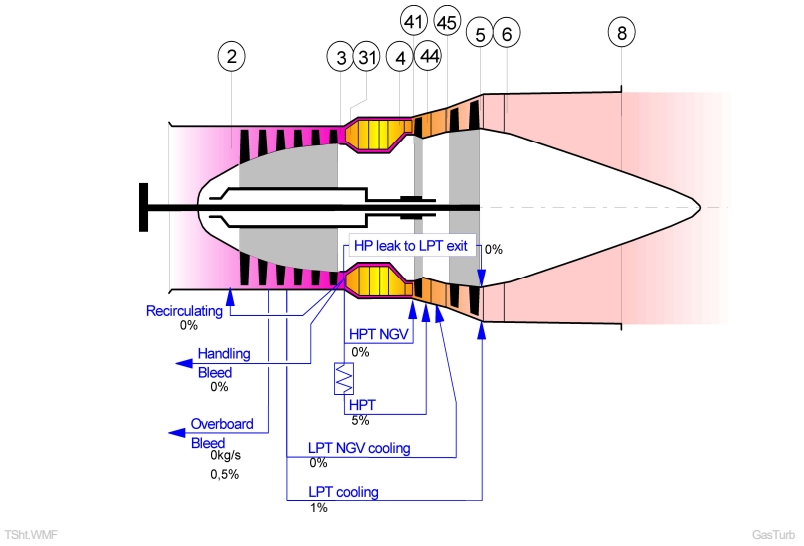

Figure 7: Two-spool gas turbine model from GasTurb with numbered stages.

The stage notations in Figure 7 are found in Table 1. The blue arrows represent the external air flows of the system. Figure 7 shows that air can be pulled from the compressor to cool the PT and the associated nozzle guide vanes (NGV) to reduce the thermal effects on the components. The same can be done for the HPT and its NGV's. Air can also be removed/bled from the compressor, this can be used as a way of preventing surge and lower the power output of the gas turbine if necessary. Recycling air from the compressor outlet to the compressor inlet can also be implemented to prevent surge.

By iterating certain parameters with regards to the LM2500+G4 performance values in Table 3 and Table 4 one can get a model in GasTurb that behaves similarly as the LM2500+G4 both off- and on-design. Parameters that determines the output of the gas turbine cycle can be calculated with regards to the known outputs of the cycle (Table 3). The software will then try to find input data between a user specified range that matches the user-set output data. The general iteration technique implemented is the Newton-Raphson iteration. The Newton-Raphson method uses influence coefficients that benchmark the change in error with regards to the specified variable. With each iteration step the error changes, the Newton-Raphson method is used to find the smallest error for the specified variable. The algorithm can be applied to multiple variables, where the influence coefficients forms the so called Jacobi matrix. The system can then be solved by using the Gauss algorithm [29]. If the iterations do not converge an error is displayed within the software and the closest iteration will be presented.

The GasTurb software also provides the thermodynamic properties along the different stages as well as a summary of some of the outputs of the cycle.

```
Date: 22feb21
Time: 11:27

Turboshaft
Alt=    0m  ISA   60% Relative Humidity ,  Rel GG Speed=1.000


          W         T         P        WRstd
Station  kg/s       K        kPa       kg/s       PWSD     =   32968,0 kW
 amb               288,15   101,325
  1     89,293     288,15   101,325                PSFC     =   0,18757 kg/(kW*h)
  2     89,293     288,15   100,312    90,368      Heat Rate=    9328,8 kJ/(kW*h)
  3     88,400     705,65  2367,357     5,932      V0       =      0,00 m/s
 31     83,489     705,65  2367,357                FN res   =     10,67 kN
  4     85,207    1500,00  2296,337     8,658      WF       =   1,71768 kg/s
 41     85,207    1500,00  2296,337     8,658      Therm Eff=   0,38590
 43     85,207    1141,79   551,741                P2/P1    =   0,99000
 44     89,671    1121,93   551,741                TRQ      =     100,0 %
 45     89,671    1121,93   537,948    33,625      P45/P44  =   0,97500
 49     89,671     807,55   106,495                Incidence=   0,00000 °
  5     90,564     805,15   106,495   145,312      P6/P5    =   0,98000
  6     90,564     805,15   104,365                PWX      =         0 kW
  8     90,564     805,15   104,365   148,278      P8/Pamb  =   1,03000
Bleed    0,446     705,65  2367,362                WBld/W2  =   0,00500
-------------------------------------------        A8       =   1,77212 m²
Efficiencies:   isentr  polytr    RNI    P/P       WCHN/W2  =   0,00000
 Compressor     0,9764  0,9842  0,990 23,600      WCHR/W2  =   0,05000
 Burner         0,9990                0,970       Loading  =    100,00 %
 HP Turbine     0,8500  0,8270  3,298  4,162      WCLN/W2  =   0,00000
 LP Turbine     0,8558  0,8286  1,078  5,051      WCLR/W2  =   0,01000
 Generator      1,0000                           PW gen   =   32968,0 kW
-------------------------------------------
HP Spool mech Eff 0,9980  Speed    38000 rpm
PT Spool mech Eff 0,9780  Speed     3600 rpm      eta t-s  =   0,83515
-------------------------------------------
hum [%]     war0       FHV     Fuel
  60,0   0,00637    49,736    Natural Gas

Input Data File:
C:\Users\trygvehs\Desktop\LM2500Estimate1.CYS (modified)
```

Figure 8: Summary stage data and output properties for the simulated LM2500+G4 GasTurb model.

Here the respective polytropic and isentropic efficiencies for the different components are presented. The massflow (W), temperature (T) and pressure (P) are shown for the different stages presented in Figure 7. Other noticeable values are PWSD (shaft power delivered $[kW]$), WF (fuel flow rate$[\frac{kg}{s}]$), Thermal Eff. (Thermal efficiency$[-]$) and FHV (Fuel Lower Heating Value$[\frac{MJ}{kg}]$). It should be noted that in the present thesis the gearing and workings of the generator will not be studied and the generator efficiency will be set to a constant value.

3.2.1 The iterations

The isentropic efficiency for both the compressor and the PT are analysed when trying to fix the power output given in Table 3 for the GasTurb model. Both efficiencies are significant when determining the power output, so it would be logical to use these variables to reach the desired power output. The isentropic efficiency for the compressor is predicted by iterating against the known thermal efficiency in Table 3. This is rationalized by analysing the gas generator system (Compressor and HPT) by using the relation presented by Equations (34) and (35) [22].

$$\Delta T_{23} = \frac{T_2}{\eta_c}[(\frac{p_3}{p_2})^{\frac{(k-1)}{k}} - 1] \tag{34}$$

$$NetPowerOutput = w \cdot c_{pg}\Delta T_{41-44} - \frac{1}{\eta_m} w \cdot \Delta T_{23} \tag{35}$$

From Equations (35) and (34) one can observe that the compressor efficiency (η_c) indirectly influences the power output. The thermal efficiency is given by Equation (36).

$$\eta_{th} = \frac{P_{shaft}}{w_f LHV} \tag{36}$$

Equation (36) shows that the power output is directly linked to the thermal efficiency. Therefore it is sensible to iterate the compressor efficiency with regards to the fixed thermal efficiency. The isentropic PT efficiency is iterated against the known exhaust gas temperature from Table 3. This relation is presented in [22] by Equation (37).

$$\Delta T_{45-5} = \eta_{PT} T_{45} [1 - (\frac{1}{p_{45}/p_5})^{\frac{(k-1)}{k}}] \tag{37}$$

Equation (37) relates the exhaust gas temperature to the PT efficiency. By managing the fixed and unknown variables this way, the iteration converges. The iteration range is purposely set to span over a wide area of efficiencies. Average values for the respective component efficiencies are collected and included in the iteration range [43] [44]. The ranges are: $\eta_{th} = 0.5 - 1$ and $\eta_{PT} = 0.5 - 1$. By filling in for the known variables in Tables 3 and 4 one gets similar outputs as the LM2500+G4 at on-design, as shown in Figure 8.

3.3 Off-design simulations in GasTurb

An off-design study of a gas turbine in GasTurb is built upon selected turbine and compressor maps. By choosing a high pressure ratio for the compressor, a two stage HPT (by inspecting Figure 6) and a medium pressure ratio for the PT, the given maps for the off-design simulation is selected. By deciding the on-design configuration for the modified two-spool gas turbine, the operation of the gas turbine for off-design can be predicted. At off-design the temperatures and pressures at the different gas turbine stages are not regarded as inputs into constructing the gas turbine (since it is already been mechanically designed in terms of the design point) but rather outputs from the off-design study.

3.3.1 Ambient temperature change

The goal of the off-design simulation is to match the given performance data in Table 3 for varying ambient temperatures. When operating a turbine the change in ambient temperature is frequent [45], therefore the effects of ambient temperature on the performance should be considered. This is done by assuming the control options for the LM2500+G4. When operating a gas turbine there are several control options. One of the options is to control the amount of fuel that enters the combustion chamber.

Regulating the fuel with regards to keeping the turbine inlet temperature (TIT) constant is a common way to control a gas turbine. An energy balance for the combustion chamber is presented in Equation (38) with the corresponding notations from Table 1.

$$w_{a31} \cdot (h_{a31} - h_{a0}) + w_f \cdot FHV \cdot \eta_{tc} + w_f (h_{f31} - h_0) = w_{g41} \cdot (h_{g41} - h_{g0}) + Q_{re} \tag{38}$$

The mass flow rate is denoted by w and h is the specific enthalpy at temperature T. The notations a and f denotes air and fuel, g denotes the combustion products and 0 is the reference state. FHV is the fuel heating value at $15°C$, η_{tc} is the efficiency of the combustion chamber and Q_{re} is the

losses in the combustion chamber due to radiation and convection. The assumption that no air is used as coolant in the turbine makes the air flow constant. No heat loss is assumed between the combustion chamber and the inlet to the turbine and the mass flow from the combustion chamber to the outlet of the turbine is constant. By expressing the enthalpy in terms of specific heat capacities and temperature differences one gets an expression for the turbine inlet temperature (TIT).

$$TIT_{ISO} = \frac{1}{c_{pg} w_{g41}} \cdot [w_{a31}(h_{a31} - h_{a0}) + w_f(h_f - h_0) + w_f FHV\eta_{tc} - Q_{re}] + \frac{h_{g0}}{w_{g4} c_{pg}} \quad (39)$$

Equation (39) shows the relation between the fuel flow and the TIT. If the ambient temperature (h_{a2}) is increased or lowered, the control system will respond by increasing or decreasing the fuel flow (w_f). By choosing TIT control as the method of control, the output parameters for the GasTurb model correlates with Table 3.

The article regarding spreadsheet calculations [46] also presents another important parameter that is related to the efficiency of the combustion chamber, namely the fuel to air ratio. For the combustion to take place one needs air to react with the fuel, the amount of air decides how much energy is released [47]. The fuel to air ratio can be found from the energy balance:

$$w_a[h_a(T_3) - h_a(T - ref)] + w_f[h_{T_f} - h_f(T_{ref})] + w_F FHV_{T_{ref}} = (w_a + w_f)[h_g(T_2) - h_g(T_{ref})] \quad (40)$$

Where subscript f, a and g stands for fuel, air and combustion/exhaust gas respectively. By letting the reference temperature be equal to the injected fuel temperature ($T_f = T_{ref}$) one can find an expression for the fuel to air ratio (FAR) $\frac{w_F}{w_A}$. By rearranging and implementing the enthalpy as a function of temperature change and specific heat Equation (40) becomes:

$$FAR = \frac{C_{p,G}(T_4 - T_{ref}) - C_{p,A}(T_3 - T_{ref})}{FHV - C_{p,G}(T_4 - T_{ref})} \quad (41)$$

Equation (41) connects the fuel to air ratio to the power output in a similar way that Equation (39) links the TIT to the power output.

Another way of controlling the turbine off-design is by changing the angle of the inlet guide vanes (IGV's), this can be applied to the system to correct desired output parameters. This is especially useful when combining the turbine with an heat exchanger, since the angle of the IGV's can help control the exhaust gas temperature. By changing the angle of the inlet guide vanes one can regulate the airflow and pressure entering the compressor. Since the gas turbine output is controlled by the fuel flow, lower loads will require less fuel. Without variable IGV's a lower fuel input will cause the original fuel air ratio to decrease. Assuming no change in reference temperature (T_{ref}) and a constant specific heat, one observes that a decrease in fuel to air ratio would cause both the TIT and exhaust gas temperature to decrease. Therefore the IGV's can be used to control the fuel air ratio by increasing or decreasing the air flow. The effect of changing the inlet air flow is observed from Equation (21) where a decrease in w_2 will directly decrease w_{41} and cause a lower enthalpy drop through the HPT.

3.3.2 Part-load performance

Another common off-design situation occurs when the gas turbine is operating at a different load than at design point, this is called the part load-performance of a gas turbine. Data from GT MASTER is used to extract the output parameters of a LM2500+G4 running at various loads. The power output, thermal efficiency, exhaust gas temperature and exhaust gas flow for the LM2500+G4 at off-design is presented in Table 5 [41].

GE LM2500+G4(RD) part-load performance at ambient conditions				
Load [%]	Power Output $[MW]$	Exhaust Temperature $[C^{\circ}]$	Exhaust mass flow rate $[\frac{kg}{s}]$	Thermal Efficiency LHV
100	32.939	532	90	38.59%
95	31.308	519	89	38.44%
90	29.678	511	87	38.16%
85	28.047	505	85	37.74%
80	26.410	512	82	36.54%
75	24.772	519	80	35.30%
70	23.132	526	78	34.01%
65	21.492	533	76	32.68%
60	19.850	540	74	31.32%
55	18.076	533	72	30.27%
50	16.574	508	67	30.85%

Table 5: Change in performance parameters of a GE LM2500+G4(RD) with regards to part-load performance. Ambient conditions at $288K$, $1.013bar$ and 60% relative humidity.

When running an off-design study in GasTurb the option to change the load directly is not available. Therefore the TIT needs to be iterated towards the given load output, this can be done for each of the part-load outputs in Table 5. As explained in Section 3.3.1, the gas turbine will be controlled by the TIT. In addition to controlling the TIT, the usage of variable IGV geometry will be implemented. IGV control can be combined with TIT control to accomplish the desired output. This is especially useful when combining the gas turbine with a steam cycle since the angle of the IGV's can help control the exhaust gas temperature. The angle of the IGV's can be plotted against different performance parameters to alter the outputs. The use of IGV's can be implemented if the GasTurb model deviates from the performance data from GT MASTER when the gas turbine is running at part-load.

The TIT and IGV will be varied and the mean average percentage error (MAPE) and root-mean-square error (RMSE) will be calculated for each data point in Table 5. By comparing the MAPE and RMSE for different IGV settings one will get an impression of how the IGV angles influence the system, and if the use of IGV's can be implemented to replicate the given performance curves from GT MASTER. The method used in determining the IGV angle that gives the closest correlation to the performance data is described in Figure 9 and the full script can be found in Appendix B.

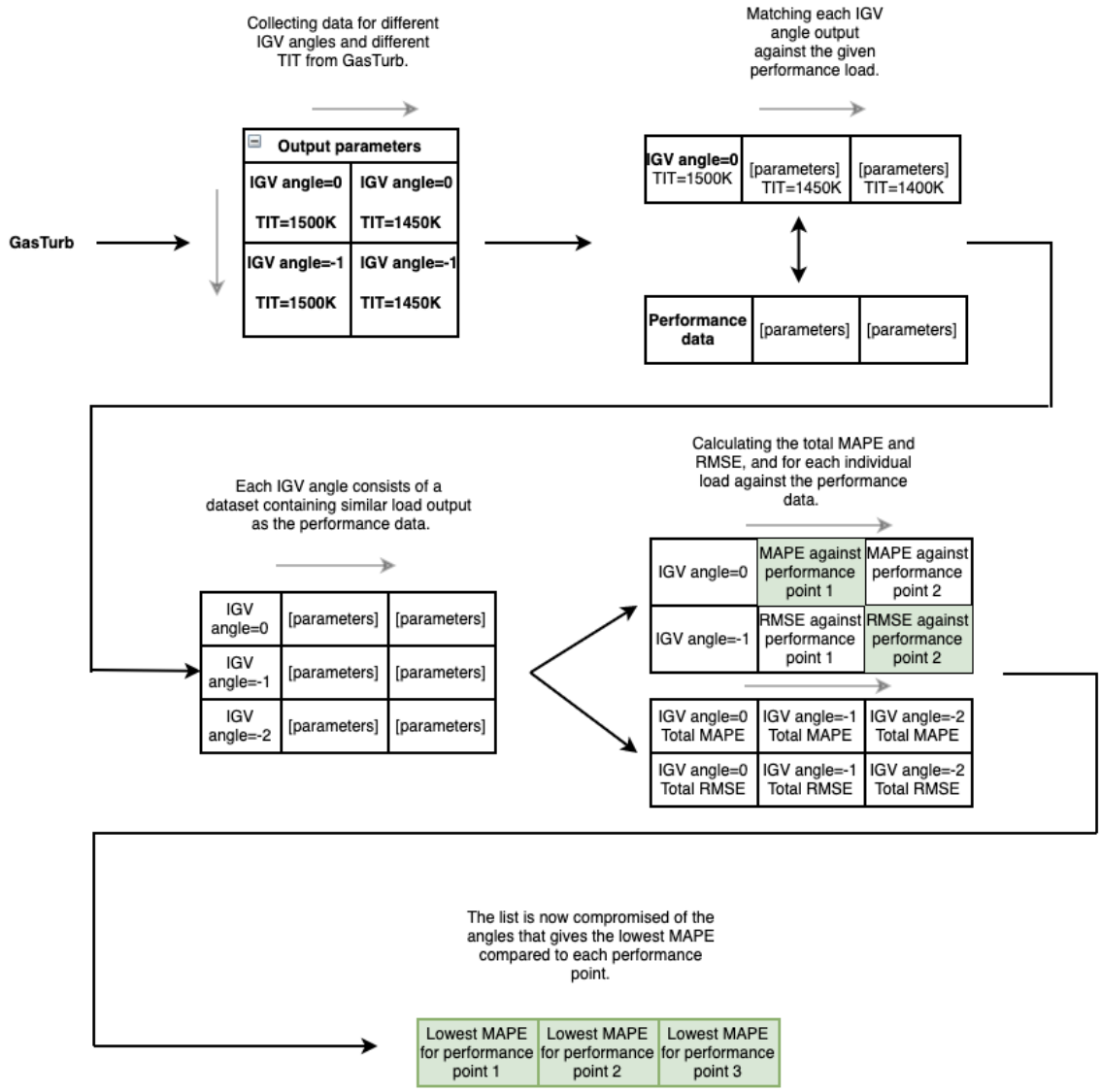

Figure 9: Process of extracting and evaluating the data for the GasTurb model running at part-load with variable geometry.

3.4 Introducing hydrogen fuel

Once the GasTurb model satisfies the given performance data for both on- and off-design with natural gas, the fuel can be changed. Since the geometry and control has been set by the given on-design point, the introduction of hydrogen will only change the output parameters. From GasTurb the performance related to hydrogen can be compared to the results from the gas turbine running on natural gas. Changing fuel in GasTurb is straight forward. From the *connections* option one can choose between the different fuels available.

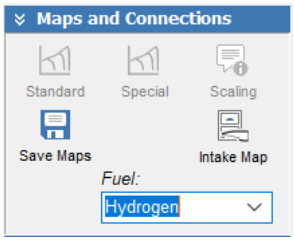

Figure 10: GasTurb interface when changing fuel.

The change of fuel automatically changes the fuel heating value and the other thermodynamic properties related to the chosen fuel.

4 GasTurb model verification

In this section the GasTurb model running on natural gas at the specified off-design conditions will be verified against the known performance data from GT MASTER presented in Table 5 and Table 3.

4.1 LM2500+G4 modelling for ambient temperature change

The results from the off-design modelling for the LM2500+G4 running on natural gas was matched against the performance data in Table 3 from GT MASTER, as described in Section 3. To clarify with regards to the entire section, the name *performance data* will be used to describe the data extracted from the GT MASTER software for the LM2500+G4 which is the performance data the GasTurb model will be verified against.

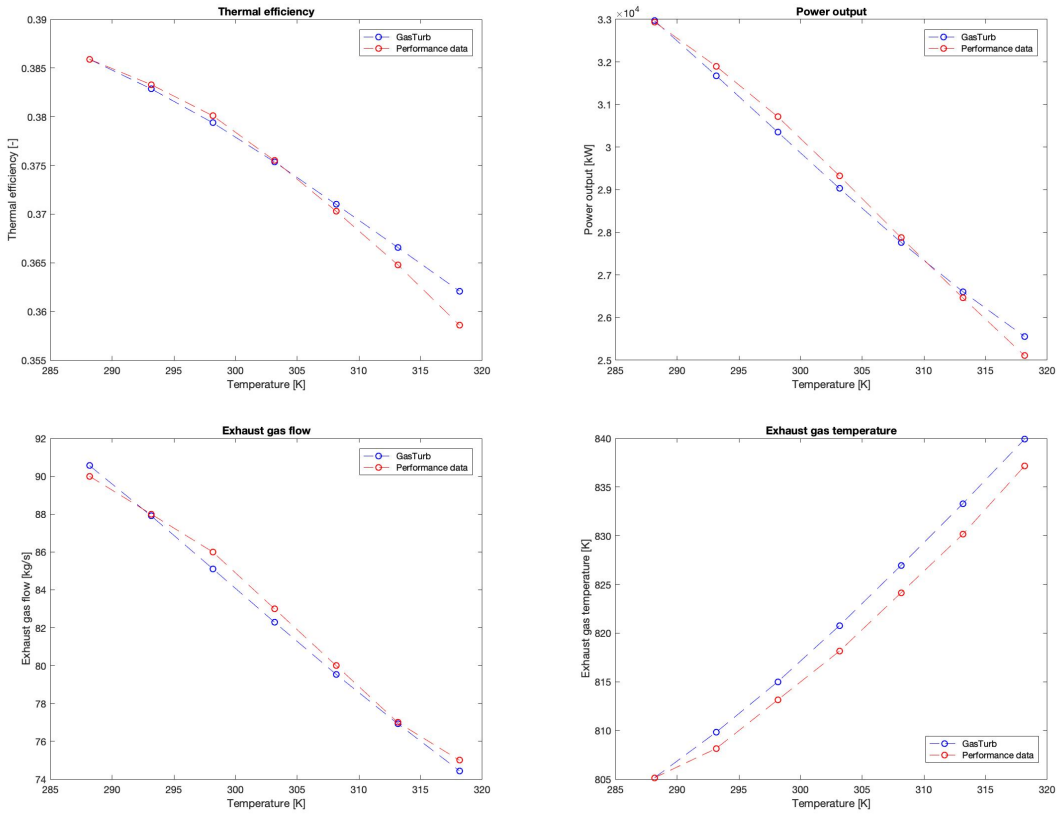

Figure 11: Thermal efficiency, power output, exhaust gas flow and exhaust gas temperature plotted against ambient temperature change for the LM2500+G4.

The mean absolute percentage error (MAPE) and the root-mean-square deviation (RMSE) is calculated for the different ambient conditions by using Equations (42) and (43). The performance data given by GT MASTER is given as F_i while A_i denotes the predicted values from the LM2500+G4 model in GasTurb and n is the number of data points.

$$MAPE = \frac{1}{n}\sum_{i=1}^{n} \mid \frac{A_i - F_i}{A_i} \mid \tag{42}$$

$$RMSE = \sqrt{\sum_{i=1}^{n} \frac{(F_i - A_i)^2}{n}} \tag{43}$$

The mean absolute percentage error and the root-mean-square deviation for the different parameters in Figure 11 are presented in Table 6.

Sensitivity analysis for the Off-design model		
Parameter	**MAPE**	**RMSE**
Power output	0.008116735	$267.1952961kW$
Thermal efficiency	0.002841655	0.001538918
Exhaust gas temperature	0.002577756	$2.344281544K$
Exhaust gas flow	0.005752997	$0.553624797\frac{kg}{s}$

Table 6: Mean absolute percentage error and root-mean-square error for the GasTurb simulation compared to the performance data from GT MASTER.

From Table 6 one observes that the mean absolute percentage error lies under a tenth of a percent for all the different parameters, this shows that the GasTurb model gives accurate results in terms of ambient temperature change. The most notable results from the root-mean square error shows that the overall power output and the exhaust gas temperature deviates with $267.20kW$ and $2.34K$ from the given performance data respectively.

Even though this model gives an accurate representation of the output parameters as shown in Table 6, the isentropic compressor efficiency is unreasonably high. The isentropic efficiency for the compressor is shown in Figure 8 to be 0.9764, this is unnaturally high compared to known compressors where the isentropic efficiency lies between 0.87 and 0.80 (the values are found from a reproduced compressor map for the LM2500 [48]).

By trial and error the system was found to be sensitive towards change in pressure ratio. By changing the pressure ratio to a slightly lower value than the given design value in Table 4 the isentropic efficiency for the compressor seems to drop to a more acceptable level. Some of the parameters at design point for the altered model is presented in Figure 12.

```
Date: 16mar21
Time: 13:05

Turboshaft
Alt=    0m  ISA

          W         T         P        WRstd
Station  kg/s       K        kPa       kg/s       PWSD     =   32831,1 kW
 amb                288,15   101,325
  1      89,000     288,15   101,325                PSFC     =   0,18757 kg/(kW*h)
  2      89,000     288,15   100,312    89,899      Heat Rate=    9328,8 kJ/(kW*h)
  3      89,000     755,70  2337,264     6,248      V0       =      0,00 m/s
 31      89,000     755,70  2337,264                FN res   =     10,66 kN
  4      90,711    1500,00  2267,146     9,314      WF       =   1,71055 kg/s
 41      90,711    1500,00  2267,146     9,314      Therm Eff=   0,38590
 43      90,711    1119,40   494,551                P2/P1    =   0,99000
 44      90,711    1119,40   494,551                TRQ      =     100,0 %
 45      90,711    1119,40   494,551    36,886      P45/P44  =   1,00000
 49      90,711     805,15   104,365                Incidence=   0,00000 °
  5      90,711     805,15   104,365   148,241      P6/P5    =   1,00000
  6      90,711     805,15   104,365                PWX      =         0 kW
  8      90,711     805,15   104,365   148,241      P8/Pamb  =   1,03000
Bleed     0,000     755,70  2337,265                WBld/W2  =   0,00000
-------------------------------------------         A8       =   1,77162 m²
Efficiencies:   isentr  polytr    RNI     P/P       WCHN/W2  =   0,00000
 Compressor     0,8640  0,9085  0,990 23,300       WCHR/W2  =   0,00000
 Burner         1,0000                0,970       Loading  =    100,00 %
 HP Turbine     0,8500  0,8252  3,257  4,584       WCLN/W2  =   0,00000
 LP Turbine     0,8837  0,8618  0,993  4,739       WCLR/W2  =   0,00000
 Generator      0,9700                             PW gen   =   31846,2 kW
-------------------------------------------
HP Spool mech Eff 1,0000  Nom Spd  38000 rpm
PT Spool mech Eff 0,9700  Nom Spd  10000 rpm       eta t-s  =   0,87027
-------------------------------------------
hum [%]     war0       FHV      Fuel
   0,0   0,00000    49,736    Natural Gas

Input Data File:
C:\Users\trygvehs\Desktop\LM2500_Trygve_modified.CYS
```

Figure 12: LM2500+G4 model data with altered pressure ratio.

The MAPE and RMSD for the altered model is presented in Table 7 .

Sensitivity analysis for the Off-design model		
Parameter	**MAPE**	**RMSE**
Power output	0.023567224	$715.6232913kW$
Thermal efficiency	0.002620107	0.0011756948
Exhaust gas temperature	0.002620107	$1.884446246K$
Exhaust gas flow	0.006607283	$0.619834937\frac{kg}{s}$

Table 7: Mean absolute percentage error and root-mean-square error for the GasTurb simulation with altered pressure ratio compared to the performance data.

Table 7 shows that the altered model gives a larger mean absolute percentage error and root-mean-square error for the power output, while the MAPE and RMSE for the other parameters seems only to slightly increase. The root-mean-square error shows that the power output deviates around $700kW$ from the performance data in Table 3. It can be argued that this result is more realistic due to the lowered isentropic compressor efficiency, even though the power output deviates more from the performance data. The altered pressure ratio will therefore be implemented and the rest of the GasTurb simulations will have a slightly lower pressure ratio than what is given in Table 4.

Regardless of the altered pressure ratio the system will be controlled by the TIT when changing the ambient temperature. The influence of TIT control for the LM2500+G4 model is presented in Figure 13.

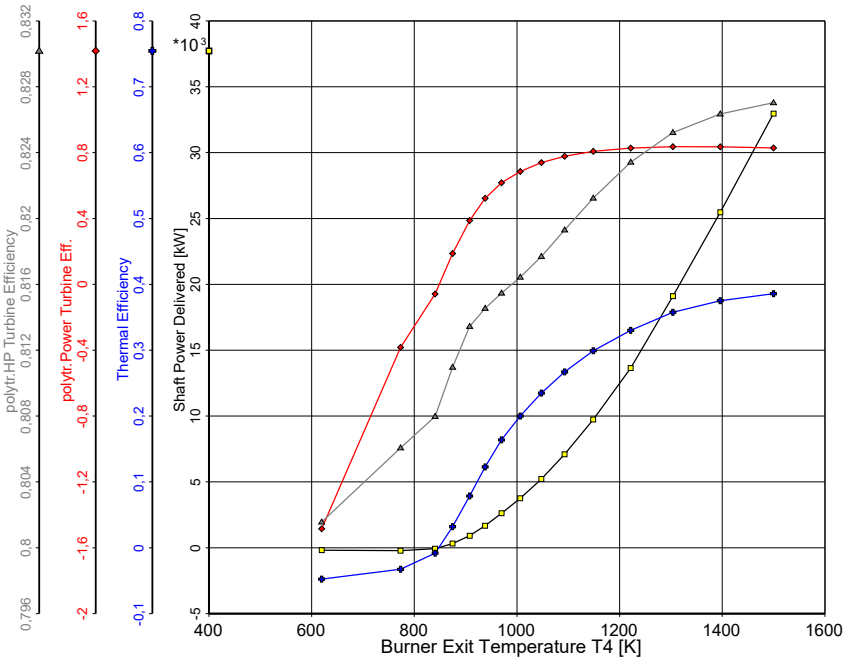

Figure 13: GasTurb plot for the influence of change in TIT with regards to power output, polytropic and thermal efficiency.

Figure 13 shows that by decreasing the TIT the polytropic efficiency for both the HPT and PT decreases as well as the thermal efficiency and power output. High temperatures are one of the main reasons for NO_x formation in the combustion chamber, and high enough TIT's will put a large thermal creep on the components in the combustion chamber and on the turbine blades. The effect of the TIT gives an understanding of how changing the fuel can affect the turbine performance characteristics. Figure 13 also shows how the TIT can be used to alter the load given by the turbine when running a part-load performance study.

4.2 LM2500+G4 modelling for part-load performance

The GasTurb model for the LM2500+G4 will be simulated at part-load by iterating the TIT as described Section 3.3.2. Significant parameters will be presented and compared to the performance data in Table 5. The GasTurb model is first simulated at part-load with only TIT-control. The parameters from Table 5 are plotted against the GasTurb model with varying load. Figure 14 shows that the power output from the GasTurb simulation is fixed against the power output from the performance data in Table 5, since this is done by controlling the TIT one would expect some of the other output parameters to vary from the performance data. Since the turbine is working at off-design, the geometry and design point is already set. This means that the only way of controlling the outputs is to decide on how the gas turbine is operated. Guessing operating strategies is what makes off-design modelling difficult since this usually tends to depend on the turbine operator and the application of the gas turbine.

Figure 14 shows that the thermal efficiency and exhaust mass flow from the GasTurb model are similar to the performance data. Both the thermal efficiency, exhaust mass flow and exhaust gas temperature starts to deviate from the performance data around 80% load. The greatest deviation from the performance data comes from the exhaust gas temperature. The deviations in parameter outputs can be caused by the operation conditions for the LM2500+G4 at part-load. The usage of variable IGV's will be implemented and the corresponding output parameters will be presented. The purpose of variable IGV geometry is presented in Section 3.3.2.

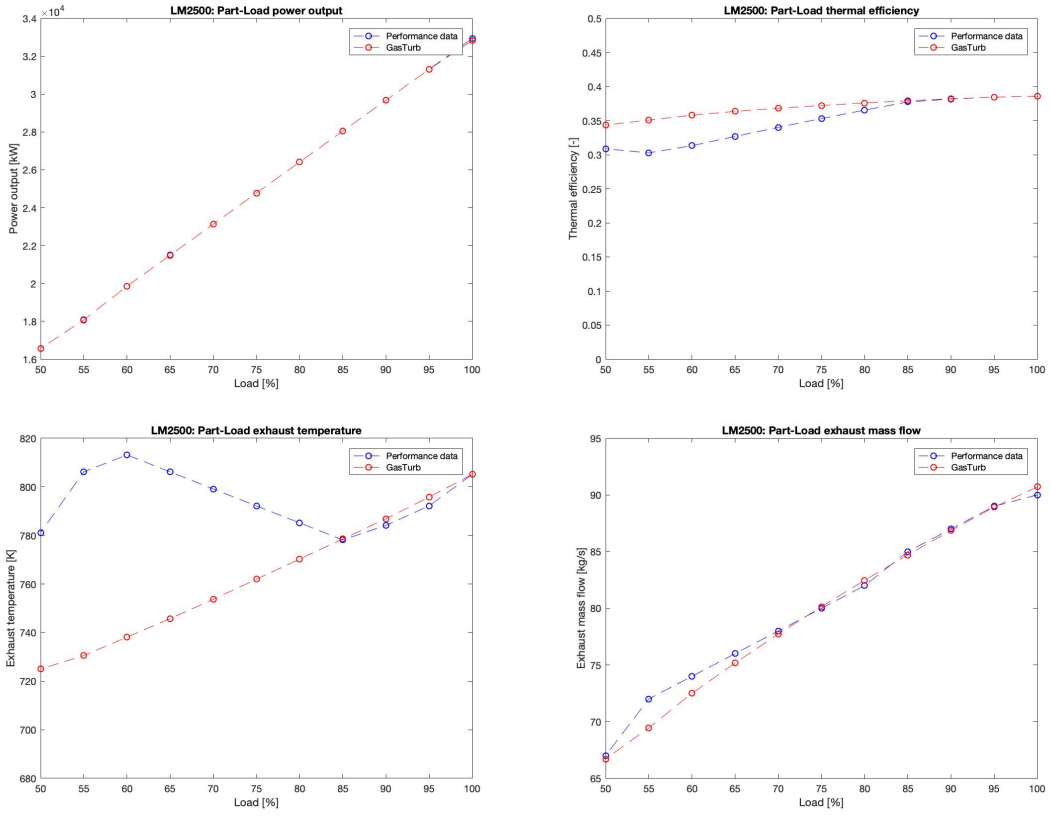

Figure 14: Power output, thermal efficiency, exhaust temperature and exhaust flow plotted against the variation in load for the LM2500+G4.

For an IGV angle varying from 0 to -45 degrees and with a TIT varying from $1500K$ to $1270K$ the MAPE and the RMSE for each angle is presented in Figure 15. Generally, Figure 15 shows

that the GasTurb simulation deviates more from the performance data with a decrease in IGV angle. For the thermal efficiency and the exhaust gas temperature the RMSE is at its lowest with an IGV setting around -20 degrees. The RMSE for the power output and exhaust gas flow seems to be lowest around an IGV setting between 0 and -5 degrees. The total MAPE shares the same characteristics as the RMSE. The power output and exhaust gas flow gives a lower MAPE close to an IGV setting of 0 degrees, while the exhaust temperature and thermal efficiency seems to be relatively unchanged before the IGV's are set to -25 degrees. Because of the large deviation in exhaust gas temperature shown in Figure 14 and because of how important exhaust gas temperature control is in a combined cycle, the IGV angles will be used to match the exhaust gas temperature profile from the performance data. This will be done by finding the TIT and IGV settings that gives the lowest MAPE for the exhaust gas temperature.

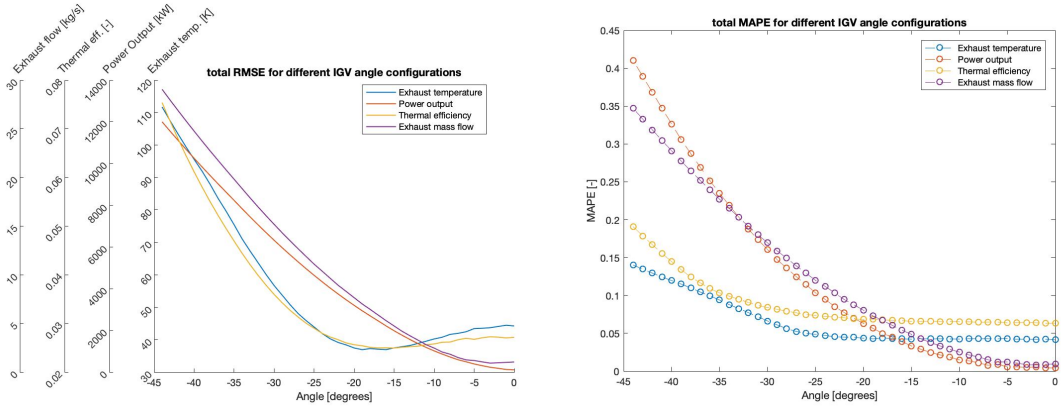

Figure 15: The total RMSE and MAPE for the LM2500+G4 with each IGV angle ranging from 0 to -45 degrees.

Using the MAPE to find the IGV setting that matches the exhaust gas temperatures given in Table 5 is presented in Figure 16. Figure 16 shows good correlation between the GasTurb model and the performance data at low power output ($1.6 - 1.8 \cdot 10^4 kW$) and at high power output ($2.8 - 3.4 \cdot 10^4 kW$). The performance points between $2 - 2.8 \cdot 10^4 kW$ can be reached by decreasing the IGV angles continuously. The increase of exhaust gas temperature with decreasing power output is not intuitive since the power output is greatly affected by the TIT as shown in Equation (35), therefore a decrease in power would intuitively decrease the TIT which again would carry over to a decreased exhaust gas temperature. The change of the IGV angle might be one of the ways of explaining what is presented from the performance data, but other ways of controlling the gas turbine at part-load could be implemented by the turbine operator. Because of the uncertainty regarding the turbine operation, it will be assumed that the way of operation will be purely TIT control and IGV variable geometry. The assumptions regarding the operation of the gas turbine limits the scope of operation and should be considered as a source of error, but given the simulation tool simplifying the methods of operation seems like the most favourable solution in terms of the objectives of the thesis and the time available.

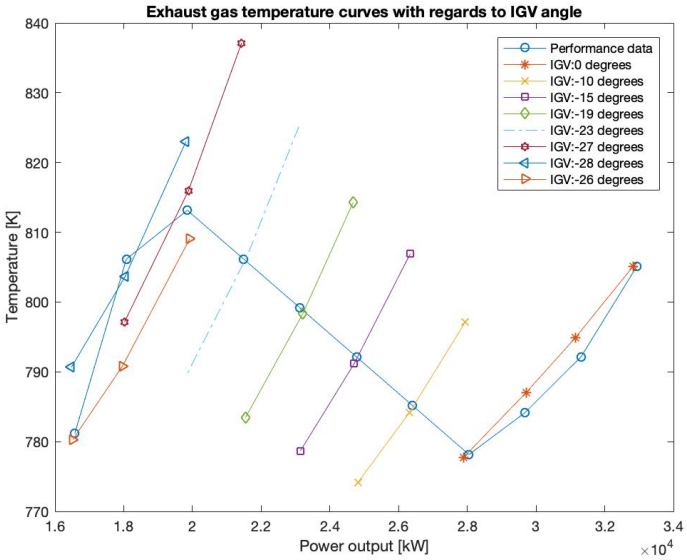

Figure 16: IGV settings for the exhaust gas temperature matching the performance data from GT MASTER

The other output parameters from Table 5 will be presented with the IGV angle that matches the exhaust gas temperature profile in Figure 16.

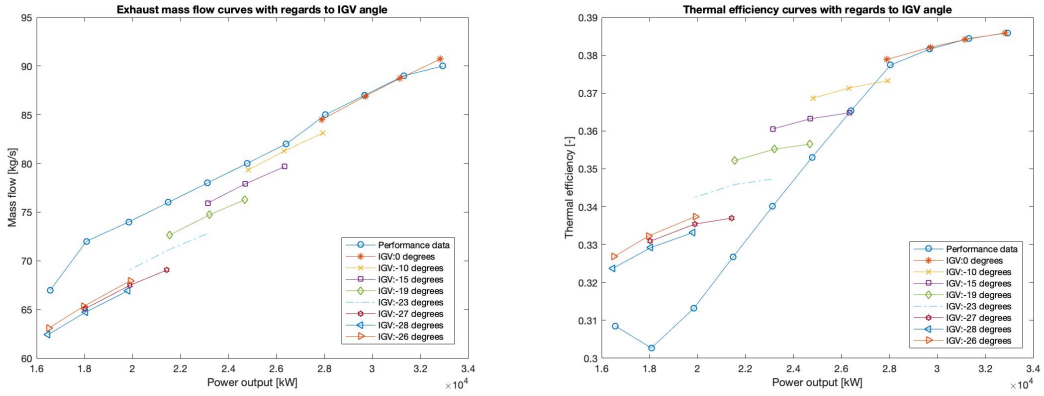

Figure 17: IGV settings meant for matching the exhaust gas temperature plotted for the thermal efficiency and exhaust mass flow

Figure 17 shows that the IGV settings used to match the exhaust gas temperature causes a general lower exhaust gas mass flow compared to the performance data. The thermal efficiency presented for the different IGV settings matches the performance data at a high power output. When the load is lowered to 70% (around $2.3 \cdot 10^4 kW$ output), the thermal efficiency from the performance data decreases more rapidly compared to the GasTurb model with IGV's. Compared to Figure 14, it is clear that the use of variable geometry for the IGV's can be used to improve the correlation between the GasTurb exhaust gas temperature and the exhaust gas temperature in Table 5. By fixing the exhaust gas temperature in GasTurb one observers that the thermal efficiency and exhaust gas flow deviates from the performance data. This might point to inaccuracies in the GasTurb model or to other ways of operating the turbine than TIT and IGV control. In general the MAPE and RMSE for each parameter is lowered when regulating the LM2500+G4 with variable IGV's. The

exception is the exhaust mass flow, which has a lower RMSE and MAPE without variable IGV as shown in Table 8.

Total MAPE and RMSE for each parameters with out without var. IGV :				
Parameter	**MAPE without var. IGV**	**MAPE with var. IGV**	**RMSE without var. IGV**	**RMSE with var. IGV**
Power output	0.0043	0.0033	$114.1246kW$	$94.7308kW$
Thermal efficiency	0.0635	0.0338	0.0272	0.0144
Exhaust gas temperature	0.0415	0.0017	$44.2546K$	$1.7372K$
Exhaust gas flow	0.0095	0.0368	$1.0501\frac{kg}{s}$	$3.6915\frac{kg}{s}$

Table 8: MAPE and RMSE for the GasTurb simulation of a LM2500+G4 with variable IGV's and without variable IGV's ($IGV = 0°$).

As mentioned earlier in the thesis, the exhaust gas temperature is significant when combining the gas turbine with a steam cycle. A combined cycle consists of two power cycles. The heat released in the primary cycle will be used as an energy input for the second cycle. By combining a gas turbine and a steam cycle one can use the exhaust gas temperature from the gas turbine to generate steam. The heated steam can then be used to drive a steam turbine or provide heat. Combined cycles increases the power output for a given amount of fuel and is therefore highly advised if possible. As mentioned in the introduction of this thesis, the gas turbine will be used to provide heat and power for an offshore facility, therefore the exhaust gas temperature should be prioritized due to its importance when using a combined cycle.

One other way to select the off-design operation would be to use the IGV setting that gives the lowest total MAPE for all the parameters combined, this can be found from Figure 15, where one clearly observers that the total MAPE is lowest with no variable geometry ($IGVangle = 0$). By doing it this way, one would have to accept the deviation in exhaust gas temperature. These two ways of evaluating the system will create two different scenarios in terms of operating the gas turbine at part-load. One without variable geometry, and one where variable geometry is used to mimic the exhaust gas temperature profile from the performance data.

Ideally the matching of the exhaust gas temperature would cause both the thermal efficiency and exhaust mass flow to match the performance data, as shown this is not the case. This might be due to other control options being used for the operation of the LM2500+G4 in GT MASTER, these control systems are complex and are dependant on the turbine operator. Another reason for the inaccuracies for the different parameters could be linked to the selected component maps in GasTurb. As mentioned in Section 3 the LM2500+G4 model is created from an existing two-spool GasTurb model, the selected compressor and turbine maps for the model are generated from limited info. One could therefore argue that the particular data for a general two-spool gas turbine that the GasTurb model is based on would create deviations when compared to a specific type of gas turbine model from GT MASTER.

5 Results and discussion for hydrogen introduction

After having verified the LM2500+G4 model in GasTurb against the available data from GT MASTER for natural gas, the results from the simulations using hydrogen will be presented and discussed.

5.1 Introduction of hydrogen for ambient temperature change

The results from the GasTurb simulation of a LM2500+G4 running on hydrogen fuel will be presented and compared to the LM2500+G4 running on natural gas. This will be done by looking at the operating point as well as how the outputs will change with regards to ambient temperature change and variation in load. The compressor and turbine maps will also be presented and compared to the natural gas case.

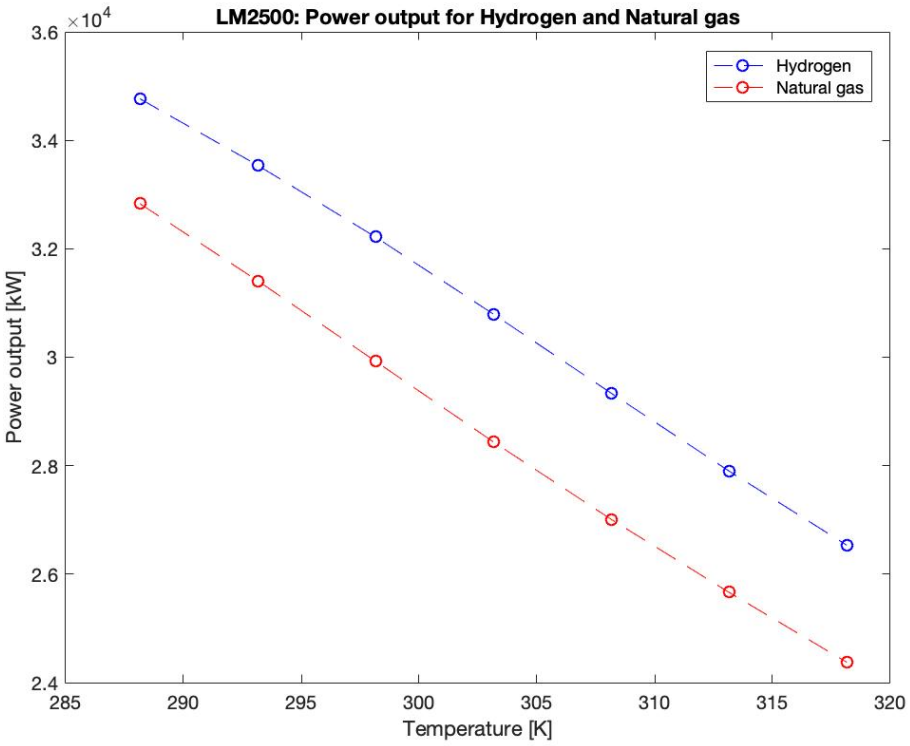

Figure 18: Power output for the LM2500+G4 with regards to ambient temperature change for hydrogen and natural gas at constant TIT.

Figure 18 shows a higher power output for hydrogen fuel than for natural gas. This can be caused by the exhaust gas products associated with hydrogen combustion. With the known fuel flow of natural gas and hydrogen from Figures 19 and 20 and the combustion reactions from Equations (33) and (32) one can determine the amount of moles for the different exhaust gas constituents. Equation (33) assumes that the natural gas only consists of methane. Natural gas often consists of a small percentage of ethane [29] but this will be disregarded when calculating the amount of moles found in the exhaust gas. Disregarding ethane due to the small mass fraction found in natural gas simplifies the chemical reaction and the corresponding calculations. From GasTurb the given fuel to air ratio will be given along with other data from the different gas turbine stages explained in Section 3.2. Figure 19 and 20 shows that the fuel to air ratio stays constant after the fuel has been introduced in the combustion chamber. Before the combustion chamber the mass flow consists only of air. By using the information presented above the fuel flow of natural gas and hydrogen is found to be:

$$w_{NG} = 1.71055 \frac{kg}{s}$$

$$w_{H2} = 0.68640 \frac{kg}{s}$$

Using the molar mass of CH_4 and H_2 the respective amount of moles is found as:

$$n_{CH4} = \frac{1.71055 \frac{kg}{s}}{16.04 \frac{kg}{kmol}} = 0.1066 \frac{kmol}{s}$$

$$n_{H2} = \frac{0.68640 \frac{kg}{s}}{2.014 \frac{kg}{kmol}} = 0.341 \frac{kmol}{s}$$

Reactions (32) and (33) can be represented as:

$$CH_4 + a(O_2 + 3.76N_2) \rightarrow bCO_2 + cH_2O + dN_2 \tag{44}$$

$$H_2 + a(O_2 + 3.76N_2) \rightarrow cH_2O + dN_2 \tag{45}$$

The subscripts a, b, c and d are found by balancing Equations (44) and (45) with regards to the amount of fuel introduced.

Natural gas: $a = 0.2132$, $b = 0.1066$, $c = 0.2132$, $d = 0.8016$

Hydrogen: $a = 0.170$, $c = 0.341$, $d = 0.6392$

From balancing Equation (44) and (45) one observes that the subscript c, that denotes the amount of H_2O formed by combustion is higher for hydrogen than for natural gas. This means that a larger amount of H_2O is produced from burning hydrogen than from burning natural gas at the same operating condition ($TIT = 1500K$). Subscript a denotes the amount of air that is needed. From subscript a one observes that less air is needed for hydrogen than for natural gas, this is not as significant since gas turbines usually operate with large amounts of excess air (often used for cooling and diluting the combustion products) [49].

By using a complete combustion reaction one observes that the main chemical changes in the exhaust gas comes from the formation of CO_2 when burning natural gas and the increased formation of H_2O when burning hydrogen. Since the excess air does not react with the fuel and the formation of CO and NO_x is assumed to be less than the formation of CO_2 and H_2O the complete combustion can be used as a reference to the actual combustion.

H_2O as a product is less dense and have a higher specific heat capacity (c_p) than both CO and CO_2. It is easy to argue for the changes that occur when switching fuel based on the chemical properties of the different exhaust gases. As mentioned in Section 2.8 the combustion products vary depending on the chosen chemical reaction and it is therefore difficult to quantify the thermodynamic properties of the exhaust gas. V. Ganapathy gives the chemical composition of the exhaust gas from a gas turbine running on natural gas as: $75\%Ni$, $15\%O_2$, $7\%H_2O$ and $3\%CO_2$ [50], the specific heat along with other parameters for this composition of exhaust gas is presented in Table 9.

Thermodynamic properties for exhaust gas from gas turbines						
Temp. [K]	**373**	**473**	**573**	**673**	**773**	**873**
Specific heat$[kJ/kgK]$	1.0610	1.0815	1.1000	1.1267	1.1501	1.1740
Viscosity $[kg/mh]$	0.0779	0.0906	0.1028	0.1145	0.1256	0.1362
Thermal conductivity $[W/mK]$	0.0319	0.0374	0.0429	0.0484	0.0537	0.0589

Table 9: Thermodynamic properties for turbine exhaust gas extracted from [50].

GasTurb takes into account some of the different combustion bi-products as well as how the change in pressure and temperature affects the system. The composition of the exhaust gas and the chemical reaction is not found in the user manual [29]. The specific heat for the exhaust gas with natural gas and hydrogen are presented by GasTurb in Figure 19 and 20 respectively. Figures 19 and 20 also include other thermodynamic properties for the different gas turbine stages presented in Section 3.2. Before entering the combustion chamber the specific heat is equal for both fuels (due to it only being air). In Stage 4 one observes that the hydrogen case has a higher specific heat capacity compared to the natural gas case. This confirms the assumption that burning hydrogen will cause a higher specific heat due to the increased production of H_2O. By confirming a higher specific heat for hydrogen combustion one can avoid making assumptions on the actual exhaust gas composition. One could calculate the average specific heat manually for the two cases by using the given fuel flow rate and assuming a distribution of exhaust gas constituents. Due to the number of assumptions needed it would not be practical to perform auxiliary calculations for the average specific heat of the exhaust gas. The specific heat provided by GasTurb alongside the specific heat for various gases in Figure 23 will therefore be used to confirm the assumption of higher specific heat for the exhaust gas products when burning hydrogen. Regardless of the accuracy of these calculations it serves to show how the exhaust gas composition influences the turbine.

	Units	St 2	St 3	St 4	St 44	St 45	St 5	St 6	St 8
Mass Flow	kg/s	89	89	90,7106	90,7106	90,7106	90,7106	90,7106	90,7106
Total Temperature	K	288,15	755,697	1500	1119,4	1119,4	805,149	805,149	805,149
Static Temperature	K	274,408	750,312	1491,16	1076,96	1076,96	772,02	799,768	799,181
Total Pressure	kPa	100,312	2337,26	2267,15	494,551	494,551	104,364	104,364	104,364
Static Pressure	kPa	84,5624	2274,83	2209,34	420,865	420,865	88,5569	101,615	101,325
Velocity	m/s	166,055	108,203	149,998	321,252	321,252	274,72	111,722	117,54
Area	m²	0,499247	0,077876	0,118803	0,210311	0,210311	0,837846	1,86003	1,77173
Mach Number		0,5	0,200002	0,2	0,499999	0,499999	0,499996	0,200001	0,210489
Density	kg/m³	1,07355	10,5621	5,09031	1,34261	1,34261	0,394094	0,436517	0,435589
Spec Heat @ T	J/(kg*K)	1004,52	1088,16	1279,47	1220,67	1220,67	1149,58	1149,58	1149,58
Spec Heat @ Ts	J/(kg*K)	1004,19	1086,87	1278,32	1212,3	1212,3	1140,85	1148,23	1148,07
Enthalpy @ T	J/kg	-10032,8	475616	1,40051E6	924018	924018	550890	550890	550890
Enthalpy @ Ts	J/kg	-23819,9	469762	1,38926E6	872417	872417	513155	544649	543982
Entropy Function @ T		-0,11924	3,34645	6,2721	5,01565	5,01565	3,67491	3,67491	3,67491
Entropy Function @ Ts		-0,290033	3,31938	6,24628	4,85431	4,85431	3,51066	3,64821	3,64535
Exergy	J/kg	-831,298	458577	1,13531E6	636496	636496	245334	245334	245334
Gas Constant	J/(kg*K)	287,05	287,05	291,067	291,067	291,067	291,067	291,067	291,067
Fuel-Air-Ratio		0	0	0,01922	0,01922	0,01922	0,01922	0,01922	0,01922
Water-Air-Ratio		0	0	0	0	0	0	0	0

Figure 19: Thermodynamic data extracted from GasTurb for the different gas turbine stages for natural gas combustion.

	Units	St 2	St 3	St 4	St 44	St 45	St 5	St 6	St 8
Mass Flow	kg/s	91,5237	91,5237	92,26	92,26	92,26	92,26	92,26	92,26
Total Temperature	K	288,15	766,854	1500	1115,58	1115,58	795,677	795,677	795,677
Static Temperature	K	273,328	761,354	1491,13	1072,83	1072,83	760,405	789,918	789,298
Total Pressure	kPa	100,312	2413,87	2341,01	508,772	508,772	104,517	104,517	104,517
Static Pressure	kPa	83,4048	2348,98	2281,58	433,044	433,044	87,76	101,632	101,325
Velocity	m/s	172,452	109,344	152,312	326,152	326,152	286,328	115,696	121,759
Area	m²	0,499247	0,077876	0,118803	0,210311	0,210311	0,837846	1,86003	1,77136
Mach Number		0,520285	0,200728	0,199783	0,500049	0,500049	0,515968	0,204798	0,21561
Density	kg/m³	1,06304	10,7482	5,09859	1,34502	1,34502	0,384576	0,428724	0,427766
Spec Heat @ T	J/(kg*K)	1004,52	1090,81	1315,06	1250,37	1250,37	1174,4	1174,4	1174,4
Spec Heat @ Ts	J/(kg*K)	1004,16	1089,5	1313,78	1241,32	1241,32	1164,88	1172,85	1172,68
Enthalpy @ T	J/kg	-10032,2	487748	1,43638E6	942570	942570	554099	554099	554099
Enthalpy @ Ts	J/kg	-24902,1	481770	1,42478E6	889382	889382	513108	547407	546687
Entropy Function @ T		-0,11924	3,40158	6,21729	4,95787	4,95787	3,59919	3,59919	3,59919
Entropy Function @ Ts		-0,303817	3,37433	6,19157	4,79671	4,79671	3,42444	3,57119	3,56817
Exergy	J/kg	-831,298	468816	1,1705E6	653606	653606	245769	245769	245769
Gas Constant	J/(kg*K)	287,05	287,05	300,103	300,103	300,103	300,103	300,103	300,103
Fuel-Air-Ratio		0	0	8,0446E-3	8,0446E-3	8,0446E-3	8,0446E-3	8,0446E-3	8,0446E-3
Water-Air-Ratio		0	0	0	0	0	0	0	0

Figure 20: Thermodynamic data extracted from GasTurb for the different gas turbine stages for hydrogen combustion.

Because of the lesser density of H_2O compared to CO_2, the speed will be higher entering the turbines. If the mass flow given by $w = \dot{V}\rho$ is constant, then the decrease in density would cause the volumetric flow rate $\dot{V}$ to increase, this is also confirmed through the volumetric heating value presented in Table 2. Volumetric flow rate is given as $\dot{V} = VA$, then by saying that the velocity V is constant one would see an increase in area A to compensate for the reduction in density. This is shown in Figure 21, where the area of the stages increase as the density reduces. If this turbine is designed for natural gas it is implied that by introducing hydrogen in the combustion chamber on would have much lighter combustion products. This would cause the velocity to be higher into the turbine for the hydrogen case than for the natural gas case as shown in Figure 22. Since the turbine extracts the energy from the working fluid, the higher velocity entering the turbine could be the reason for the slight increase in power output. This reasoning can also be tied up to Equation (19), that gives a higher spool speed for higher volumetric flow rate.

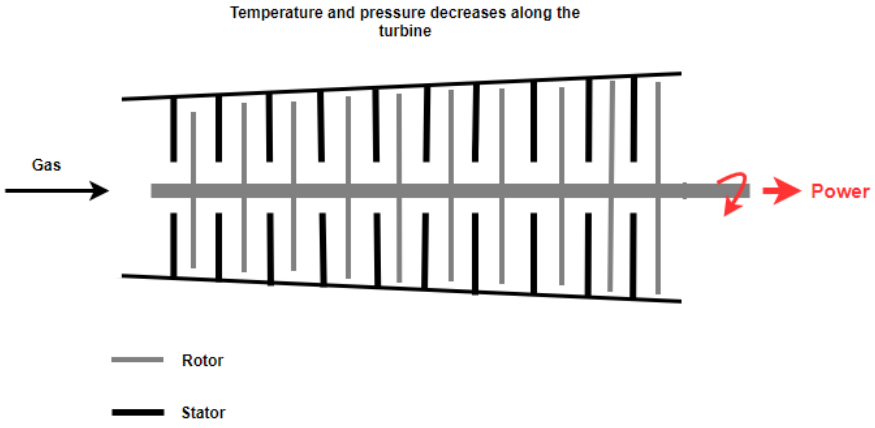

Figure 21: Generic sketch of the side view of the different stages in a general turbine.

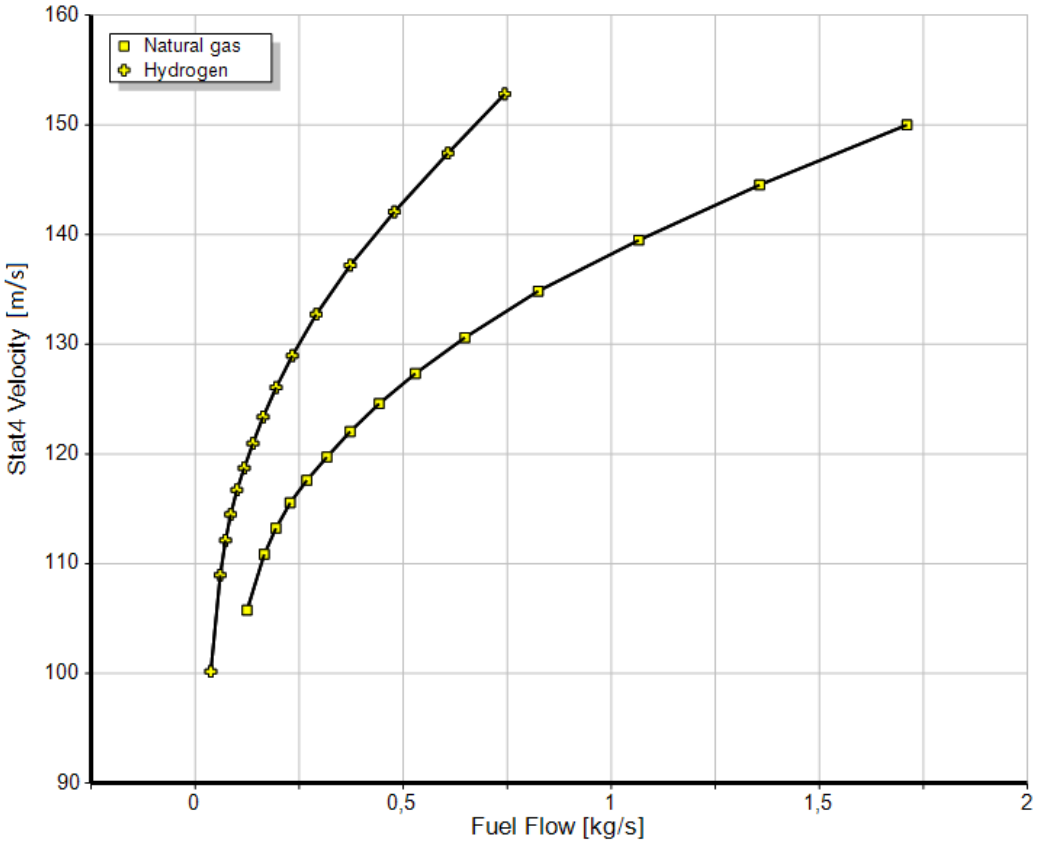

Figure 22: Velocity of the working fluid in the LM2500 upon entering the HPT.

As shown in Figure 24 the higher heating value of hydrogen will cause the specific power to increase when switching fuel. This is because of the higher energy density for hydrogen compared to natural gas. The core efficiency and thermal efficiency is presented in Figure 25. Both the core efficiency and the thermal efficiency decreases when the ambient temperature rises this is due to the decrease in air density which lowers the mass flow rate [51]. Figure 25 shows that the core and thermal efficiency is slightly higher for hydrogen than for natural gas. From the GasTurb manual, the thermal efficiency (η_{th}) and core efficiency (η_{core}) is given by Equations (46) and (47) respectively.

$$\eta_{th} = \frac{w_9 V_9^2/2 - w_0 V_0^2/2}{w_f FHV} \tag{46}$$

Equation (46) defines the thermal efficiency as the increase of the gas streams kinetic energy passing through the engine divided by the amount of heat introduced in terms of the fuel mass flow and the heating value of the fuel. This shows that the velocity of the working fluid influences the thermal efficiency. As explained above, the exhaust gas produced by injecting hydrogen will have a higher velocity due to the lower density. The higher velocity related to hydrogen combustion can be one explanation to why GasTurb calculates a higher thermal efficiency for hydrogen than for natural gas.

$$\eta_{core} = \frac{w_{core}(dh_{is} - V_0^2/2)}{w_f FHV} \tag{47}$$

Similarly the core efficiency in Equation (47) is defined as the ratio between the energy available after the combined power requirements of the core stream compression processes are fulfilled and the energy related to the fuel insertion. Because of the pre-determined TIT control, the product of fuel flow and FHV will be similar across both fuels. This means that the denominator in

Equation (47) will not change drastically when switching fuels. V_0 is the ambient speed entering the compressor, and it can be influenced by the increased power output from the turbines. Since the HPT drives the compressor, one could argue that this would increase the speed entering the core of the engine, hence increasing the core efficiency when switching to hydrogen. The GasTurb 13 manual states that dh_{is} is evaluated by assuming an isentropic expansion from the core exit to ambient conditions. The rate of isentropic enthalpy change can be related to the specific heat capacity of the exhaust gas, as shown in the Equation (48).

$$\Delta h = c_p \Delta T \tag{48}$$

By assuming a constant specific heat capacity, one can observe from Equation (48) that a higher specific heat capacity will cause a greater enthalpy change. For hydrogen the exhaust gas that enters the turbine will consist of air and H_2O as shown by Equation (32). Table 10 shows that the specific heat capacity for H_2O is higher than that of gases associated with combustion of natural gas (CO_2, CO). This could explain the difference in core efficiency when switching fuel from natural gas to hydrogen.

Specific specific heats for various gases		
Gas	**Formula**	c_p $[\frac{kJ}{kg \cdot K}]$
Air	–	1.005
Carbon dioxide	CO_2	0.846
Carbon monoxide	CO	1.040
Nitrogen	N_2	1.039
Steam	H_2O	1.872

Table 10: The specific heat capacity for different gases at $300K$.

By treating the specific heat capacity as a function of temperature one can observe from Equation (47) that a greater change in specific heat capacity will cause a larger value for dh_{is} and give a higher core efficiency. Figure 23 shows the specific heat for different gases in $\frac{kJ}{kgK}$. The specific heat was calculated by using the formula: $\overline{c_p} = a + bT + cT^2 + dT^3$ where a, b, c and d are constants. These constants vary for different gases and are extracted from [52]. From Figure 23 one observes that the change in specific heat with regards to temperature is much greater for H_2O than for CO and CO_2. Therefore the combustion products produced by using hydrogen as a fuel will have a higher specific heat capacity than the combustion products produced by natural gas.

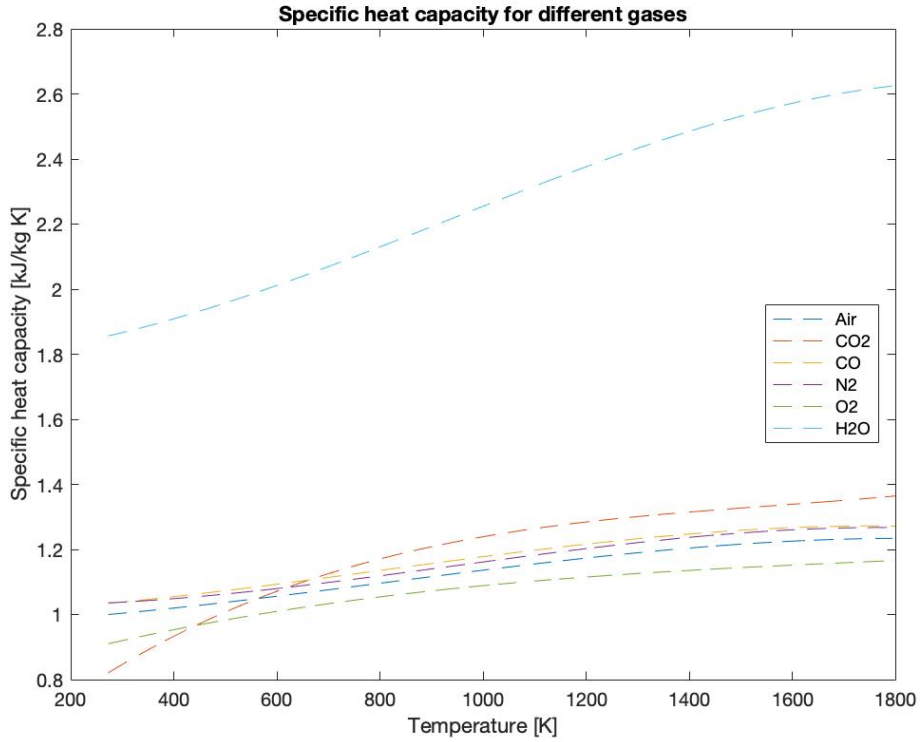

Figure 23: The specific heat for different gases with varying temperature.

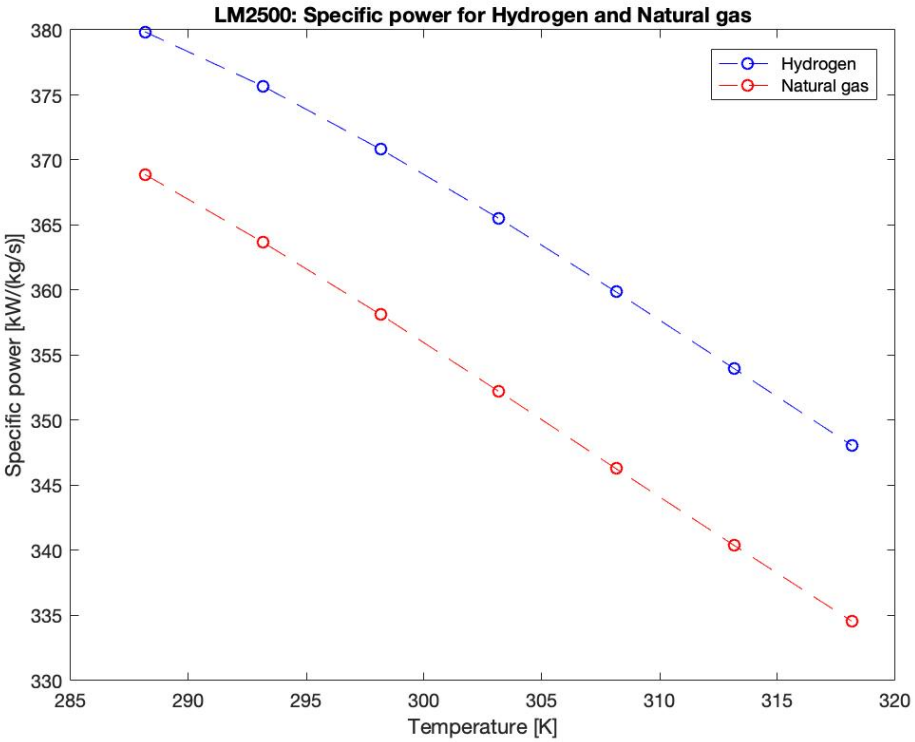

Figure 24: Specific power for hydrogen and natural gas combustion at constant TIT.

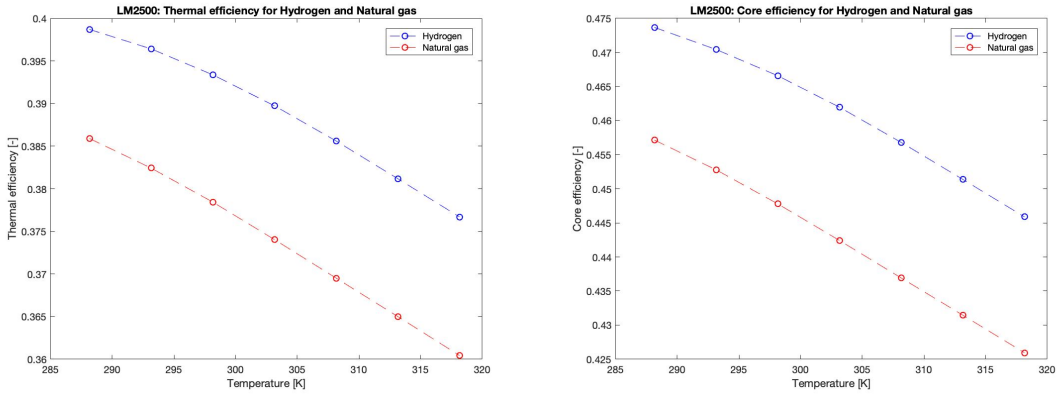

Figure 25: Thermal efficiency and core efficiency for hydrogen and natural gas with regards to ambient temperature change at constant TIT.

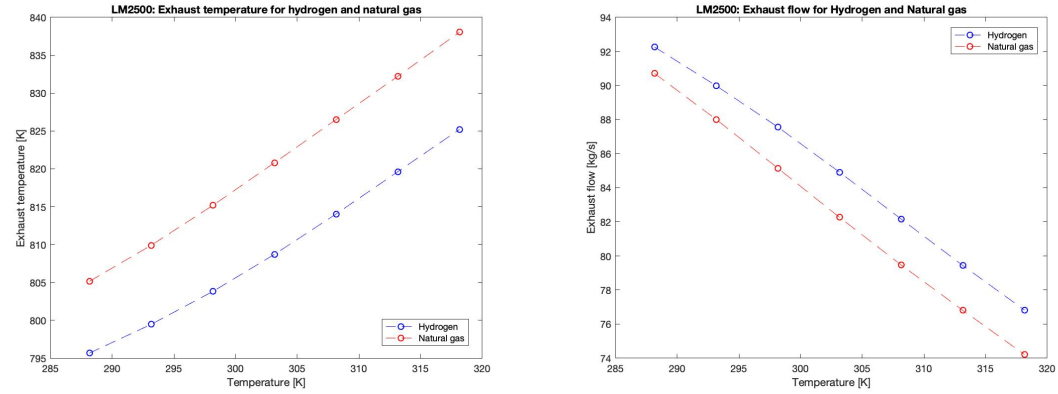

Figure 26: Exhaust temperature and exhaust flow for hydrogen and natural gas with regards to ambient temperature change at constant TIT.

The data from Figures 26, 25 and 18 are used to calculate the average percentage difference between natural gas and hydrogen at varying ambient temperatures. With ambient temperature change the power output is shown to increase by 7.8% for hydrogen fuel. The thermal efficiency is found to increase by an average of 4% when switching to hydrogen while the exhaust flow is increased by 2.9%. The exhaust gas temperature is found to decrease by 1.4% when changing fuel from natural gas to hydrogen.

5.1.1 Difference in operating point

When changing the fuel type to hydrogen the general operating point of the gas turbine is shifted. The operating point is noted by a yellow square (■) and the corresponding design point with a white circle (○). The total power output with a TIT of $1500K$ for hydrogen is $34765.1kW$ compared to $32830.8kW$ for natural gas which is a 5.9% increase in power output when changing fuel to hydrogen. With the TIT at $1500K$ the thermal efficiency is increased by 3.95% when switching to hydrogen and the exhaust gas temperature is decreased by 1.18%.

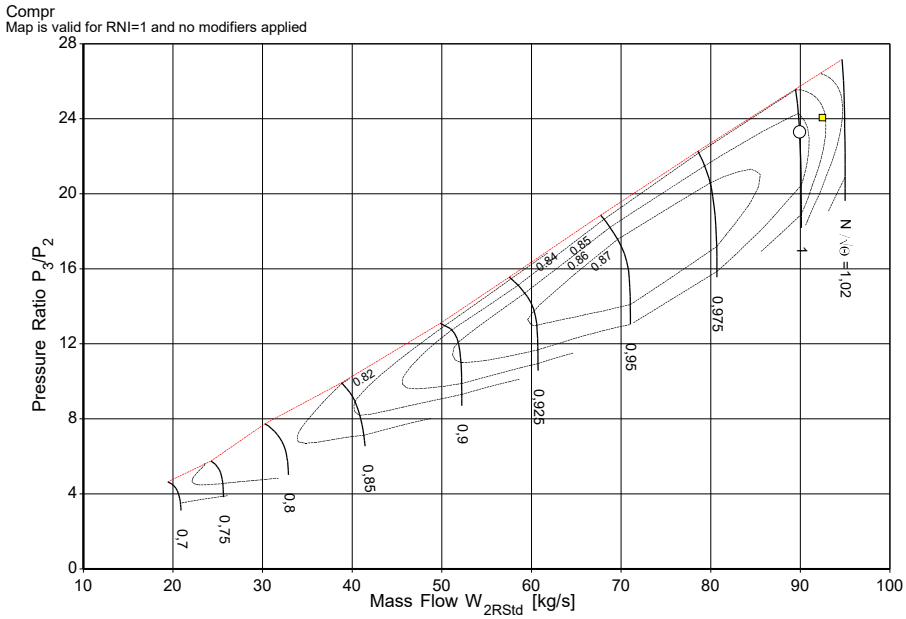

Figure 27: Operating point for hydrogen compared to the design point for natural gas presented on a compressor map.

Figure 27 shows that the operating point for hydrogen lies above and to the right of the design point. Referring to Figure 4 one observes that the two points are lying at the same $\frac{T_{41}}{T_2}$ line. Equation (15) implies a higher pressure ratio through the compressor when switching to hydrogen due to the increase in w_2. The increase in inlet mass flow (w_2) comes from the higher volumetric flow rate associated with hydrogen upstream of the compressor. The increased volumetric flow rate is introduced in Section 2.8 and discussed in Section 5.1.

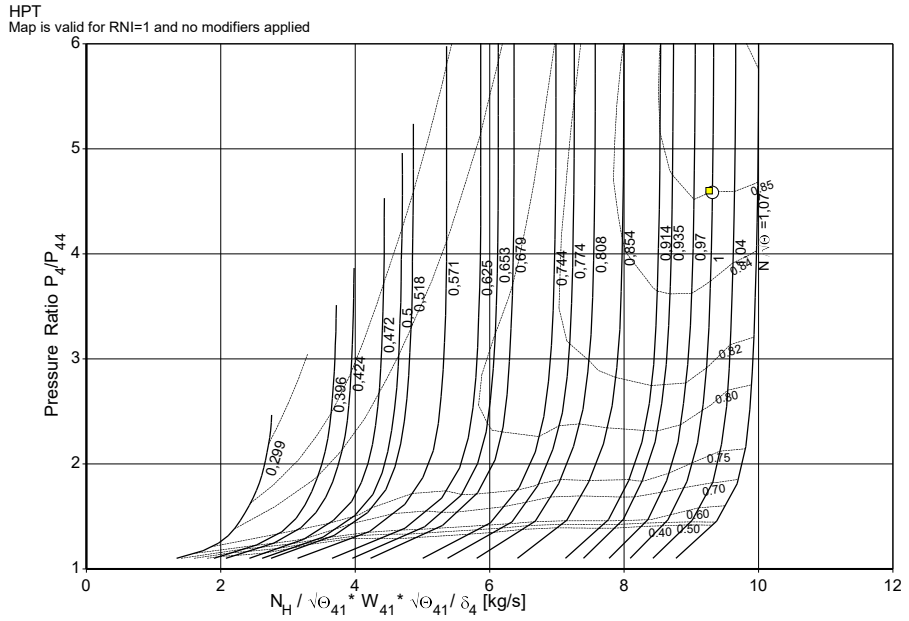

Figure 28: Operating point for hydrogen compared to the design point for natural gas presented on a HPT map.

Figure 28 shows that the operating point for the HPT lies close to the design point. This might be caused by the fixed TIT. The spreadsheet calculations from [46] presents the polytropic efficiency for a turbine as:

$$\eta_p = \frac{\psi(T_4) - \psi(T_{44})}{ln(\frac{p_4}{p_{44}})} \tag{49}$$

where ψ is the entropy function and is given as:

$$\psi = \int_{T_{ref}}^{T} \frac{C_p}{R} \frac{dT}{T} \tag{50}$$

By assuming that the working fluid entering the HPT is mainly air (small mass fraction of combustion products), then the specific heat capacity (c_p) and gas constant (R) would remain unchanged when switching fuel. By this assumption one observes from Equation (50) that the entropy function will not deviate greatly when switching fuels. Since the TIT is fixed, T_{41} will remain constant for both fuels. By these assumptions the operating point for the HPT with hydrogen would lie on the same efficiency curve as the design point as shown in Figure 28. Because of this the operation point for the HPT will lie close to the design point.

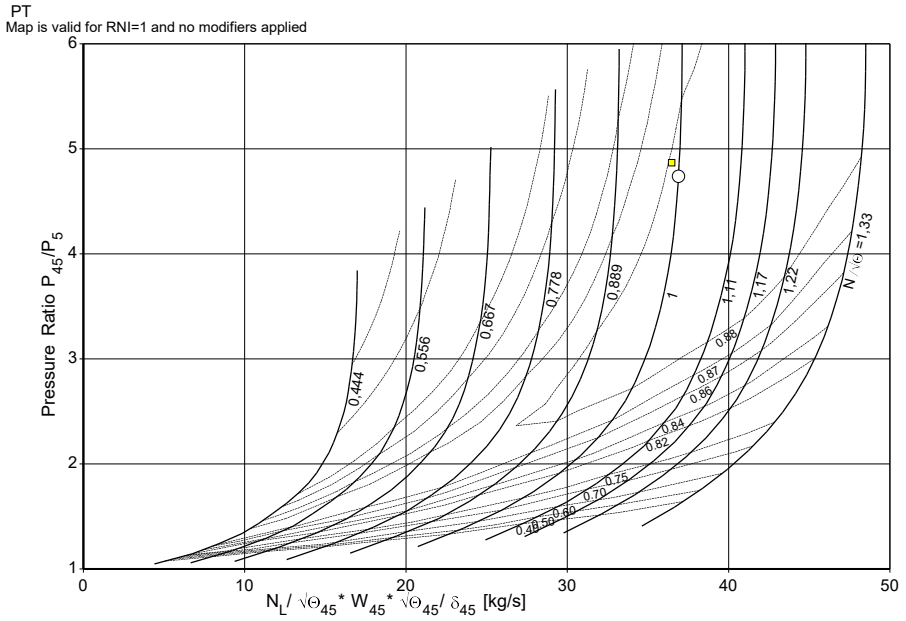

Figure 29: Operating point for hydrogen compared to the design point for natural gas presented on a PT map.

Figure 29 shows that the operating point for the PT is slightly above the design point. The increase in pressure ratio could be explained by using the ideal gas law as a reference. The ideal gas law is given by Equation (51).

$$p = \rho RT \tag{51}$$

Since hydrogen is less dense than natural gas, the combustion products in exhaust gas that enters the PT will have lower density than at design point. By lowering the density one increases the pressure as shown by Equation (51). The higher pressure can also be explained by the increased velocity that is gained by using hydrogen. This explanation correlates with the accommodating plots in Appendix C. The cause in deviation from design point for the PT compared to the HPT could be caused by the TIT control. The fixed TIT directly affects the inlet to the HPT, while no form of regulation or control downstream could cause larger deviations for the PT.

In general one observes that a fixed TIT at $1500K$ controls the operating point for the HPT when switching fuel, but the components downstream and upstream of the HPT (i.e. the compressor and PT) gets more affected by the change in fuel.

5.2 Introduction of hydrogen for part-load performance

At part-load the GasTurb model will be evaluated with variable IGV's and without variable IGV's for hydrogen and natural gas in correlation with the two scenarios presented in Section 4.2. The power output will be varied for both fuels by changing the TIT.

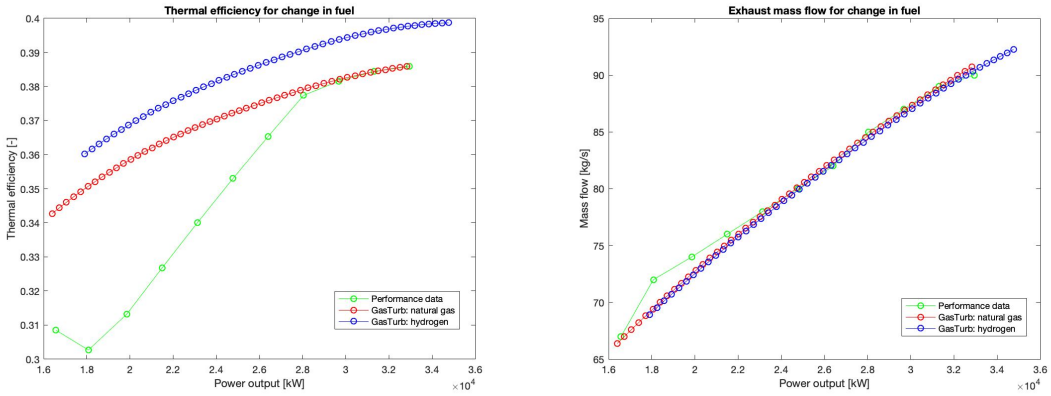

Figure 30: Thermal efficiency and exhaust gas flow for the LM2500+G4 running part-load with hydrogen fuel.

Figure 30 shows a change in both thermal efficiency and exhaust gas temperature when switching from natural gas to hydrogen without changing the IGV's. At part-load the thermal efficiency is generally increased by 4.2% when using hydrogen while the exhaust gas flow is increased by 3%. The increase in thermal efficiency at part-load can again be explained by the higher velocity of the exhaust gas resulting in a higher thermal efficiency given by Equation (46). It is also worth noting that the energy transfer for an axial turbine can be represented by the speed of the turbine blades, U, and the change in the tangential component of the absolute velocity that passes through the rotor section of the turbine, c_Θ. Equation (52) assumes adiabatic flow [53]. One would expect the velocity triangles entering the gas turbine to change in both size and direction when switching fuels, but the effect on the actual performance is small due to the adversity of the turbine blades [19].

$$\Delta W = \frac{\dot{W}}{w} = U \Delta c_\Theta \tag{52}$$

At part-load the exhaust gas flow is increased for hydrogen compared to natural gas. At the same power output one would expect a similar mass flow for natural gas and hydrogen due to the relation between flow rate and velocity influencing the power output as described in Equation (52). But at constant TIT one observes from Figure 26 that hydrogen combustion will cause a higher exhaust gas mass flow due to the increased velocity and volumetric flow rate. This correlates with Figure 30 which shows a similar mass flow for hydrogen and natural gas at the same power output with a deviation at high power output and low power output for the respective fuels.

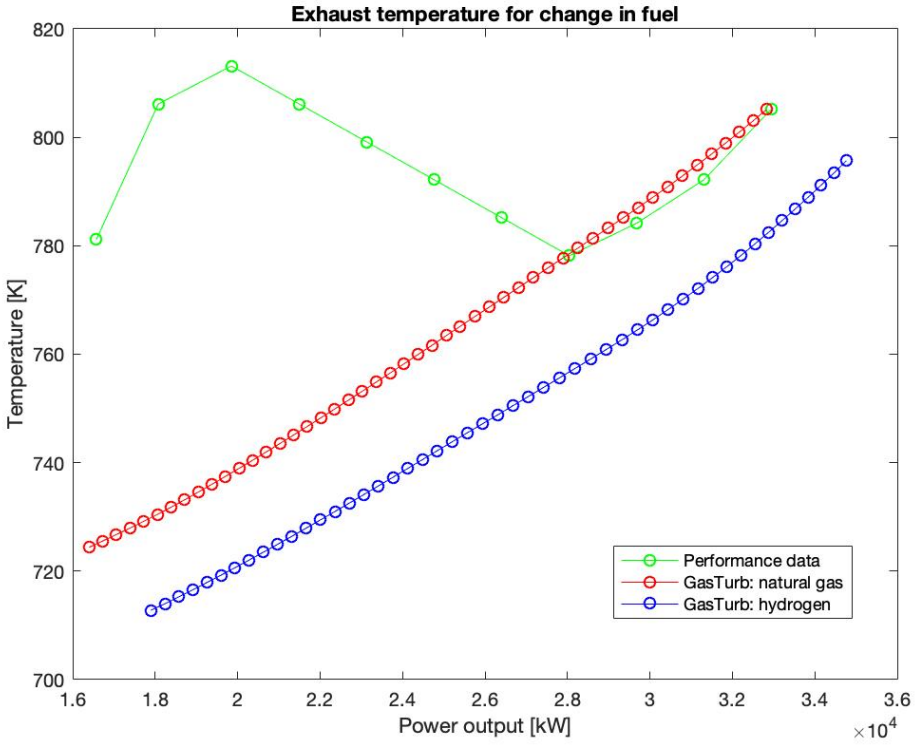

Figure 31: Exhaust gas temperature for the LM2500+G4 running part-load with hydrogen fuel.

Figure 31 shows that the exhaust gas temperature for the LM2500+G4 model is lower for hydrogen than for natural gas. On average the exhaust gas flow temperature is found to decrease by 1.4% at part-load when using hydrogen. The lower exhaust gas temperature indicates that the properties of hydrogen as a fuel directly influences the rate at which the exhaust gas temperature is lowered. Since the temperature is fixed when entering the HPT, the pressure would be higher for hydrogen combustion because of the lower density of the exhaust products. The lower density would again increase the speed as explained in Section 5.1. One could also expect a decrease in temperature due to the increased pressure with regards to the ideal gas law relation presented in Equation (51). Equation (37) then implies a decrease in exhaust gas temperature as shown in Figure 31. The specific heat of exhaust gas might affect the change in exhaust gas temperature, but the main contribution would be expected to come from the change in pressure. The specific heat capacity is a measurement of how much energy in terms of heat that needs to be applied to a substance to raise its temperature with one degree. A high heat capacity will imply that more energy needs to be removed or added to change the temperature of a substance. Although the working fluid is mostly air, the change in exhaust gas composition when switching fuels are mainly the increased steam produced by burning hydrogen and the CO_2 produced by burning natural gas. From Figure 23 one observes that steam has the highest specific heat capacity which would imply that more energy needs to be extracted from the steam to change its temperature compared to that of CO_2. The higher specific heat capacity for steam does not support what is presented in Figure 31 since this would imply a higher exhaust gas temperature for hydrogen than for natural gas. Therefore the influence the specific heat has on the temperature drop through the turbine is uncertain. Another possibility is that GasTurb does not implement temperature change through the turbine in terms of heat transfer between the exhaust gas and the turbine blades, but rather temperature change as a function of reduction in pressure only. The increase of specific heat capacity would increase

the enthalpy drop as shown by Equation (53).

$$\Delta h_{is} = \int c_p(T)dT = \bar{c_p}(T_{inlet} - T_{outlet}) \tag{53}$$

As discussed the change in the average specific heat will cause a larger enthalpy drop through a general expansion process which might again correlate with the decreased exhaust gas temperature for hydrogen. Another parameter that influences the temperature drop is the specific-heat ratio k [19]. The specific-heat ratio influences the temperature change in an expansion process and is given by Equation (54). [54]:

$$k = \frac{c_p}{c_v} \tag{54}$$

Specific heat ratios at 300K for various gases		
Gas	**Formula**	k [−]
Air	−	1.400
Carbon dioxide	CO_2	1.289
Carbon monoxide	CO	1.400
Nitrogen	N_2	1.400
Steam	H_2O	1.327

Table 11: The specific heat capacity for various gases at $300K$.

Table 11 shows that carbon dioxide has the lowest specific heat ratio at $300K$. The thermodynamic relation for an adiabatic expansion process is given by Equation (55) [55].

$$\frac{T_{out}}{T_{in}} = (\frac{p_{out}}{p_{in}})^{[1-\frac{1}{k}]} \tag{55}$$

Due to the nature of an expansion process the outlet temperature T_{out} will always be lower than the inlet temperature T_{in} and p_{out} will always be lower than p_{in}, therefore one observes that a high value for k will result in a low $\frac{T_{out}}{T_{in}}$. Therefore the higher specific heat ratio will increase the temperature drop and therefore decrease the outlet temperature [19]. Values for the specific heat with constant volume (c_v) is not commonly found in thermodynamic tables, therefore the specific heat at constant volume will be calculated by the ideal gas relation in Equation (56) [56].

$$c_v = c_p - R \tag{56}$$

From Equation (56) the specific heat at constant volume is found by using the values for c_p from Figure 23, the specific gas constant R is to remain constant. The corresponding values for the different specific heat ratios are found from Equations (56), (54) and tabulated data in [57].

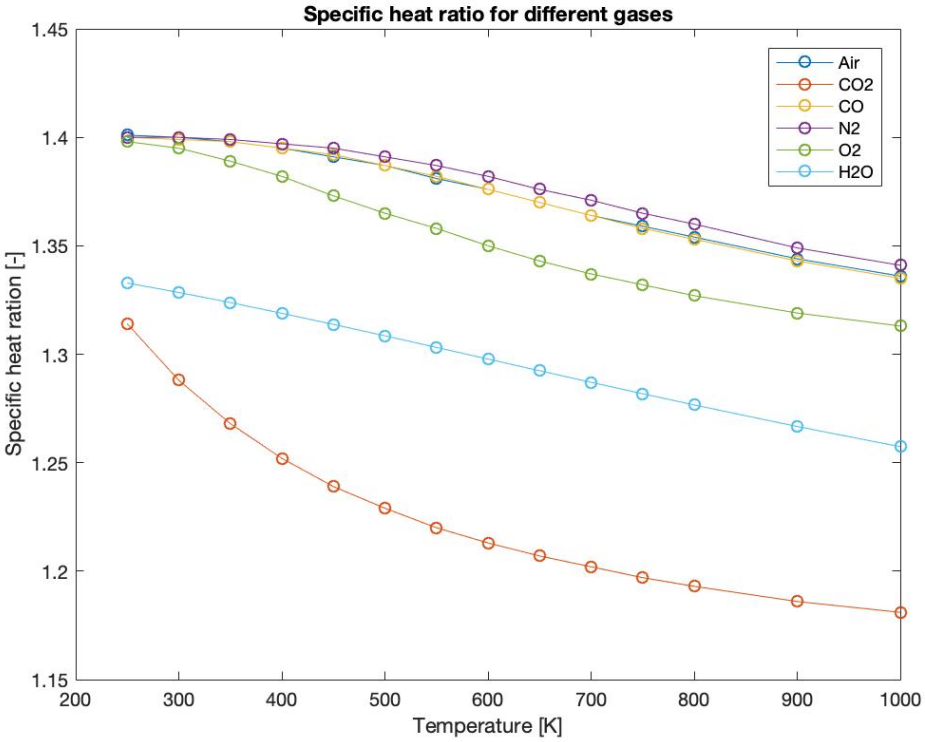

Figure 32: Specific heat ratio for different gases with varying temperature.

Constituents such as oxygen, nitrogen and air will naturally be included when burning both fuels due to the usage of air as a working fluid. As mentioned CO_2 has the lowest specific heat ratio of the selected gases followed by H_2O. It is worth to note that CO has similar specific heat ratio as air, a higher specific heat ratio would again increase the temperature drop and decrease the exhaust gas temperature, but the formation of CO would be significantly lower than the CO_2 formation [58] [59]. From Figure 32 one observes that H_2O has a higher specific heat ratio than CO_2. The lower specific heat ratio for CO_2 compared to H_2O could be one reasons to why the exhaust gas temperature is lower when burning hydrogen compared to natural gas. It is worth noting that the main contributor to the lower exhaust gas temperature for hydrogen in Figure 31 is most likely the increased pressure ratio associated with hydrogen combustion. The increased pressure ratio through a turbine can be caused by the increased velocity due to lower density as mentioned in Section 5.1.1. A higher pressure ratio will increase the cycle efficiency and again reduce the exhaust gas temperature, but as observed from Figure 32 the chemical composition of the exhaust gas should be considered.

The same procedure as described in Figure 9 is used when changing the fuel type to hydrogen. The IGV settings used in Figure 16 will be the same used in Figure 33 and the only change will be the change in fuel. The exhaust gas temperature for the LM2500+G4 running on hydrogen with the IGV settings for natural gas is presented in Figure 33. Generally one observes that the exhaust gas temperature for hydrogen "lags" behind the exhaust gas temperature for natural gas at the same IGV setting. When having the IGV angle set at zero degrees one gets the exact same exhaust gas temperature profile as shown in Figure 31, the arguments made previously for the difference in exhaust gas temperature profile are still applicable. The increased velocity associated with hydrogen causes the power output to increase. The increase in power output shifts the IGV curves for hydrogen in Figure 33 to the right. The shift in power seems to propagate when decreasing the IGV settings. This indicates that the operation of the gas turbine needs to be altered when changing fuel, especially when using a combined cycle where the exhaust gas temperature profile is significant. To get the desired exhaust gas temperature profile when using hydrogen it is implied that the IGV settings needs to be changed. From Figure 31 one observes that the IGV angles for hydrogen needs to be reduced to match the power output of the performance data.

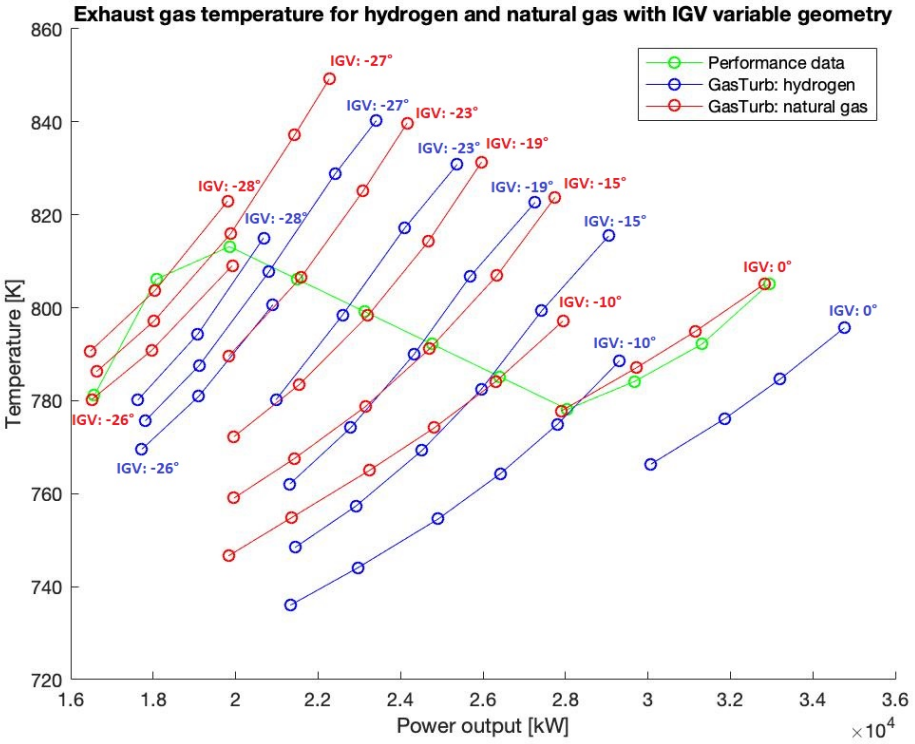

Figure 33: The exhaust gas temperature with matching IGV settings for both natural gas and hydrogen.

In Figure 34 the same IGV settings found for natural gas are used to plot the thermal efficiency and the exhaust gas flow for hydrogen. The thermal efficiency curves are shifted upwards due to the increased speed when introducing hydrogen. The difference in exhaust gas flow for the two fuels is not as significant. The exhaust gas flow for natural gas and hydrogen seems to correlate at the same power output, this is again due to the relationship between mass flow rate and power output as described when discussing Figure 30. The small difference in exhaust gas flow could be caused by the need to introduce less hydrogen than natural gas due to the higher heating value associated with hydrogen.

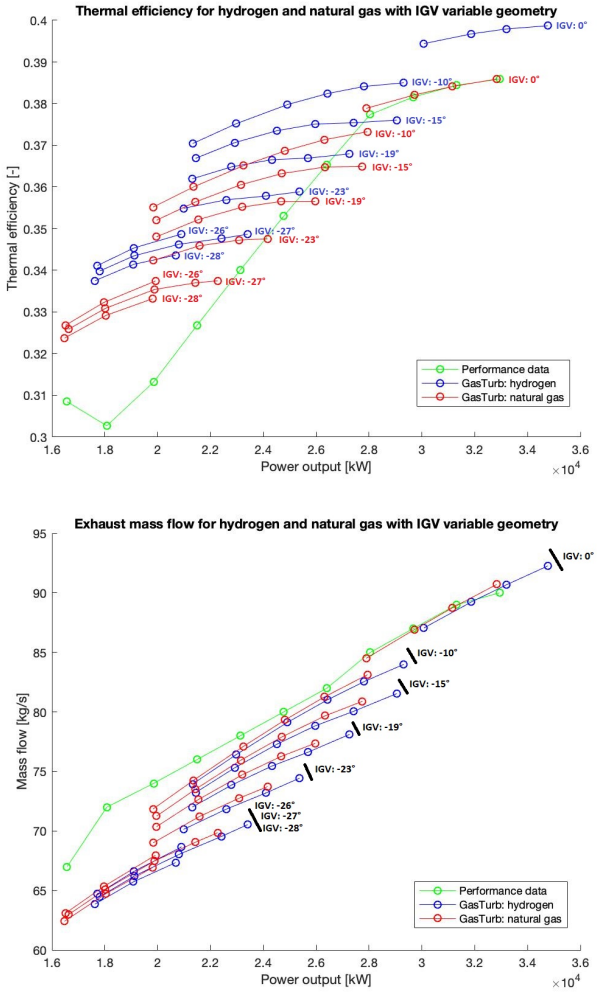

Figure 34: Thermal efficiency and exhaust gas flow for the LM2500+G4 running part-load with hydrogen fuel with variable geometry.

The script used for matching the exhaust gas temperature profile from GT MASTER by changing the TIT and IGV settings in the GasTurb model for natural gas is used for hydrogen. Figure 35 presents the IGV settings that matches the performance data from GT MASTER when using hydrogen.

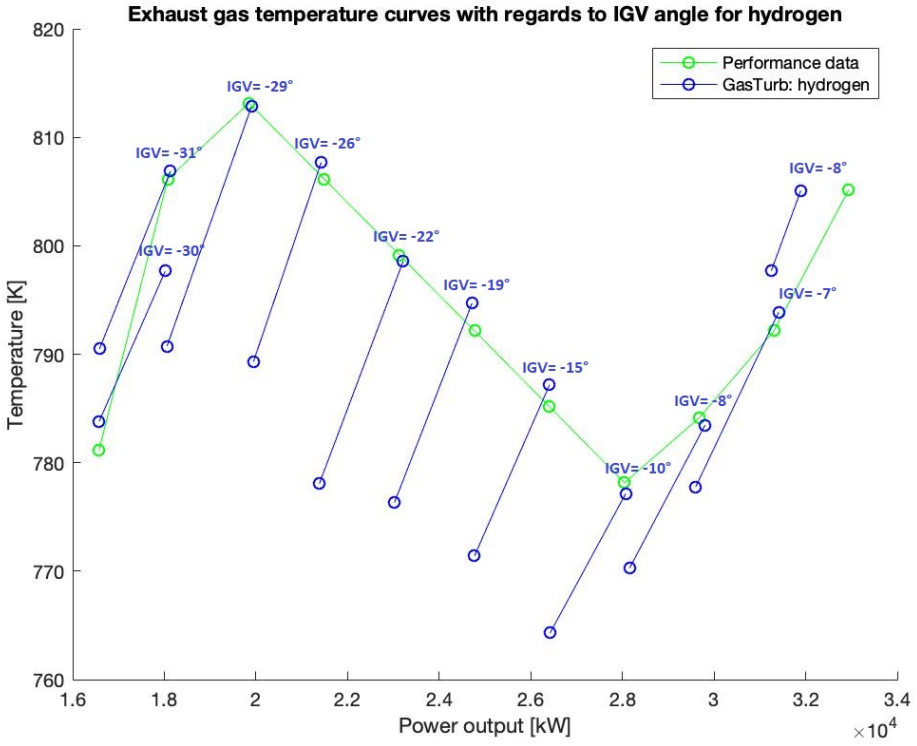

Figure 35: Matching the exhaust gas temperature for the LM2500+G4 running on hydrogen by using variable IGV settings.

The attempt to replicate the exhaust gas temperature profile from the GT MASTER performance data has been done by TIT control and variable IGV geometry. A certain IGV geometry will not give the desired exhaust gas temperature if the TIT is not specified. The TIT and IGV settings needed to replicate the exhaust gas temperature from the performance data is given in Table 12 for both fuels. Table 12 is graphically represented in Figure 36.

IGV and TIT for matching the exhaust gas temperature from GT MASTER									
Performance data		**GasTurb: natural gas**				**GasTurb: hydrogen**			
Load $[kW]$	**Exh.Temp** $[K]$	**Exh.Temp** $[K]$	**IGV** $[deg.]$	**TIT** $[K]$	**Load** $[kW]$	**Exh.Temp** $[K]$	**IGV** $[deg.]$	**TIT** $[K]$	**Load** $[kW]$
32939	805.15	805.15	0	1500	32831	805.07	−8	1500	31893
31308	792.15	794.87	0	1476	31142	793.88	−7	1481	31412
29678	784.15	787.10	0	1457	29714	783.47	−8	1457	29804
28047	778.15	777.76	0	1433	27894	777.14	−10	1438	28071
26410	785.15	784.13	−10	1433	26311	787.19	−15	1443	26410
24772	792.15	791.18	−15	1433	24708	794.70	−19	1443	24717
23132	799.15	798.32	−19	1433	23210	791.46	−22	1423	22646
21492	806.15	806.54	−23	1433	21588	807.70	−26	1438	21426
19850	813.15	815.91	−27	1433	19879	812.82	−29	1433	19901
18076	806.15	803.69	−28	1399	18045	806.89	−31	1409	18136
16574	781.15	780.28	−26	1352	16515	780.23	−30	1352	16130

Table 12: IGV and TIT settings at part-load for matching GasTurb model and GT MASTER performance data with regards to exhaust gas temperature for natural gas and hydrogen.

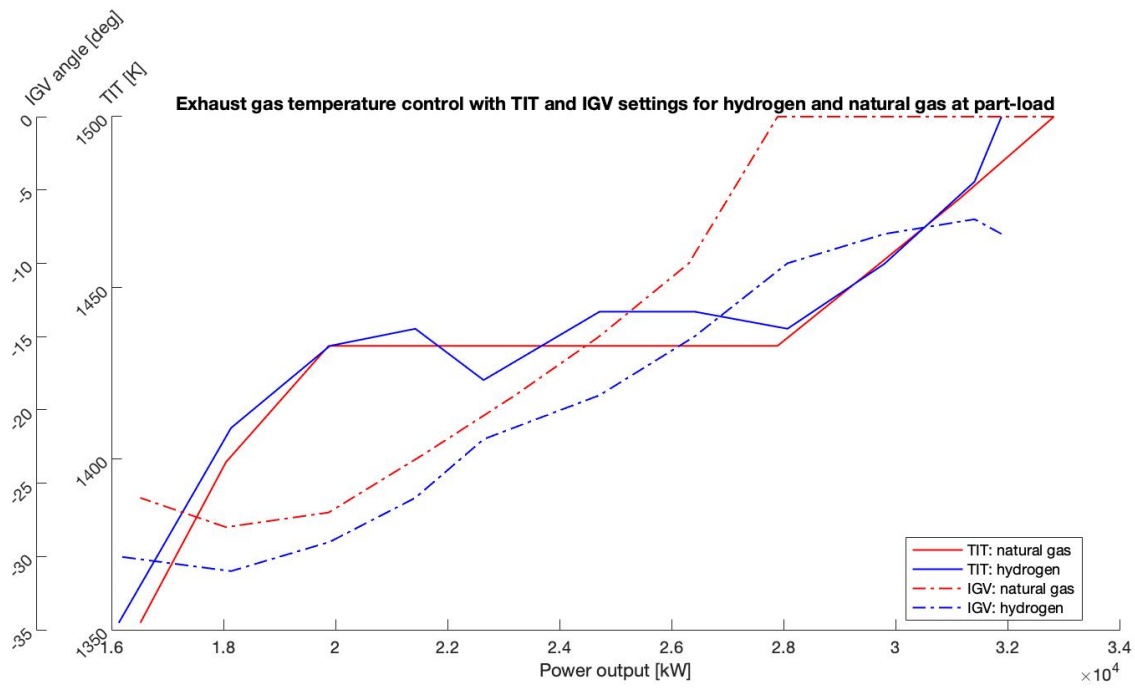

Figure 36: Graphical representation of Table 12 for the operation of the gas turbine with regards to the exhaust gas temperature for hydrogen and natural gas.

Figure 36 implies a more stable operation with regards to change of TIT and IGV settings for natural gas than for hydrogen.

5.3 Considerations when using hydrogen

Due to the performance data available from the GT MASTER software for the LM2500+G4, much of the comparison so far has revolved around the thermal efficiency, exhaust gas temperature and exhaust gas flow. In this subsection the model for the LM2500+G4 will be used to investigate some of the other parameters significant to the performance of the gas turbine. Other considerations regarding the usage of hydrogen in gas turbines will also be presented and discussed based on the results from the GasTurb model.

5.3.1 NOx-formation

One of the most prominent challenges with the use of hydrogen fuel in gas turbines is the formation of NO_x in the combustion process. It is found that the formation of NO_x is strongly dependant on the TIT. In general there have been implemented three different solutions to decrease the NO_x formation and emissions associated with the operation of gas turbines [19]: dilution of the fuel, exhaust gas removal and premixed combustion. The premixed combustion solution is the most common for turbines running on natural gas. The premixing of the fuel is touched upon in Section 3.1. By premixing the fuel one decreases the stoichiometric flame temperature of the combustion. GasTurb uses an index to represent the likelihood of NO_x-formation, the NO_x *severity parameter* is given by GasTurb in Equation (57).

$$S_{NO_x} = \left(\frac{p_3}{2965kPa}\right)^{0.4} \cdot e^{\frac{T_3-826K}{194K}+\frac{6.29-100war}{53.2}} \tag{57}$$

Equation (57) shows that an increase in temperature and pressure increases the severity for NO_x formation, while an increase in the water to air ratio (war) will lower the NO_x severity index. The severity index for NO_x will only be used as a reference to get a general overview of how the introduction of hydrogen might affect the gas turbine operation. Since the formation of NO_x happens on a molecular level it is very difficult to create an overall equation that accurately predicts the amount of NO_x formed in a combustion process. Therefore the NO_x severity parameter will only serve as an indicator when comparing hydrogen and natural gas. Figure 37 shows a higher NO_x severity index for hydrogen than for natural gas, the NO_x severity parameter decreases with decreasing TIT, which again would result in a lower power output. Hydrogen has a lower ignition temperature and a larger flammability limit than natural gas. The increased reactivity of hydrogen makes it difficult to pre-mix since one could experience ignition between the air and the fuel in unwanted sections of the combustion chamber. The main reason for the increase in NO_x severity index for hydrogen in Figure 37 is the increase in pressure caused by the lower density of the combustion products. Because of the uncertainty revolving around premixing hydrogen, the safest and most sensible solution would be to dilute the hydrogen with either nitrogen or steam. Dilution of the hydrogen would have a direct effect on the exhaust gas temperature. As touched upon earlier the specific heat ratio of a fluid affects the temperature drop. By diluting the hydrogen with steam one would effectively increase the specific heat of the mixture as shown in Figure 23. Steam dilution would increase the enthalpy drop through the turbine but would decrease the specific heat ratio as shown in Figure 32. A larger enthalpy drop would result in a larger power output, but a lower specific heat ratio would result in a higher exhaust gas temperature. When diluting with nitrogen, the specific heat is lowered resulting in a lower power output compared to steam dilution, but the higher specific heat ratio would cause a lower exhaust gas temperature. Due to the already lowered exhaust temperature for hydrogen due to the increased pressure ratio through the turbine it would be beneficial to dilute with steam. When diluting with steam it is possible to raise the exhaust gas temperature so that it correlates with the exhaust gas temperature for natural gas. Matching the exhaust gas temperature profile for the fuels would simplify the operation of the gas turbine in a combined cycle, especially if the combined cycle is designed for natural gas. Therefore, the increased power output associated with steam dilution has to be weighted against matching the exhaust gas temperature profile for natural gas.

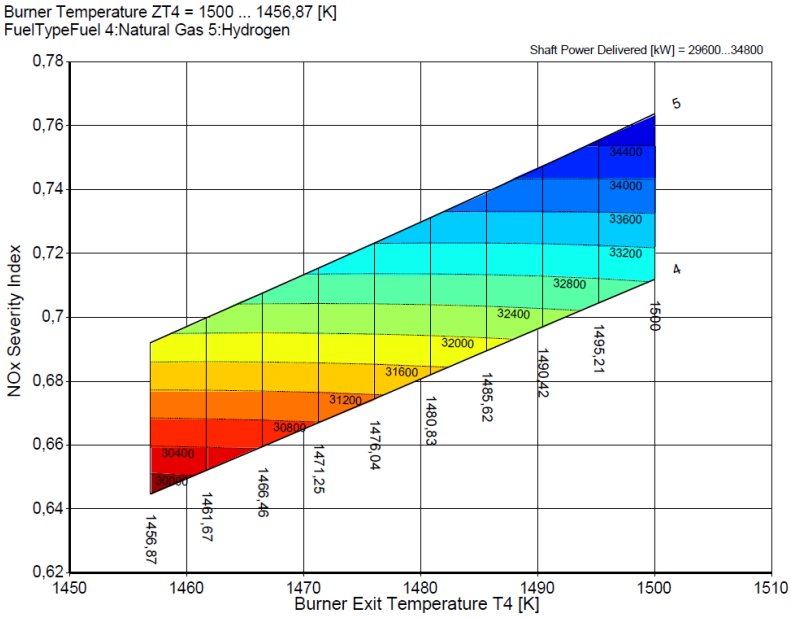

Figure 37: The NO_x severity index for hydrogen (5) and natural gas (4) with shaft power contour lines for the LM2500+G4 model.

5.3.2 TIT-control

One topic that often comes to mind when discussing hydrogen as a fuel is the high temperature associated with burning hydrogen. The high reactivity of hydrogen and oxygen has been discussed, but because of the increased enthalpy drop through the expansion process one would expect the temperature to increase in the turbine blades. Even though the TIT is held constant, the heat transfer and the rate at which heat is produced varies for the two fuels. In this thesis the TIT control has been used as a common denominator to validate the changes in performance between hydrogen and natural gas, but the effects on the turbomachinery caused by the high TIT when switching fuel has not been considered. The energy change due to change in temperature is proportional to the specific heat capacity. A higher specific heat capacity would cause more heat to be transferred when changing the temperature. The combustion products from burning pure hydrogen will therefore have higher heat transfer capabilities than the combustion products associated with natural gas. A proposed average heat-transfer coefficient for the outer side of a turbine blade is presented in Equation (58) [60].

$$\alpha_{out} = 0.285 \frac{(\rho V)^{0.63} c_p^{1/3} \kappa^{2/3}}{D^{0.37} \mu^{0.7}} \tag{58}$$

In Equation (58) μ is the viscosity of the exhaust gas, D is the characteristic length , V is the general stream velocity and κ is the thermal conductivity. The heat transfer coefficient for both CO_2 and H_2O will be evaluated at the burner outlet. CO_2 and H_2O is chosen because they represent the general change in exhaust gas composition when burning natural gas and hydrogen respectively. Figures 19 and 20 are used to extract the temperature and pressure at stage 4 for natural gas and hydrogen. The thermodynamic properties are then found from the Wolfram Alpha database for the respective temperatures and pressures [61]. The characteristic length is assumed to be equal for both cases and will not be included. To validate the thermal properties from WolframAlpha, the thermal properties was cross checked against [62], [63], [57], [52] and the ideal gas law.

$$CO_2\text{: } c_p = 1328 \tfrac{J}{kgK},\ \mu = 5.42 \cdot 10^{-5} Pas,\ \rho = 7.958 \tfrac{kg}{m^3},\ \kappa = 0.1 \tfrac{W}{mK}$$

$$\alpha_{out.CO2} = 241.51 \cdot V^{0.63}$$

$$H_2O\text{: } c_p = 2623 \tfrac{J}{kgK},\ \mu = 5.59 \cdot 10^{-5} Pas,\ \rho = 3.382 \tfrac{kg}{m^3},\ \kappa = 0.169 \tfrac{W}{mK}$$

$$\alpha_{out.H2O} = 245.41 \cdot V^{0.63}$$

The heat transfer coefficient is higher for steam than it is for CO_2 regardless of the velocity. As mentioned one would also expect a velocity increase for steam due to the increased enthalpy drop and lesser density. A higher heat transfer coefficient would cause the turbine blades to absorb more heat. The increased steam formation in the exhaust gas when burning hydrogen will increase the heat transfer properties of the exhaust gas. The increased heat transfer will cause a larger thermal creep/strain on the turbomachinery which again will cause corrosion, thermal barrier coating degradation and fouling [64]. Due to the increased heat transfer associated with hydrogen having the TIT set at $1500K$ for both fuels would not be advisable. This would imply that the LM2500+G4 would need to run on a lower TIT than $1500K$ when switching to hydrogen. The reduction of TIT due to the increased heat transfer associated with hydrogen was addressed in a study by P. Chiesa and G. Lozza [19].

When suggesting a TIT for the LM2500+G4 running on hydrogen one can refer to the heat transfer coefficient for the LM2500+G4 running on natural gas. From Figure 19 one can calculate the heat

transfer coefficient for the CO_2 in the exhaust gas as:

$$\alpha_{out.CO2} = 241.51 \cdot (149.998\frac{m}{s})^{0.63} = 5673.8\frac{W}{m^2 \cdot K}$$

As a reference, the heat transfer coefficient for hydrogen combustion should be lower or equal to $5673.8\frac{W}{m^2 \cdot K}$ to prevent thermal damage to the turbine blades. One way to investigate an alternative TIT for hydrogen combustion would be to look at the power output provided at various TIT's. Figure 38 gives the correlation between power output and TIT, the effects on the exhaust gas temperature is also included due to its significance in a combined cycle.

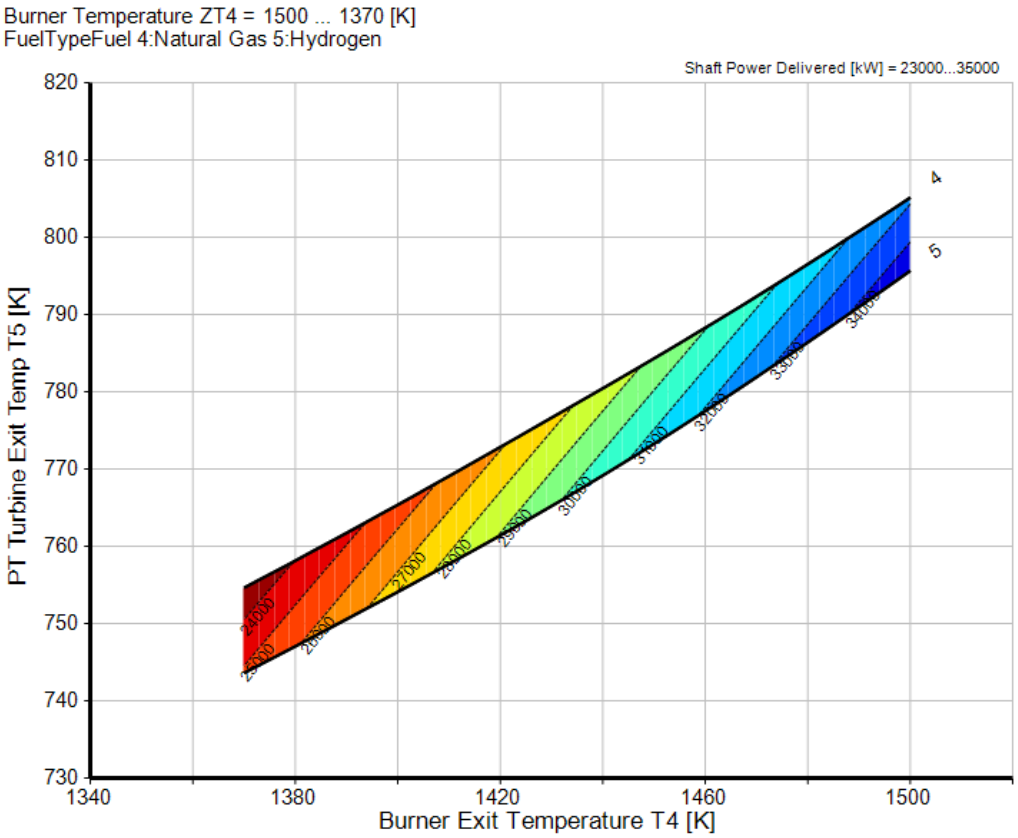

Figure 38: Varying TIT for the LM2500+G4 running on hydrogen (5) and natural gas (4) against the exhaust temperature with power output contours.

To represent the exhaust gas temperature as a function of the TIT with the correlating power output gives a good view of how the choice of fuel influences the system. The power output associated with natural gas at design point ($TIT = 1500K$) can be found for hydrogen combustion at a lower TIT. Matching the power output for hydrogen against the power output for natural gas at design point would provide a lower TIT for hydrogen combustion which would lower the heat transfer coefficient. If one were to lower the TIT for hydrogen to reduce the thermal creep/strain on the turbine one should do it in such a way that some other corresponding parameter matches the base case for natural gas. Having both fuels at the same power output would provide stable operation when switching fuels (if the gas turbine is meant to provide a constant load). Matching the power output for both fuels was done in GasTurb for the LM2500+G4 model as shown in Figure 38. Figure 38 shows a power output of $33000kW$ at design point for natural gas, the same power output is found for hydrogen with a TIT of $1475K$. Running the GasTurb model on hydrogen with a TIT ranging from $1470K$ to $1475K$ the closest match to the power output

at design point for natural gas was found out to be $1470.5K$. From Figure 38 one observes that hydrogen combustion at $1470.5K$ gives an exhaust gas temperature of $782.15K$. The exhaust gas temperature for hydrogen with a $TIT = 1470.5K$ is around $23K$ lower than the exhaust gas temperature for natural gas with a $TIT = 1500K$. If both fuels were using a $TIT = 1500K$ the exhaust gas temperature difference would be lowered ($9.52K$ difference). This implies that if one were to reduce the thermal effects of the turbine blades by lowering the TIT one effectively reduces the exhaust gas temperature which might affect the combined cycle. The blade heat transfer coefficient for hydrogen combustion at $1470.5K$ and $2266.68kPa$ is given as:

The velocity exiting the burner is given from GasTurb as: $V = 150\frac{m}{s}$

The properties for steam is found at $1470.5K$ and $2266.68kPa$ using WolframAlpha [61]:

$$H_2O\text{: } c_p = 2606\frac{J}{kgK},\ \mu = 5.49 \cdot 10^{-5}Pas,\ \rho = 3.341\frac{kg}{m^3},\ \kappa = 0.164\frac{W}{mK}$$

This gives a heat transfer coefficient equal to:

$$\alpha_{out.H2O} = 5666.9\frac{W}{m^2 \cdot K}$$

The heat transfer coefficient for steam at a $TIT = 1470.5K$ is lower than that for CO_2 at a $TIT = 1500K$. This would imply that if the turbine was designed for natural gas with a $TIT = 1500K$ it would be safe to use hydrogen with a $TIT = 1470.5K$ at least with regards to the blade heat transfer coefficient. The specific heat capacity of the gases are of great importance to both the blade heat transfer coefficient and the enthalpy drop through the turbine. In Figure 39 the specific heat capacity for both fuels is presented along with the TIT. From Figure 39 one observes that the specific heat capacity for natural gas combustion at a $TIT = 1500K$ would be equal to the specific heat capacity for hydrogen combustion at around $TIT = 1360K$. The blade heat transfer coefficient for steam at $1360K$ and $1911.593kPa$ is given as:

The velocity exiting the burner is given from GasTurb as: $V = 144.432\frac{m}{s}$

The properties for steam is found at $1360K$ and $1911.593kPa$ using WolframAlpha [61]:

$$H_2O\text{: } c_p = 2542\frac{J}{kgK},\ \mu = 5.1 \cdot 10^{-5}Pas,\ \rho = 3.175\frac{kg}{m^3},\ \kappa = 0.148\frac{W}{mK}$$

This gives a heat transfer coefficient equal to:

$$\alpha_{out.H2O} = 227.8 \cdot 144.432^{0.63} = 5215.7\frac{W}{m^2 \cdot K}$$

Again, the heat transfer coefficient for steam at $1360K$ is lower than the heat transfer coefficient for CO_2 at $1500K$, but now the TIT will be so low that the power output will be severely reduced ($24401.1kW$). To hold the TIT around $1470K$ when using hydrogen would be recommended due to the matching power output with natural gas at a $TIT = 1500K$. The only problem that might occur when using a lower TIT for hydrogen is the even lower exhaust gas temperature. It should be noted that the blade heat transfer coefficient used is only a proposal for capturing the heat transfer in a turbine blade. In a real case the heat transfer would also be dependant on the turbine blade material and the combustion products would be not be exclusive to H_2O and CO_2. The model for the LM2500+G4 in GasTurb is meant to imitate the real gas turbine and due to the

lack of performance data it is reasonable to assume that some of the configurations in the model does not match the actual turbine. However the proposed TIT of $1470K$ when using hydrogen fuel should be considered for the LM2500+G4. The suggested TIT ($1470K$) serves to show that the increased heat transfer qualities of hydrogen combustion products should be considered when changing fuel. As mentioned in Section 2.4 the use of cooling air will not be focused on in this thesis, but its worth noting that the increased heat transfer on the turbine blades when burning hydrogen could be solved by increasing the amount of cooling air on the turbine blades.

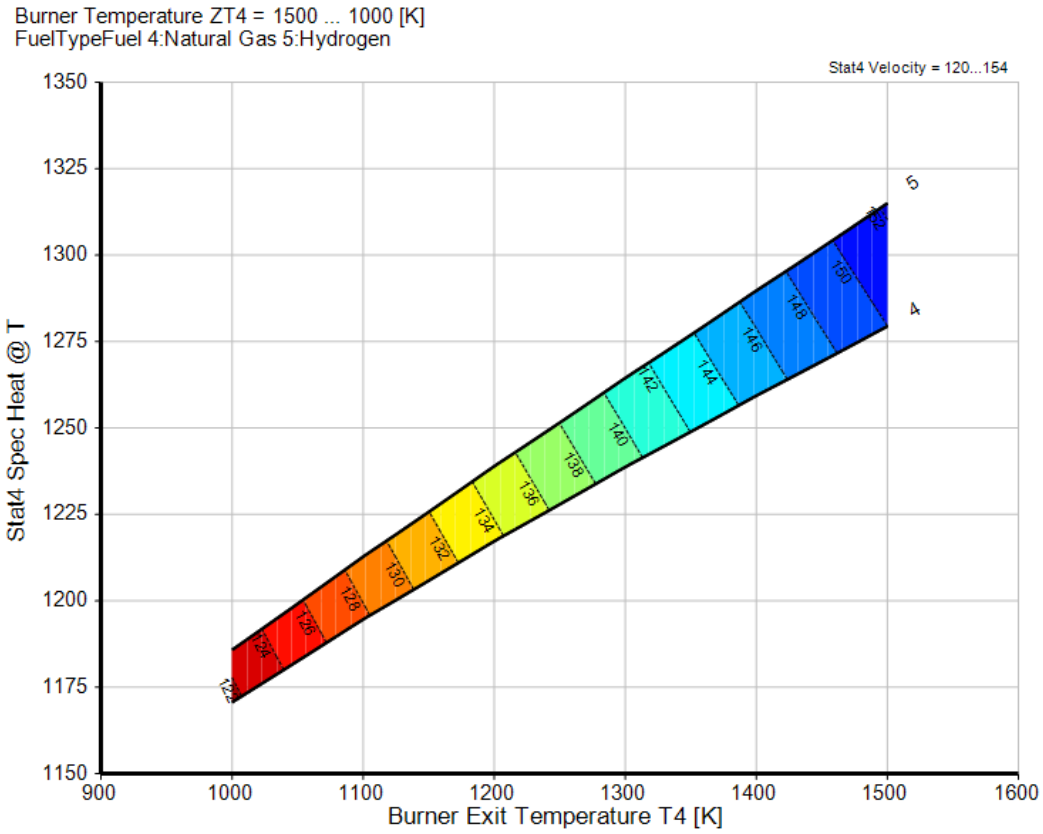

Figure 39: The specific heat for the LM2500+G4 model running on hydrogen(5) and natural gas(4) with regards to varying TIT with velocity contours.

The heat transfer coefficient is also found for the proposed chemical composition of gas turbine exhaust gas presented by V. Ganapathy [50]. In accordance with Section 5.1 the composition given for the gas turbine exhaust gas is: $75\%N_2$, $15\%O_2$, $7\%H_2O$ and $3\%CO_2$ given in volume percent. By converting the volume percent to mass percent and finding the average thermal properties for the exhaust gas one can determine the heat transfer coefficient. The heat transfer coefficient is evaluated at design point for natural gas i.e. $T = 1500K$ and $p = 2267.15kPa$ with an exhaust gas velocity at $V = 149.998\frac{m}{s}$ (from Figure 19). The thermal properties for each constituent is given in Table 13.

Thermal properties of gas turbine exhaust gases					
Gas	**Formula**	$c_p\ [\frac{kJ}{kg \cdot K}]$	$\kappa\ [\frac{W}{mK}]$	$\mu\ [Pa \cdot s]$	$\rho\ [\frac{kg}{m^3}]$
Carbon dioxide	CO_2	1.328	0.1000	$5.42 \cdot 10^{-5}$	7.958
Steam	H_2O	2.622	0.1690	$5.59 \cdot 10^{-5}$	3.275
Nitrogen	N_2	1.248	0.0882	$5.41 \cdot 10^{-5}$	5.064
Oxygen	O_2	1.143	0.0984	$6.41 \cdot 10^{-5}$	5.791

Table 13: Thermal properties of gas turbine exhaust gas constituents at $1500K$ and $2267.15kPa$.

The average thermal properties are given by the mass fractions (X) of the constituents:

$$\bar{\kappa}_{exh.gas} = X_{CO2}\kappa_{CO2} + X_{N2}\kappa_{N2} + X_{O2}\kappa_{O2} + X_{H2O}\kappa_{H2O} = 0.0938\frac{W}{mK}$$

$$\bar{\mu}_{exh.gas} = X_{CO2}\mu_{CO2} + X_{N2}\mu_{N2} + X_{O2}\mu_{O2} + X_{H2O}\mu_{H2O} = 5.578 \cdot 10^{-5} Pa \cdot s$$

$$\bar{c_p}_{exh.gas} = X_{CO2}c_{p.CO2} + X_{N2}c_{p.N2} + X_{O2}c_{p.O2} + X_{H2O}c_{p.H2O} = 1.2927\frac{kJ}{kgK}$$

$$\bar{\rho}_{exh.gas} = X_{CO2}\rho_{CO2} + X_{N2}\rho_{N2} + X_{O2}\rho_{O2} + X_{H2O}\rho_{H2O} = 5.2321\frac{kg}{m^3}$$

The heat transfer coefficient for the turbine blade is then given as:

$$\alpha_{exh.gas} = 4054.9\frac{W}{m^2K}$$

The heat transfer coefficient for the exhaust gas composition given by V. Ganapathy is even lower than $\alpha_{out.CO2}$, this is most likely due to the large fraction of nitrogen and oxygen in the exhaust gas. From $\alpha_{exh.gas}$ one observes that the suggested TIT for hydrogen could actually be an over estimate due to a large portion of the air not reacting with the fuel. The large quantity of air compared to the exhaust gas from the fuels (H_2O and CO_2) would lower the heat transfer coefficient. This implies that it is possible to keep the TIT even closer to $1500K$ when using hydrogen fuel.

5.3.3 Polytropic and isentropic efficiencies

In this thesis the isentropic efficiency for the compressor and the PT was used to match the given performance data from GT MASTER (Section 3.2.1). The change in isentropic and polytropic efficiencies for the ambient temperature change and the part-load study will therefore be presented.

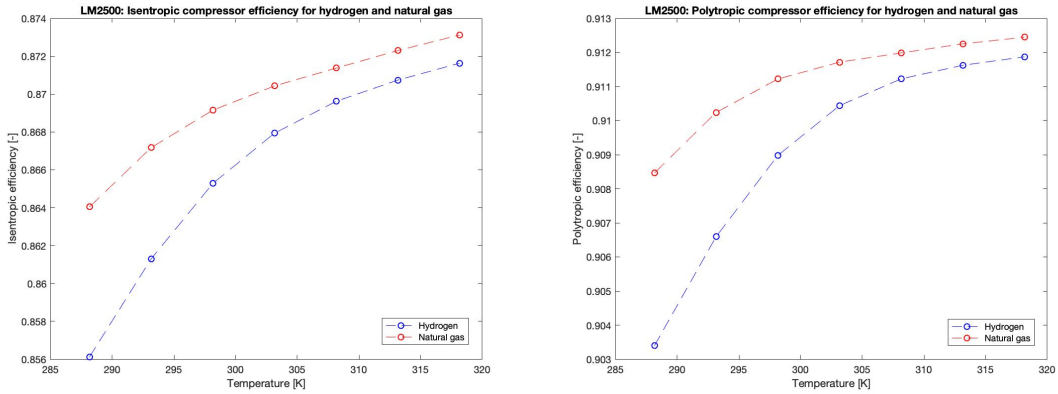

Figure 40: The polytropic and isentropic efficiencies for the compressor with ambient temperature change for hydrogen and natural gas.

Figure 40 shows that both the isentropic and polytropic efficiency seems to increase when increasing the ambient temperature. This is not intuitive since the compressors use less work when the ambient temperature is lowered due to the increased density of the working fluid [51]. One would expect the respective compressor efficiencies to have its peak at the design point i.e. at the set ambient condition ($288.15K$ and $101.325kPa$). The reason for the lower efficiency can be explained by the relation between the individual component efficiencies and the overall cycle efficiency (thermal efficiency). The maximum thermal efficiency decides the relation between the overall thermal energy in the gas turbine cycle and the overall work delivered. Even though the compressor efficiency is an important parameter it is the pressure ratio of the compressor that decides the energy available for the turbines. The efficiency curves presented in Figure 40 might be a little bit misleading since it does not show the full scope of the efficiency curve. In Figure 41 the isentropic compressor efficiency is plotted against the thermal efficiency and the compressor pressure ratio for a larger ambient temperature range. The wider range of ambient temperatures shows that the GasTurb model gives the highest isentropic compressor efficiency when the ambient temperature is approximately $325K$, this implies that the curves in Figure 40 will decrease once the ambient temperature is increased beyond $325K$. The form of the curve in Figure 41 matches that of other isentropic efficiency curves for compressors found in literature [65]. Figure 41 shows that at design point ($288.15K$) the thermal efficiency and the compressor ratio is at their highest, this comes at the cost of a lower compressor efficiency. It is also worth noting that the isentropic efficiency range for the compressor is relatively small (a $37K$ change in ambient temperature would result in a 1% change in compressor efficiency). One way of interpreting the result in Figure 40 is that the usage of hydrogen fuel demands a lower compressor efficiency and would therefore be more flexible in terms of compressor performance, this is most likely due to the increased power output and increased thermal efficiency associated with hydrogen. Another explanation for the lower efficiency for the hydrogen fuel is that the compressor is designed for natural gas combustion (design point), any deviation from the design point (increased mass flow, higher temperature or lower input pressure) would lower the efficiency of the component.

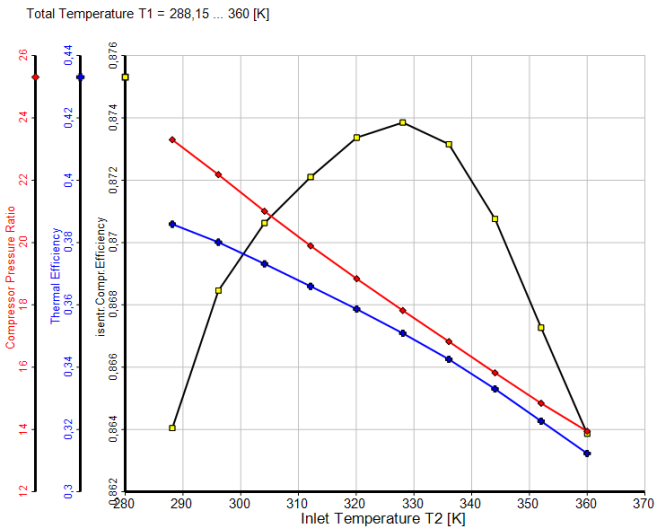

Figure 41: Isentropic compressor efficiency for a wider ambient temperature range for the LM2500+G4 model in GasTurb.

The corresponding isentropic and polytropic effciency for the compressor at part-load is presented in Figure 42. It seems the change in fuel does not cause large differences in the isentropic and polytropic efficiency curves for the compressor at part-load. The higher the load the lower the compressor efficiency. The lowest compressor efficiency is when the LM2500+G4 is operating at full load with hydrogen. The highest compressor efficiency is found around $21000kW$, this is not chosen as the design point due to its lower power output and lower thermal efficiency. The variation in load does not cause a large variation in the compressor efficiency (around 1% drop in efficiency from $16000kW$ to $34000kW$).

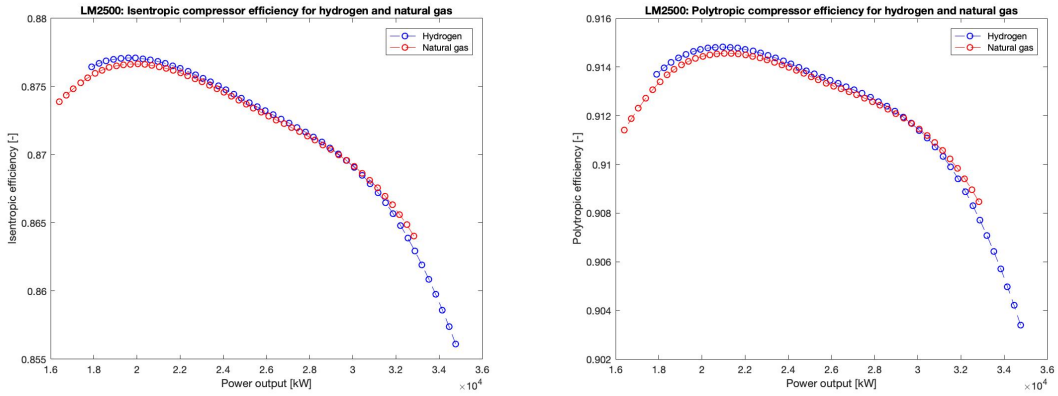

Figure 42: The polytropic and isentropic efficiencies for the compressor running on part-load.

The efficiencies for the HPT with regards to the ambient temperature change is shown in Figure 43. The turbine efficiency displays the opposite behaviour of the compressor, the efficiency decreases with increasing ambient temperature. What is interesting to note is that the hydrogen case has a higher isentropic efficiency than the natural gas case, but a lower polytropic efficiency compared to the natural gas case. The higher isentropic efficiency for the hydrogen case through the turbine would most likely be caused by the increased enthalpy drop due to the exhaust gas composition as discussed. The polytropic efficiency represents the actual compression process, this would imply that the turbine using hydrogen combustion has a better theoretical efficiency (isentropic) than

actual (polytropic) efficiency. The increased pressure ratio when using hydrogen would increase the isentropic efficiency according to Equation (3), but the increase in isentropic efficiency should make for a higher polytropic efficiency given by Equation (6). In general the isentropic efficiency is dependant on the working conditions (the pressure ratio) while the polytropic efficiency is less dependant on the working conditions. Therefore the isentropic efficiency will be a better criteria for evaluating the component efficiencies when changing fuel, this is because the change in fuel directly changes the working conditions. If the working conditions for both fuels were the same the polytropic efficiency would be the preferred efficiency to evaluate.

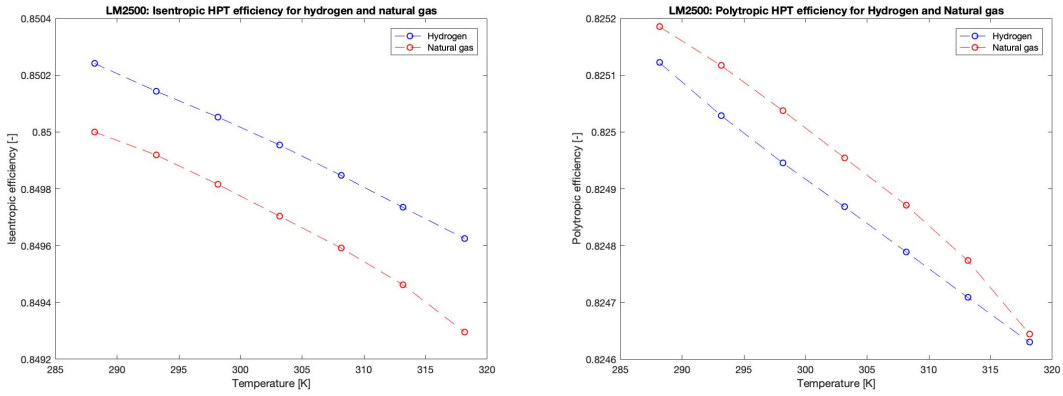

Figure 43: The polytropic and isentropic efficiencies for the HPT with ambient temperature change running on hydrogen and natural gas.

The HPT efficiencies for the LM2500+G4 model running on part-load is given in Figure 44. As for the compressor efficiency at part-load the isentropic and polytropic efficiencies for the HPT seems to decrease with a decrease in load. The polytropic efficiency for the hydrogen case is lower than the natural gas case while the isentropic efficiency is higher for the hydrogen case than for the natural gas case. The general explanation for this phenomenon could be explained by the same reasoning as for the HPT with ambient temperature change. Generally the component efficiencies are not sensitive to the change in load or ambient temperature.

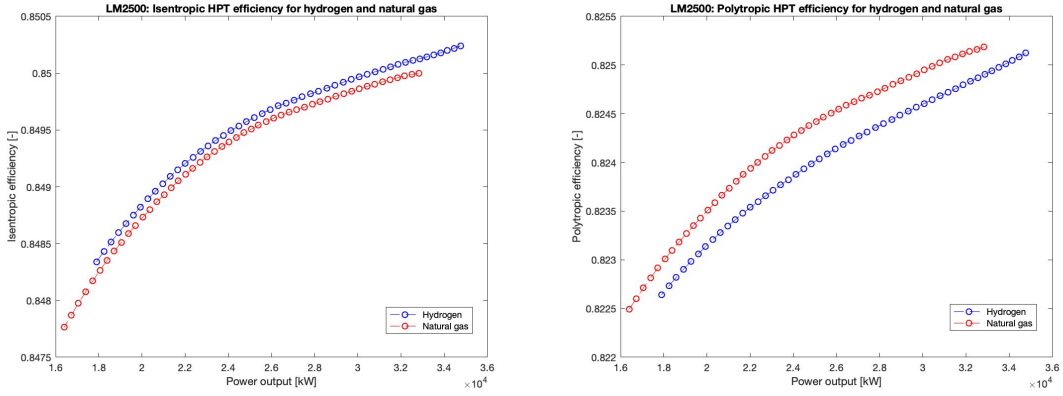

Figure 44: The polytropic and isentropic efficiencies for the HPT running on part-load for hydrogen and natural gas.

The PT is directly influenced by the components upstream of it (compressor and HPT). Similarly for the PT as for the other components the percent change in component efficiencies with regards to ambient temperature change and change in load is small. The natural gas case seems to give

a generally higher PT component efficiency than the hydrogen case when changing the ambient temperature (Figure 45), while at part-load (Figure 46) the efficiencies for hydrogen are slightly higher than for natural gas. These graphs shows that hydrogen fired gas turbines can operate with lower component efficiencies and that the component efficiencies only experience small changes when changing fuel at off-design. There aren't any large changes in the polytropic or isentropic efficiencies when running at off-design, and the outputs of the cycle seems to be influenced by other parameters such as TIT, pressure ratio and exhaust gas temperature. But it is important to acknowledge the component efficiencies as they represent how well the turbomachinery is adapting to changes in the operation of the gas turbine.

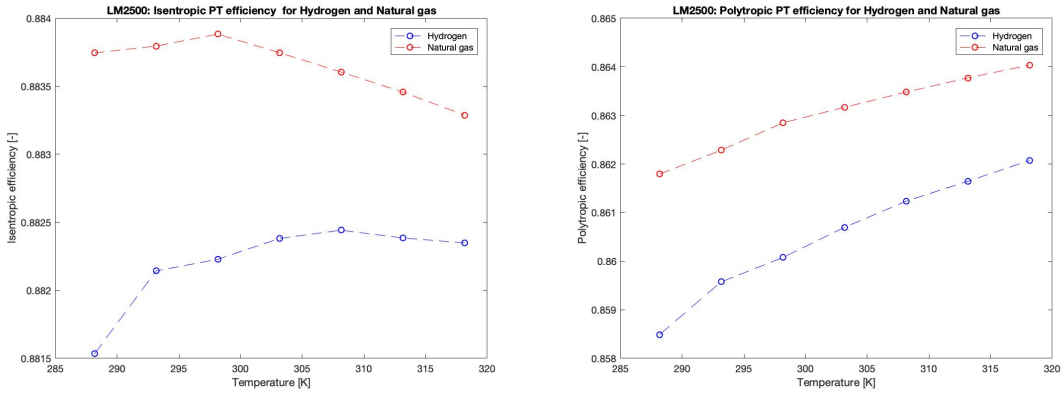

Figure 45: The polytropic and isentropic efficiencies for the PT with ambient temperature change for natural gas and hydrogen.

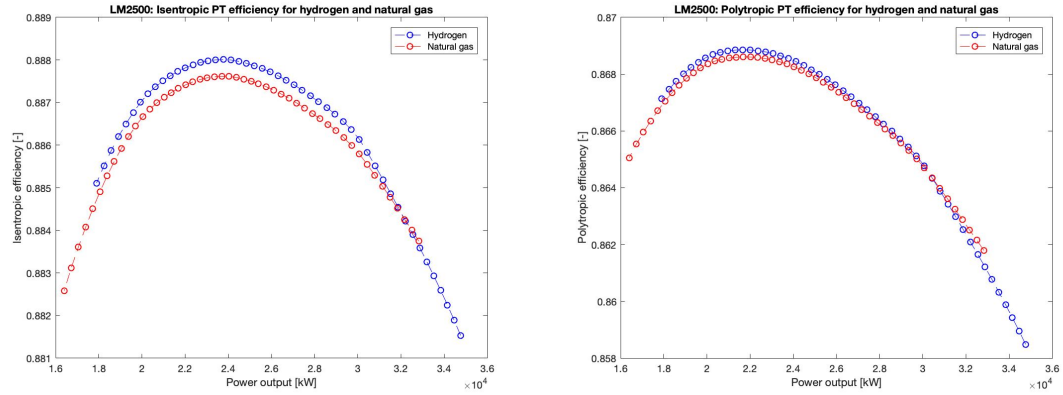

Figure 46: The polytropic and isentropic efficiencies for the PT running on part-load for hydrogen and natural gas.

5.3.4 The combined cycle

As mentioned in previous sections the exhaust gas temperature becomes important when combining the gas turbine with a heat recovery steam generator (HRSG). The exhaust gas produced from the gas turbine generates steam that is used in another turbine to increase the efficiency and power output of the combined cycle. The main components of a HRSG are as follows: economizer, evaporator and superheater. The economizer works as a heat exchanger between the hot exhaust gas from the gas turbine and the water in the HRSG. The water is turned into steam in the evaporator by an external energy source. The wet steam is turned into dry steam by a superheater

that is heating the steam to superheated conditions before it enters the turbine. Due to the increased efficiency the HRSG could be implemented along with the LM2500+G4. The reason for including this section in the discussion is to refer to some of the changes that might affect a combined cycle when introducing hydrogen fuel.

The lower exhaust gas temperature when using hydrogen could pose a problem in the economizer. The low temperature combined with small changes in mass flow would cause less steam generated and depending on the pressure in the economizer could cause the steam to reach its saturation temperature [50]. Some of the options available to avoid steaming in the economizer will be presented:

- Using supplementary firing to increase the steam formation and flow rate of steam through the economizer.
- Using a flow control valve between the economizer and the evaporator. This would cause the economizer to operate closer to the discard pressure of the feed pump which again would cause a higher saturation temperature that will avoid steaming.
- Implementing a bypass on the gas side of the economizer. The bypass would reduce the general duty of the economizer.

All of these options should be considered when firing hydrogen in a combined cycle because of the lower exhaust gas temperature as shown in Figures 31 and 33. Another option is to specifically design the HRSG to match hydrogen combustion. The efficiency for the HRSG would be lower due to less heat being introduced in the economizer when using hydrogen. The lower heat extraction is caused by larger power extraction in the turbines caused by the increased enthalpy drop for hydrogen combustion. One could argue that the increased efficiency and power output when burning hydrogen in a gas turbine would make up for the eventual decrease in efficiency and power output in a combined cycle.

For the HES-OFF project the LM2500+G4 is meant to work in a combined cycle offshore. In offshore applications space is of great importance as mentioned in Section 3.1, therefore the HRSG connected to the LM2500+G4 needs to be compact. One solution is to use a once-through heat recovery steam generator (OTSG). An OTSG combines the economizer, evaporator and superheater into one unit, this negates the problem of steaming in the economizer. As far as the author is aware, specific data for the HRSG is not defined. Due to the limited time on this thesis, the efficiency and workings of the combined cycle will not be included. The inclusion of an OTSG motivates further work regarding the performance of hydrogen combustion systems.

5.3.5 Surge Margin

The surge margin at part-load is shown in Figure 47 in terms of the total engine mass flow and the compressor spool speed (HPC spool speed) for natural gas (4) and hydrogen fuel (5). From an operational standpoint one observes that the surge margin decreases when the inlet mass flow and compressor spool speed increases. For a given mass flow rate GasTurb calculates the surge margin higher when using hydrogen than natural gas. Since the surge margin is a representation of the distance between the current operating point and the surge line, one would not expect the margin for surge to be accurate for a physical turbine. Since the GasTurb model is based on a generic two-spool gas turbine provided by the software the surge margin presented would be expected to deviate from the actual gas turbine. There are also uncertainties connected to the occurrence of surge as mentioned in Section 2.7. Therefore the surge margin presented in GasTurb should be

viewed as more of a reference than certain value. Even though the values might be incorrect, the scaling and change in surge margin with regards to the engine mass flow should be considered.

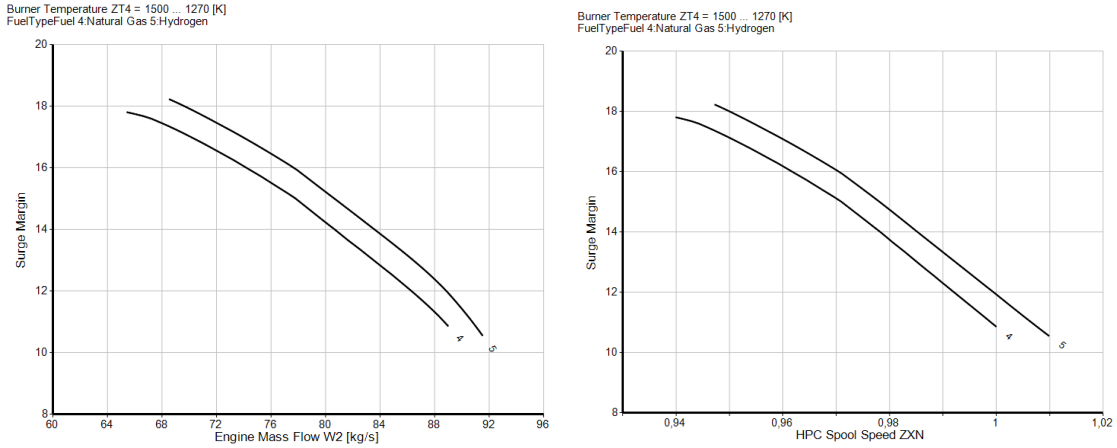

Figure 47: The surge margin with regards to mass flow and relative compressor spool speed for both natural gas (4) and hydrogen (5).

One explanation to Figure 47 would be the increase of angle of attack and the increased blade stall. Since the only component at fixed speed is the PT ($3600rpm$), this implies that the compressor speed depends on the mass flow of air entering. At a constant mass flow rate (defined by Equation (29)) one can assume that decreasing the blade speed would lower the angle of attack and therefore increase the surge margin. This explanation might describe the plots in Figure 47. The increased mass flow entering the compressor due to the higher enthalpy drop through the turbines when using hydrogen fuel, causes the velocity triangle to shift and the angle of attack to decrease. This reasoning might explain why the surge margin is higher for hydrogen than for natural gas at part-load.

5.3.6 Operating line

Earlier in the thesis the compressor and turbine maps have been mentioned with regards to how the surge line is constructed (Section 2.7) and how the on and off-design point change when changing the fuel (Section 5.1.1). The off-design point is merely one point in the operating line. The theory presented in Section 2.6 will be used to analyze the difference when changing fuel. The operating lines for the HPT, PT and compressor are presented in Figure 48 for natural gas ( ) and hydrogen ( ).

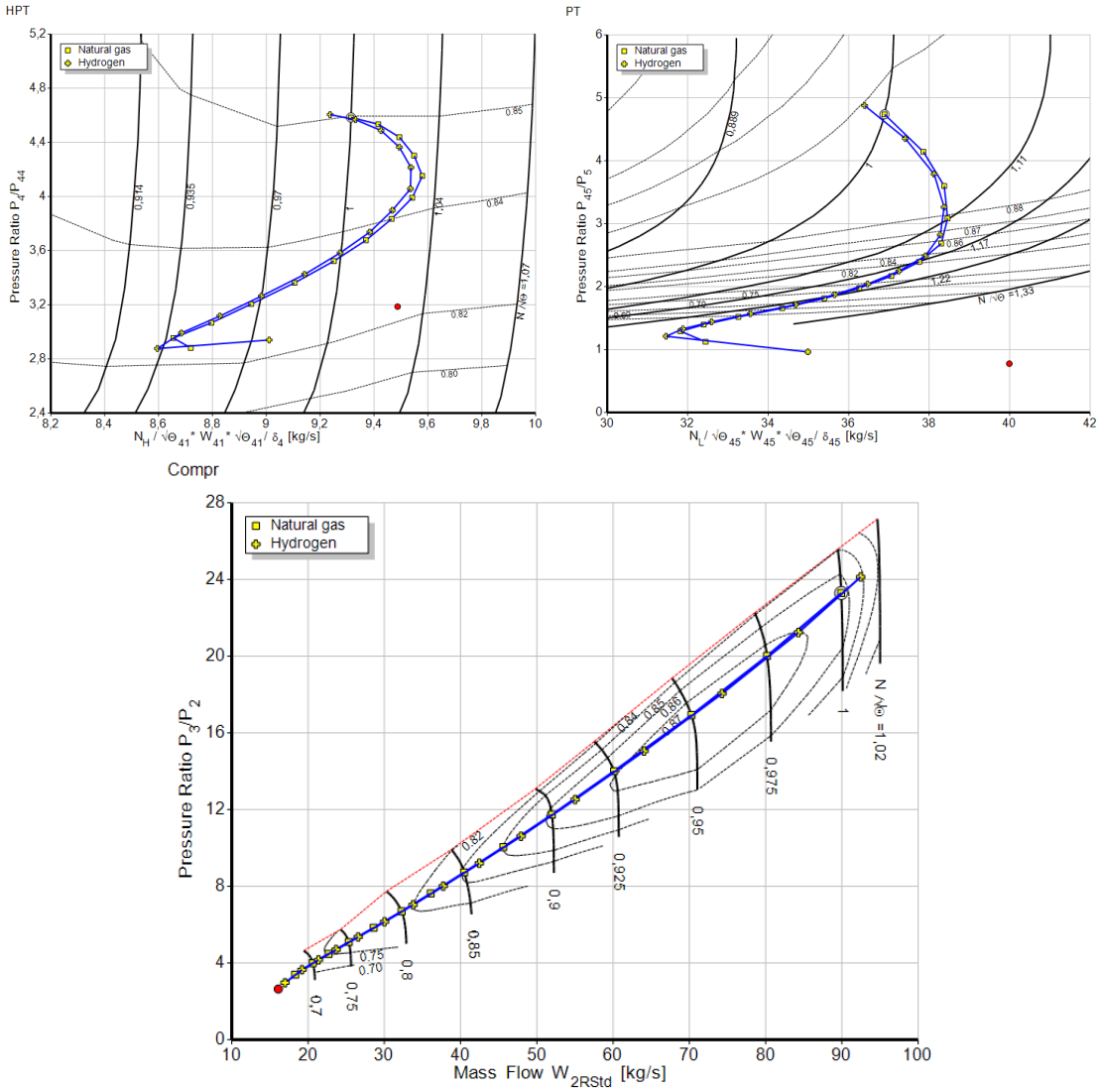

Figure 48: The operating lines for the compressor, HPT and PT of a LM2500+G4 running on natural gas and hydrogen.

The operating lines for the compressor seems to correlate with each other regardless of the fuel. The difference is found at the end points of the operating line. As mentioned in Section 5.1.1, the operating line is shifted more up to the left, meaning a higher pressure ratio and a slightly higher mass flow at $1500K$. The TIT is fixed and visualized by the operating line following an imaginary TIT-line referenced to in Figure 4. The shift in operating line for hydrogen is due to the increased turbine power upstream of the compressor, that forces more air and higher pressure ratio's through the compressor. From Equation (14) one can observe that an increase in mass flow will increase the pressure ratio. This is observed from the compressor map with regards to the relative corrected spool speed increasing ($N/\sqrt{\Theta}$) when using hydrogen due to the connection between spool speed for the HPT and compressor given by Equation (19). This indifference propagates to low mass flows as well, where one observes that the natural gas operates at lower mass flow and pressure ratio at the same TIT.

The maps for both the HPT and PT have been zoomed in on to capture the slight changes when switching fuels. At low power output and low pressure ratio the HPT operating line starts at

a high mass flow that is decreasing with a decreasing pressure ratio. From the HPT operating line one observes that the gas turbine is increasing the spool speed and mass flow along with the increasing pressure ratio. The pressure ratio is defined as $\frac{p_4}{p_{44}}$, so an increase in pressure ratio for the HPT implies a higher turbine inlet pressure which is due to a higher TIT. This relation correlates with Equation (24). At a pressure ratio around 4.2, the product of corrected speed and mass flow seems to decrease while still increasing the pressure ratio. One observes that the HPT operating line for natural gas curves slightly more to the right than the operating line for hydrogen. Equation (24) gives a correlation between turbine pressure ratio, TIT and mass flow rate. Due to the lower heating value and smaller enthalpy drop trough a turbine when using natural gas, the system would need a larger mass flow to give the same pressure ratio compared to using hydrogen. The HPT operating line for hydrogen extends longer than the operating line for natural gas due to the increased specific heat capacity of the exhaust gases when burning hydrogen. A similar curve is observed for the PT map. The red dot on all of the maps is a point that has not converged, this might be caused by inaccuracies in the GasTurb model.

Overall the operating lines in the component maps for hydrogen and natural gas combustion exhibit similar behaviour, with slight changes. From an operational point of view this would mean that the change of fuel will not influence the overall behaviour of the gas turbine significantly. Control options such as IGV control and TIT control needs to be altered when switching to hydrogen to match the outputs for natural gas. The surge margin that was discussed in Section 2.7 does not change greatly when switching fuels and by GasTurb's definition the margin slightly increases when using hydrogen. This implies that there is no need to significantly alter the operation lines for the different component maps in terms of bleeding air or implementing speed control.

6 Conclusion and further work

The present thesis has presented and investigated some of the changes in specified performance parameters for an aeroderivative gas turbine using hydrogen fuel. This has been done by creating a model of a LM2500+G4 in the software GasTurb. The GasTurb model has been verified against known data for the specific turbine running on natural gas at design point and off-design. The parameters used for verifying the GasTurb model are the power output, thermal efficiency, exhaust gas temperature and exhaust mass flow. The GasTurb model created for the LM2500+G4 correlates with the external data provided for a LM2500+G4 at design point. At off-design point, two scenarios where presented based on available data, namely ambient temperature change and part-load performance. Running the model with ambient temperature change gives good a correlation with the external data, with the MAPE for each parameter lying under one percent. The model is then altered giving a slightly higher MAPE for the power output, but a more plausible compressor efficiency. For the part-load performance TIT and IGV-control is used to operate the turbine. Without variable geometry for the IGV's the exhaust gas temperature deviates from the external data, while the power output, thermal efficiency and exhaust mass flow gives a good correlation. Due to the importance of a reliable exhaust gas temperature profile in a combined cycle, the variable geometry for the IGV's was implemented to specifically match the exhaust gas temperature from the external data. An optimal IGV angle was found for each part-load data point with regards to the exhaust gas temperature from the external data. With variable IGV's the total MAPE was found to be lowered for all parameters except the exhaust gas flow. Having received satisfactory results from verifying the model, the fuel was changed to hydrogen.

From the simulation results it was observed a 5.1% increase in power output for hydrogen fuel compared to natural gas at the same TIT. This was deduced to be due to the composition of the exhaust gas from burning hydrogen having a higher specific heat and creating a higher enthalpy

drop during the expansion. The increase in power output for hydrogen could also be explained by the higher volumetric flow rate due to the lower energy density of hydrogen. Along with the lesser energy density of hydrogen, the lesser density of the combustion products when using hydrogen would cause a higher velocity and spool speed. The increased velocity for hydrogen was found to increase the mechanical energy extracted giving a higher thermal efficiency than for natural gas. For a TIT at $1500K$ the thermal efficiency increased by 3.95% when switching from natural gas to hydrogen. Because of the high FHV for hydrogen one will require less hydrogen to produce the same amount of power compared to the amount of natural gas needed.

With the TIT at $1500K$ the exhaust gas temperature was found to decrease by 0.64% when changing from natural gas to hydrogen fuel. The decrease in exhaust gas temperature for hydrogen is most likely influenced by the increased volumetric flow rate which would cause a higher pressure ratio through the turbines. The higher specific heat ratio for H_2O compared to CO_2 could also cause a decrease in exhaust gas temperature for hydrogen combustion. The changes in outputs when switching fuel at a $TIT = 1500K$ seems to carry over when operating at off-design for ambient temperature change and part-load.

With ambient temperature change the general increase in power output and thermal efficiency is found to be 7.8% and 4% for hydrogen compared to natural gas, while the exhaust gas temperature is decreased by 1.4%. These changes are similar when running at part-load. The part-load simulations gave a general decrease of 1.4% for the exhaust gas temperature when using hydrogen compared to natural gas, while the thermal efficiency was observed to increase by 4.2% when switching fuel. No notable change was observed for the power output at part-load since the power output was fixed for both natural gas and hydrogen. Variable IGV angles was implemented to match the exhaust gas temperature when running at part-load. The IGV settings found for the natural gas case was implemented when using hydrogen fuel, it was found that the IGV settings would need to be changed when switching fuels. The IGV angles set for natural gas needs to be decreased when using hydrogen in order to match the given exhaust gas temperature profile.

The NO_x formation is more severe when changing from natural gas to hydrogen due to the high reactivity and high flame speed. Premixing the fuel with air is not an option because of the high chance of spontaneous ignition. A more realistic and sensible approach to reduce the formation of NO_x would be to dilute the hydrogen with either steam or nitrogen. Due to steam having a lower specific heat ratio than nitrogen it would be beneficial to dilute with steam to match the exhaust gas temperature profile for the gas turbine running on natural gas. Nitrogen dilution would be better in terms of matching the natural gas power output (due to a lower specific heat capacity), but this would result in an even lower exhaust gas temperature (due to a higher specific heat ratio).

The thermodynamic properties of the exhaust gas for hydrogen and natural gas combustion is evaluated against a proposed equation for the turbine blade heat transfer coefficient. The exhaust gas produced from hydrogen (H_2O) has better heat transfer properties than the exhaust gas produced from natural gas (CO_2). The increased heat transferring properties of H_2O might damage the turbine blades if hydrogen where to be burned at the maximum TIT ($1500K$). By matching the power output for hydrogen against the power output for natural gas at design point a firing temperature of $1470K$ is proposed for hydrogen.

The polytropic and isentropic efficiencies are evaluated for the compressor, HPT and PT. The component efficiencies are found to be insensitive towards change in load and ambient temperature. The surge margin is found to be slightly higher for natural gas than for hydrogen, but the uncertainty regarding surge should be investigated further. The operating lines for the compressor, HPT and PT are similar for both fuels. The operating lines for hydrogen is shifted slightly due to the higher pressure ratio associated with the increased volumetric flow rate. Overall, the im-

plementation of hydrogen as fuel does not seem to cause any major changes to the parameters investigated, and from an operational point of view both fuels behave similarly. However, extra precautions needs to be taken when incorporating hydrogen fuel due to high flammability and various combustion characteristics. From this work the following objectives have been met:

- Determination of the two spool gas turbine performance in the GasTurb software have been done by defining the term *gas turbine performance* and evaluate the corresponding parameters from the software up against external data.
- Gas turbine performance benchmarking for natural gas and hydrogen fuel are presented with regards to the selected parameters and the results and variations when changing the fuel are discussed.
- The analyses done are linked towards a specific gas turbine model namely the LM2500+G4.

These results and fulfillment of objectives are of course dependant on the accuracy of the GasTurb model and the scope set by the thesis. To gain a more detailed analysis of the effects and challenges related to hydrogen combustion in gas turbines one needs to study the individual components. The development of new technology is also linked to the topic, due to much of the implementation being in the research phase.

The current thesis presents several topics that could be studied further. It would be interesting to study what implications the combined cycle has on the LM2500+G4 performance when implementing hydrogen fuel. Due to ammonia and hydrogen having similar chemical properties the introduction of ammonia as a fuel should also be investigated. Other ways of controlling the turbine when switching fuels would also be interesting to look at (speed control, inlet throttling, discharge throttling and re-circulation). Using a different simulation tool to model a LM2500+G4 could also be done to verify the model for the LM2500+G4 in GasTurb. In correlation to the HES-OFF project the performance of a LM6000 PF running on hydrogen should also be studied further.

Bibliography

[1] F. Landis. (2008). 'Gas-turbine engine'. https://www.britannica.com/technology/gas-turbine-engine , (accessed: 09.08.2020).

[2] GasTurb, *GasTurb 13*, https://www.gasturb.de/download.html, (accessed: 2020).

[3] D. Robb. (2017). 'Aeroderivative gas turbines'. https://www.turbomachinerymag.com/view/aeroderivative-gas-turbines , (accessed: 02.05.2021).

[4] L. Riboldi, E. F. Alves, M. Pilarczyk, E. Tedeschi and L. O. Nord, 'Optimal design of a hybrid energy system for the supply of clean and stable energy to offshore installations', *Frontiers in Energy Research*, vol. 8, p. 346, 2020, ISSN: 2296-598X. DOI: 10.3389/fenrg.2020.607284. [Online]. Available: https://www.frontiersin.org/article/10.3389/fenrg.2020.607284.

[5] Norwegian Petroleum directorate. (2020). 'Emissions to air'. https://www.norskpetroleum.no/en/environment-and-technology/emissions-to-air/, (accessed: 24.05.2021).

[6] Y. Koç, H. Yağlı, A. Görgülü and A. Koç, 'Analysing the performance, fuel cost and emission parameters of the 50 mw simple and recuperative gas turbine cycles using natural gas and hydrogen as fuel', *International Journal of Hydrogen Energy*, vol. 45, no. 41, pp. 22 138–22 147, 2020, ISSN: 0360-3199. DOI: https://doi.org/10.1016/j.ijhydene.2020.05.267. [Online]. Available: http://www.sciencedirect.com/science/article/pii/S0360319920321248.

[7] U.S. Energy Information Administration. (2020). 'Hydrogen explained'. https://www.eia.gov/energyexplained/hydrogen/production-of-hydrogen.php, (accessed: 08.12.2020).

[8] H. Sayyaadi, 'A conceptual design of a dual hydrogen-power generation plant based on the integration of the gas-turbine cycle and copper chlorine thermochemical plant', *International Journal of Hydrogen Energy*, vol. 42, no. 48, pp. 28 690–28 709, 2017, ISSN: 0360-3199. DOI: https://doi.org/10.1016/j.ijhydene.2017.09.070. [Online]. Available: http://www.sciencedirect.com/science/article/pii/S0360319917336984.

[9] I. L. Drell and F. E. Belles, 'Survey of hydrogen combustion properties', 1958.

[10] A. Valera-Medina, S. Morris, J. Runyon, D. Pugh, R. Marsh, P. Beasley and T. Hughes, 'Ammonia, methane and hydrogen for gas turbines', *Energy Procedia*, vol. 75, pp. 118–123, 2015, Clean, Efficient and Affordable Energy for a Sustainable Future: The 7th International Conference on Applied Energy (ICAE2015), ISSN: 1876-6102. DOI: https://doi.org/10.1016/j.egypro.2015.07.205. [Online]. Available: https://www.sciencedirect.com/science/article/pii/S187661021500973X.

[11] P. Gobbato, M. Masi, A. Toffolo and A. Lazzaretto, 'Numerical simulation of a hydrogen fuelled gas turbine combustor', *International Journal of Hydrogen Energy*, vol. 36, no. 13, pp. 7993–8002, 2011, Hysydays, ISSN: 0360-3199. DOI: https://doi.org/10.1016/j.ijhydene.2011.01.045. [Online]. Available: https://www.sciencedirect.com/science/article/pii/S0360319911000875.

[12] N. Tekin, M. Ashikaga, A. Horikawa and H. Funke, 'Enhancement of fuel flexibility of industrial gas turbines by development of innovative hydrogen combustion systems', *Gas Energy*, vol. 2, pp. 18–23, 2018.

[13] M. Gazzani, P. Chiesa, E. Martelli, S. Sigali and I. Brunetti, 'Using hydrogen as gas turbine fuel: Premixed versus diffusive flame combustors', *Journal of engineering for gas turbines and power*, vol. 136, no. 5, 2014.

[14] D. M. Todd *et al.*, 'Demonstrated applicability of hydrogen fuel for gas turbines', 2000.

[15] M. Moliere, N. Hugonnet and G. Energy, 'Hydrogen-fuelled gas turbines: Experience and prospects', *Power-Gen Asia*, 2004.

[16] R. Sierens and E. Rosseel, 'Variable Composition Hydrogen/Natural Gas Mixtures for Increased Engine Efficiency and Decreased Emissions ', *Journal of Engineering for Gas Turbines and Power*, vol. 122, no. 1, pp. 135–140, Jul. 1999, ISSN: 0742-4795. DOI: 10.1115/1.483191. eprint: https://asmedigitalcollection.asme.org/gasturbinespower/article-pdf/122/1/135/5547904/135_1.pdf. [Online]. Available: https://doi.org/10.1115/1.483191.

[17] NCCS - Norwegian CCS Research. (2019). 'Hydrogen-firing of gas turbines'. https://www.sintef.no/projectweb/nccs/annual-report-2019/nccs-2019-case-c-hydrogen-firing-of-gas-turbines-task-5/, (accessed: 26.05.2021).

[18] General Electric. (2021). 'Hydrogen fueled gas turbine'. https://www.ge.com/gas-power/future-of-energy/hydrogen-fueled-gas-turbines, (accessed: 26.05.2021).

[19] P. Chiesa, G. Lozza and L. Mazzocchi, 'Using hydrogen as gas turbine fuel', *Journal of Engineering for Gas Turbines and Power-transactions of The Asme - J ENG GAS TURB POWER-T ASME*, vol. 127, Jan. 2005. DOI: 10.1115/1.1787513.

[20] F. Haglind and R. Singh, 'Design of aero gas turbines using hydrogen', 2006.

[21] 'Index', in *Modern Gas Turbine Systems*, ser. Woodhead Publishing Series in Energy, P. Jansohn, Ed., Woodhead Publishing, 2013, pp. 791–816, ISBN: 978-1-84569-728-0. DOI: https://doi.org/10.1533/9780857096067.backmatter. [Online]. Available: https://www.sciencedirect.com/science/article/pii/B9781845697280500215.

[22] H. Cohen, G. F. C. Rogers and H. I. H. Saravanamuttoo, *Gas turbine theory*. Longman, 1972.

[23] G. Rogers and Y. Mayhew, *Engineering Thermodynamics: Work and Heat Transfer, 4th Edition*. Pearson, 1992.

[24] A. Razak, '11 - gas turbine performance modelling, analysis and optimisation', in *Modern Gas Turbine Systems*, ser. Woodhead Publishing Series in Energy, P. Jansohn, Ed., Woodhead Publishing, 2013, pp. 423–514, ISBN: 978-1-84569-728-0. DOI: https://doi.org/10.1533/9780857096067.3.423. [Online]. Available: https://www.sciencedirect.com/science/article/pii/B9781845697280500112.

[25] R. Bhaskar and A. Pradeep, *Jet aircraft propulsion*, https://nptel.ac.in/content/storage2/courses/101101002/downloads/Lect-25.pdf, (accessed: 06.12.2020).

[26] Y. Lee, S. Teramoto and K. Okamoto, 'Prediction of profile losses in an axial compressor cascade using large eddy simulation', Nov. 2019.

[27] J. M. Schultz, 'The polytropic analysis of centrifugal compressors', 1962.

[28] L. Bakken, *Thermodynamics, compression and expansion processes*, Compendium TEP04 Gas Turbines and Compressors, 2020.

[29] J. Kurzke and GasTurb GmbH. (2018). 'GasTurb 13'. https://www.gasturb.de/Downloads/Manuals/GasTurb13.pdf, (accessed: 07.12.2020).

[30] J. Kurzke and I. Halliwell, 'Understanding off-design behavior', in. May 2018, pp. 577–610, ISBN: 978-3-319-75977-7. DOI: 10.1007/978-3-319-75979-1_13.

[31] J. Kurzke, 'Achieving maximum thermal efficiency with the simple gas turbine cycle', *MTU Aero Engines, Dachauer Str*, vol. 665, p. 80 995, 2003.

[32] T. Wang, '15 - the gas and steam turbines and combined cycle in igcc systems', in *Integrated Gasification Combined Cycle (IGCC) Technologies*, T. Wang and G. Stiegel, Eds., Woodhead Publishing, 2017, pp. 497–640, ISBN: 978-0-08-100167-7. DOI: https://doi.org/10.1016/B978-0-08-100167-7.00028-7. [Online]. Available: https://www.sciencedirect.com/science/article/pii/B9780081001677000287.

[33] V. V. N. K. S. Koyyalamudi and Q. H. Nagpurwala, 'Stall margin improvement in a centrifugal compressor through inducer casing treatment', *International Journal of Rotating Machinery*, vol. 2016, p. 2 371 524, Apr. 2016, ISSN: 1023-621X. DOI: 10.1155/2016/2371524. [Online]. Available: https://doi.org/10.1155/2016/2371524.

[34] SKYbrary. (2020). 'Stall'. https://www.skybrary.aero/index.php/Stall , (accessed: 10.05.2021).

[35] M. Noor, A. Wandel and T. Yusaf, 'The development of mild combustion open burner experimental setup', Jul. 2013.

[36] J. Backman and J. Kaikko, '7 - microturbine systems for small combined heat and power (chp) applications', in *Small and Micro Combined Heat and Power (CHP) Systems*, ser. Woodhead Publishing Series in Energy, R. Beith, Ed., Woodhead Publishing, 2011, pp. 147–178, ISBN: 978-1-84569-795-2. DOI: https://doi.org/10.1533/9780857092755.2.147. [Online]. Available: https://www.sciencedirect.com/science/article/pii/B9781845697952500076.

[37] M. Escudier and T. Atkins, *A Dictionary of Mechanical Engineering (2 ed.)* Oxford University Press, 2019.

[38] *Dry Low Emissions Combustor Development*, vol. Volume 3: Coal, Biomass and Alternative Fuels; Combustion and Fuels; Oil and Gas Applications; Cycle Innovations, Turbo Expo: Power for Land, Sea, and Air, V003T06A027, Jun. 1998. DOI: 10.1115/98-GT-310. eprint: https://asmedigitalcollection.asme.org/GT/proceedings-pdf/GT1998/78644/V003T06A027/2411197/v003t06a027-98-gt-310.pdf. [Online]. Available: https://doi.org/10.1115/98-GT-310.

[39] Forecast International. (2010). 'The market for gas turbine marine engines'. https://www.forecastinternational.com/samples/F649_CompleteSample.pdf, (accessed: 28.05.2021).

[40] C. E. Neilson, 'LM2500 gas turbine modifications for biomass fuel operation', *Biomass and Bioenergy*, vol. 15, no. 3, pp. 269–273, 1998, ISSN: 0961-9534. DOI: https://doi.org/10.1016/S0961-9534(98)00021-X. [Online]. Available: https://www.sciencedirect.com/science/article/pii/S096195349800021X.

[41] Thermoflow Inc., *GT MASTER ®*, https://www.thermoflow.com/index.html, (accessed: 2020).

[42] GE Aviation. (2021). 'The LM2500+G4 Engine'. https://www.geaviation.com/marine/engines/military/lm2500-plus-g4, (accessed: 22.02.2020).

[43] E. Lemmon, M. Huber and M. McLinden, *Nist standard reference database 23: Reference fluid thermodynamic and transport properties-refprop, version 9.1*, en, May 2013. [Online]. Available: https://tsapps.nist.gov/publication/get_pdf.cfm?pub_id=912382.

[44] M. J. Moran and H. N. Shapiro, *Fundamentals of engineering thermodynamics*, 6th ed. John Wiley and Sons Inc., New York, NY, 2009. [Online]. Available: http://eu.wiley.com/WileyCDA/WileyTitle/productCd-0470540192.html.

[45] S. Ebigenibo and N. Promise, 'Off-design performance analysis of gas turbines', *Global Journal of Engineering and Technology Advances*, vol. 4, p. 4, Aug. 2020. DOI: 10.30574/gjeta.2020.4.2.0046.

[46] J. Kurzke and I. Halliwell, 'Spreadsheet calculations', in. May 2018, pp. 619–637, ISBN: 978-3-319-75977-7. DOI: 10.1007/978-3-319-75979-1_15.

[47] Q. Xin, '4 - fundamentals of dynamic and static diesel engine system designs', in *Diesel Engine System Design*, Q. Xin, Ed., Woodhead Publishing, 2013, pp. 299–347, ISBN: 978-1-84569-715-0. DOI: https://doi.org/10.1533/9780857090836.2.299. [Online]. Available: http://www.sciencedirect.com/science/article/pii/B9781845697150500042.

[48] E. Tsoutsanis, Y.-G. Li, P. Pilidis and M. Newby, 'Part-load performance of gas turbines – part i: A novel compressor map generation approach suitable for adaptive simulation', Dec. 2012. DOI: 10.1115/GTINDIA2012-9580.

[49] U.S. Environmental Protection Agency Combined Heat and Power Partnership. (2015). 'Catalog of chp technologies'. https://www.epa.gov/sites/production/files/2015-07/documents/catalog_of_chp_technologies_section_3._technology_characterization_-_combustion_turbines.pdf, (accessed: 26.05.2021).

[50] V. Ganapathy, *Steam Generators and Waste Heat Boilers: For Process and Plant Engineers*. Oct. 2014, pp. 1–496, ISBN: 9780429159329. DOI: 10.1201/b17519.

[51] K. Brun and R. Kurz. (2019). 'In what all ways ambient temperature affects performance of gas turbines'. https://www.turbomachinerymag.com/view/in-what-all-ways-ambient-temperature-affects-performance-of-gas-turbines , (accessed: 28.04.2021).

[52] B. G. Kyle, *Chemical and Process Thermodynamics*. Prentice-Hall, 1984.

[53] S. L. Dixon, 'Chapter 4 – axial-flow turbines: Mean-line analysis and design', 2010.

[54] S. S. Rashwan, I. Dincer, A. Mohany and B. G. Pollet, 'The sono-hydro-gen process (ultrasound induced hydrogen production): Challenges and opportunities', *International Journal of Hydrogen Energy*, vol. 44, no. 29, pp. 14 500–14 526, 2019, ISSN: 0360-3199. DOI: https://doi.org/10.1016/j.ijhydene.2019.04.115. [Online]. Available: https://www.sciencedirect.com/science/article/pii/S0360319919315447.

[55] National Aeronatics and Space Administration: Nancy Hall, *Isentropic compression (or expansion)*, https://www.grc.nasa.gov/www/k-12/airplane/compexp.html, Accessed: 2021–04-21.

[56] I. Kolmanovsky, P. Morall, M. Van Nieuwstadt and A. Stefanopoulou, 'Issues in modelling and control of intake flow in variable geometry turbocharged engines', *Chapman and Hall CRC research notes in mathematics*, pp. 436–445, 1999.

[57] K. Wark, *Thermodynamics 4th ed.* McGraw-Hill, 1983.

[58] K. Edward, 'Chapter 18 - air pollution', in *Environmental Pollution and Control (Fourth Edition)*, J. J. Peirce, R. F. Weiner and P. A. Vesilind, Eds., Fourth Edition, Woburn: Butterworth-Heinemann, 1998, pp. 245–269, ISBN: 978-0-7506-9899-3. DOI: https://doi.org/10.1016/B978-075069899-3/50019-5. [Online]. Available: https://www.sciencedirect.com/science/article/pii/B9780750698993500195.

[59] B. G. Miller, '4 - the effect of coal usage on human health and the environment', in *Clean Coal Engineering Technology*, B. G. Miller, Ed., Boston: Butterworth-Heinemann, 2011, pp. 85–132, ISBN: 978-1-85617-710-8. DOI: https://doi.org/10.1016/B978-1-85617-710-8.00004-2. [Online]. Available: https://www.sciencedirect.com/science/article/pii/B9781856177108000042.

[60] J. F. Louis, 'Systematic studies of heat transfer and film cooling effectiveness', *AGARD High Temp. Probl. in Gas Turbine Eng. 36 p(SEE N 78-21118 12-07)*, 1978.

[61] Wolfram—Alpha Knowledgebase, *Wolframalpha*, https://www.wolframalpha.com/, Accessed: 14.04.2021.

[62] M. L. Huber, E. Sykioti, M. J. Assael and R. A. Perkins, 'Reference correlation of the thermal conductivity of carbon dioxide from the triple point to 1100 k and up to 200 mpa', *Journal of physical and chemical reference data*, vol. 45, no. 1, p. 013 102, 2016.

[63] A. Fenghour, W. Wakeham and V. Vesovic, 'The viscosity of carbon dioxide', *Journal of Physical and Chemical Reference Data - J PHYS CHEM REF DATA*, vol. 27, pp. 31–44, Jan. 1998. DOI: 10.1063/1.556013.

[64] M. Ditaranto, H. Li and T. Løvås, 'Concept of hydrogen fired gas turbine cycle with exhaust gas recirculation: Assessment of combustion and emissions performance', *International Journal of Greenhouse Gas Control*, vol. 37, Jun. 2015. DOI: 10.1016/j.ijggc.2015.04.004.

[65] Z. Liu, X. Ren, Z. Yan, H. Zhu, T. Zhang and W. Zhu, 'Effect of inlet air heating on gas turbine efficiency under partial load', *Energies*, vol. 12, p. 3327, Aug. 2019. DOI: 10.3390/en12173327.

Appendix

A Model of gas turbine performance data from GT MASTER

GT MASTER LM2500+G4(RD) data	
Name	GE LM2500+RD
Revised	30.03.2015
Frequency and engine	Geared version of a $60Hz$ engine
Combustor	Dry Low NOx combustor (25)
Power turbine stages	6
Max model errors in test range	$Mex < 1\%$, $kW < 1\%$, $HR < 1\%$, $Tex < 8F$ $(4.4C)$
Test range	0 to $120F$ $(-18$ to $49°C)$, full load dry
Model range	-28.9 to $48.9°C$
Fuel	Gas only
Load	5 to 100%

Table 14: Model data for the LM2500+G4(RD) extracted from GT MASTER 29 (Thermoflow) [41].

B Script for calculating MAPE, RMSE and IGV settings for natural gas and hydrogen


```
%Values for GasTurb simulations are imported from Excel to the Workspace,
%with the notation: TITIGVMatlab for natural gas and TITIGVMatlabH2 for
%hydrogen.


%Given performance data for natural gas:
TIT=[1500   1495.20833  1490.41666  1485.62499  1480.83332  1476.04165  1471.24998↙
1466.45831  1461.66664  1456.87497  1452.0833   1447.29163  1442.49996  1437.70829↙
1432.91662  1428.12495  1423.33328  1418.54161  1413.74994  1408.95827  1404.1666↙
1399.37493  1394.58326  1389.79159  1384.99992  1380.20825  1375.41658  1370.62491↙
1365.83324  1361.04157  1356.2499   1351.45823  1346.66656  1341.87489  1337.08322↙
1332.29155  1327.49988  1322.70821  1317.91654  1313.12487  1308.3332   1303.54153↙
1298.74986  1293.95819  1289.16652  1284.37485  1279.58318  1274.79151  1269.99984];
TITGiven=[1500 1475.953 1453.628 1431.719 1409.373 1386.197 1362.513 1338.726 1314.771↙
1288.886 1267.044];
ShfPwrGiven=[32939 31308 29678 28047 26410 24772 23132 21492 19850 18076 16574];
ExhTempGiven=[805.15    792.15  784.15  778.15  785.15  792.15  799.15  806.15  813.15↙
806.15  781.15];
ExhflowGiven=[90 89 87  85  82  80  78  76  74  72  67];
ThermalEffGiven=[0.3859 0.3844  0.3816  0.3774  0.3654  0.353   0.3401  0.3268  0.3132↙
0.3027  0.3085];

%Allocating space:
ThermalEff=zeros(45,49);
PowerOutput=zeros(45,49);
ExhTemp=zeros(45,49);
ExhMassFlow=zeros(45,49);
ThermalEffH2=zeros(45,49);
PowerOutputH2=zeros(45,49);
ExhTempH2=zeros(45,49);
ExhMassFlowH2=zeros(45,49);
ItVar=1;
Points=zeros(45,11);
PointsH2=zeros(45,11);
OGsens=0.01;
j=1;
x=2;


y=1;
yIT=1;

%Arranging data
while y<=312
    for x=1:49
        ThermalEff(yIT,x)=TITIGVMatlab(y,x+2);
        PowerOutput(yIT,x)=TITIGVMatlab(y+1,x+2);
        ExhTemp(yIT,x)=TITIGVMatlab(y+2,x+2);
        ExhMassFlow(yIT,x)=TITIGVMatlab(y+3,x+2);
        ThermalEffH2(yIT,x)=TITIGVMatlabH2(y,x+2);
        PowerOutputH2(yIT,x)=TITIGVMatlabH2(y+1,x+2);
        ExhTempH2(yIT,x)=TITIGVMatlabH2(y+2,x+2);
        ExhMassFlowH2(yIT,x)=TITIGVMatlabH2(y+3,x+2);
    end
    y=y+7;
    yIT=1+yIT;
end
%Finding the minimal difference in for the GasTurb simulation data (NG) and the performance
%data
minDiff=zeros(45,11);
for angle=1:45
    for performance=1:11
    minDiff(angle,performance)=min(abs(ShfPwrGiven(performance)-PowerOutput(angle,:)));
```

```
    end
end

%Finding the correlating points to the given power output in the
%performance data
for angle=1:45
    for performance=1:11
        for x=1:49
            if abs(ShfPwrGiven(performance)-PowerOutput(angle,x))==minDiff(angle,performance)
            Points(angle,performance)=x;
            end
        end
    end
end

%Extracting the parameters with regards to power output
for a=1:45
    for i=1:11
        SelThermalEff(a,i)=ThermalEff(a,Points(a,i));
        SelPowerOutput(a,i)=PowerOutput(a,Points(a,i));
        SelExhMass(a,i)=ExhMassFlow(a,Points(a,i));
        SelExhTemp(a,i)=ExhTemp(a,Points(a,i));
        SelThermalEffH2(a,i)=ThermalEffH2(a,Points(a,i));
        SelPowerOutputH2(a,i)=PowerOutputH2(a,Points(a,i));
        SelExhMassH2(a,i)=ExhMassFlowH2(a,Points(a,i));
        SelExhTempH2(a,i)=ExhTempH2(a,Points(a,i));
    end
end


%Check the Overall RMSE & MAPE for the different angles:
for a=1:45
for z=1:11
    MAPE_PowerOutput(a)=1/11*abs((ShfPwrGiven(z)-SelPowerOutput(a,z))/ShfPwrGiven(z));
    MAPE_ThermalEff(a)=1/11*abs((ThermalEffGiven(z)-SelThermalEff(a,z))/ThermalEffGiven(z));
    MAPE_ExhGasTemp(a)=1/11*abs((ExhTempGiven(z)-SelExhTemp(a,z))/ExhTempGiven(z));
    MAPE_ExhGasFlow(a)=1/11*abs((ExhflowGiven(z)-SelExhMass(a,z))/ExhflowGiven(z));
    RMSE_PowerOutput(a)=1/11*(SelPowerOutput(a,z)-ShfPwrGiven(z))^2;
    RMSE_ThermalEff(a)=1/11*(SelThermalEff(a,z)-ThermalEffGiven(z))^2;
    RMSE_ExhGasTemp(a)=1/11*(SelExhTemp(a,z)-ExhTempGiven(z))^2;
    RMSE_ExhGasFlow(a)=1/11*(SelExhMass(a,z)-ExhflowGiven(z))^2;







end

end

%MAPE and RMSE for each of the performance points with regards to angle:

for a=1:45
for z=1:11
    MAPEP_PowerOutput(a,z)=abs((ShfPwrGiven(z)-SelPowerOutput(a,z))/ShfPwrGiven(z));
    MAPEP_ThermalEff(a,z)=abs((ThermalEffGiven(z)-SelThermalEff(a,z))/ThermalEffGiven(z));
    MAPEP_ExhGasTemp(a,z)=abs((ExhTempGiven(z)-SelExhTemp(a,z))/ExhTempGiven(z));
    MAPEP_ExhGasFlow(a,z)=abs((ExhflowGiven(z)-SelExhMass(a,z))/ExhflowGiven(z));
    RMSEP_PowerOutput(a,z)=(SelPowerOutput(a,z)-ShfPwrGiven(z))^2;
    RMSEP_ThermalEff(a,z)=(SelThermalEff(a,z)-ThermalEffGiven(z))^2;
    RMSEP_ExhGasTemp(a,z)=(SelExhTemp(a,z)-ExhTempGiven(z))^2;
    RMSEP_ExhGasFlow(a,z)=(SelExhMass(a,z)-ExhflowGiven(z))^2;
```

```
end

end

%Total MAPE and RMSE for each angle:
for a=1:45
MAPE_PowerOutput(a)=1/11*sum(MAPEP_PowerOutput(a,:));
MAPE_ThermalEff(a)=1/11*sum(MAPEP_ThermalEff(a,:));
MAPE_ExhGasTemp(a)=1/11*sum(MAPEP_ExhGasTemp(a,:));
MAPE_ExhGasFlow(a)=1/11*sum(MAPEP_ExhGasFlow(a,:));
RMSE_PowerOutput(a)=sqrt(1/11*sum(RMSEP_PowerOutput(a,:)));
RMSE_ThermalEff(a)=sqrt(1/11*sum(RMSEP_ThermalEff(a,:)));
RMSE_ExhGasTemp(a)=sqrt(1/11*sum(RMSEP_ExhGasTemp(a,:)));
RMSE_ExhGasFlow(a)=sqrt(1/11*sum(RMSEP_ExhGasFlow(a,:)));

end

%Finding the lowest MAPE angle for each interval with regards
%to the exhaust gas temperature:
OptimalAnglePath=zeros(1,11);
for interval=1:11
    for angle=1:45
        if MAPEP_ExhGasTemp(angle,interval)==min(MAPEP_ExhGasTemp(:,interval))
        OptimalAnglePath(interval)=angle;

        end
    end
end

%Finding the total MAPE sum for each given IGV setting:
for t=1:45
SumMAPEVector(t)=(MAPE_PowerOutput(t)+MAPE_ThermalEff(t)+MAPE_ExhGasFlow(t)+MAPE_ExhGasTemp↙
(t))/4;
end
%Lowest total MAPE for all parameters combined:
smallestToTMape=min(SumMAPEVector);
for i=1:45
    if SumMAPEVector(i)==smallestToTMape
        anglenum=i;
    end
end


%Plotting the total MAPE and RMSE for the given parameters:
angle=1:45;
figure(1)
plot(angle,MAPE_ExhGasTemp,'--o',angle,MAPE_PowerOutput,'--o',angle,MAPE_ThermalEff,'--o',↙
angle,MAPE_ExhGasFlow,'--o')
title('total MAPE for different IGV angle configurations')
xlabel('Angle [degrees]')
ylabel('MAPE [-]')
legend('Exhaust temperature','Power output','Thermal efficiency','Exhaust mass flow')

figure2=plotNy(angle,RMSE_ExhGasTemp,1,...
    angle,RMSE_PowerOutput,2,...
    angle,RMSE_ThermalEff,3,...
    angle,RMSE_ExhGasFlow,4,...
'Linewidth',1,...
'YAxisLabels',{'Exhaust temp.' 'Power Output' 'Thermal eff.' 'Exhaust flow'},...
'xAxisLabel','Angle [degrees]',...
'TitleStr','total RMSE for different IGV angle configurations',...
'LegendString',{'Exhaust temperature' 'Power output' 'Thermal efficiency' 'Exhaust mass↙
flow'});
```

```
%Plotting the performance data alongside the outputs for specific IGV
%settings:
figure(10)
plot(ShfPwrGiven,ExhTempGiven,'-o',SelPowerOutput(28,:),SelExhTemp(28,:),'-+',SelPowerOutput↙
(1,1:4),SelExhTemp(1,1:4),'-*',SelPowerOutput(24,4:9),SelExhTemp(24,4:9),'-.',SelPowerOutput↙
(11,4:9),SelExhTemp(11,4:9),'-x',SelPowerOutput(16,4:9),SelExhTemp(16,4:9),'-s',↙
SelPowerOutput(20,4:9),SelExhTemp(20,4:9),'-d',SelPowerOutput(28,4:9),SelExhTemp(28,4:9),'-↙
p',SelPowerOutput(28,9:11),SelExhTemp(28,9:11),'-h',SelPowerOutput(29,9:11),SelExhTemp(29,9:↙
11),'-<',SelPowerOutput(27,9:11),SelExhTemp(27,9:11),'->')
title('Exhaust gas temperature curves with regards to IGV angle')
xlabel('Power output [kW]')
ylabel('Temperature [K]')
legend('Performance data','IGV:-27 degrees','IGV:0 degrees','IGV:-23 degrees','IGV:-10↙
degrees','IGV:-15 degrees','IGV:-19 degrees','IGV:-27 degrees','IGV:-27 degrees','IGV:-28↙
degress','IGV:-26 degrees')


figure(4)
plot(ShfPwrGiven,ThermalEffGiven,'-o',SelPowerOutput(28,:),SelThermalEff(28,:),'-+',↙
SelPowerOutput(1,1:4),SelThermalEff(1,1:4),'-*',SelPowerOutput(24,4:9),SelThermalEff(24,4:↙
9),'-.',SelPowerOutput(11,4:9),SelThermalEff(11,4:9),'-x',SelPowerOutput(16,4:9),↙
SelThermalEff(16,4:9),'-s',SelPowerOutput(20,4:9),SelThermalEff(20,4:9),'-d',SelPowerOutput↙
(28,4:9),SelThermalEff(28,4:9),'-p',SelPowerOutput(28,9:11),SelThermalEff(28,9:11),'-h',↙
SelPowerOutput(29,9:11),SelThermalEff(29,9:11),'-<',SelPowerOutput(27,9:11),SelThermalEff↙
(27,9:11),'->')
title('Thermal efficiency curves with regards to IGV angle')
xlabel('Power output [kW]')
ylabel('Thermal efficiency [-]')
legend('Performance data','IGV:-27 degrees','IGV:0 degrees','IGV:-23 degrees','IGV:-10↙
degrees','IGV:-15 degrees','IGV:-19 degrees','IGV:-27 degrees','IGV:-27 degrees','IGV:-28↙
degress','IGV:-26 degrees')


figure(5)
plot(ShfPwrGiven,ExhflowGiven,'-o',SelPowerOutput(28,:),SelExhMass(28,:),'-+',SelPowerOutput↙
(1,1:4),SelExhMass(1,1:4),'-*',SelPowerOutput(24,4:9),SelExhMass(24,4:9),'-.',SelPowerOutput↙
(11,4:9),SelExhMass(11,4:9),'-x',SelPowerOutput(16,4:9),SelExhMass(16,4:9),'-s',↙
SelPowerOutput(20,4:9),SelExhMass(20,4:9),'-d',SelPowerOutput(28,4:9),SelExhMass(28,4:9),'-↙
p',SelPowerOutput(28,9:11),SelExhMass(28,9:11),'-h',SelPowerOutput(29,9:11),SelExhMass(29,9:↙
11),'-<',SelPowerOutput(27,9:11),SelExhMass(27,9:11),'->')
title('Exhaust mass flow curves with regards to IGV angle')
xlabel('Power output [kW]')
ylabel('Mass flow [kg/s]')
legend('Performance data','IGV:-27 degrees','IGV:0 degrees','IGV:-23 degrees','IGV:-10↙
degrees','IGV:-15 degrees','IGV:-19 degrees','IGV:-27 degrees','IGV:-27 degrees','IGV:-28↙
degress','IGV:-26 degrees')

%Hydrogen and Natural gas models compared without IGV var geometry.
figure(6)
plot(ShfPwrGiven,ThermalEffGiven,'-og',PowerOutput(1,:),ThermalEff(1,:),'-or',PowerOutputH2↙
(1,:),ThermalEffH2(1,:),'-ob')
title('Thermal efficiency for change in fuel')
xlabel('Power output [kW]')
ylabel('Thermal efficiency [-]')
legend('Performance data','GasTurb: natural gas','GasTurb: hydrogen')

figure(7)
plot(ShfPwrGiven,ExhflowGiven,'-og',PowerOutput(1,:),ExhMassFlow(1,:),'-or',PowerOutputH2↙
(1,:),ExhMassFlowH2(1,:),'-ob')
title('Exhaust mass flow for change in fuel')
xlabel('Power output [kW]')
```

```
ylabel('Mass flow [kg/s]')
legend('Performance data','GasTurb: natural gas','GasTurb: hydrogen')

figure(8)
plot(ShfPwrGiven,ExhTempGiven,'-og',PowerOutput(1,:),ExhTemp(1,:),'-or',PowerOutputH2(1,:),↙
ExhTempH2(1,:),'-ob')
title('Exhaust temperature for change in fuel')
xlabel('Power output [kW]')
ylabel('Temperature [K]')
legend('Performance data','GasTurb: natural gas','GasTurb: hydrogen')

%Plotting variable geometry for both hydrogen and natural gas:
figure(9)
hold on
p=plot(ShfPwrGiven,ExhTempGiven,'-og');
h2=plot(SelPowerOutputH2(28,:),SelExhTempH2(28,:),'-ob',SelPowerOutputH2(1,1:4),SelExhTempH2↙
(1,1:4),'-ob',SelPowerOutputH2(24,4:9),SelExhTempH2(24,4:9),'-ob',SelPowerOutputH2(11,4:9),↙
SelExhTempH2(11,4:9),'-ob',SelPowerOutputH2(16,4:9),SelExhTempH2(16,4:9),'-ob',↙
SelPowerOutputH2(20,4:9),SelExhTempH2(20,4:9),'-ob',SelPowerOutputH2(28,4:9),SelExhTempH2↙
(28,4:9),'-ob',SelPowerOutputH2(28,9:11),SelExhTempH2(28,9:11),'-ob',SelPowerOutputH2(29,9:↙
11),SelExhTempH2(29,9:11),'-ob',SelPowerOutputH2(27,9:11),SelExhTempH2(27,9:11),'-ob')
ng=plot(SelPowerOutput(28,:),SelExhTemp(28,:),'-or',SelPowerOutput(1,1:4),SelExhTemp(1,1:↙
4),'-or',SelPowerOutput(24,4:9),SelExhTemp(24,4:9),'-or',SelPowerOutput(11,4:9),SelExhTemp↙
(11,4:9),'-or',SelPowerOutput(16,4:9),SelExhTemp(16,4:9),'-or',SelPowerOutput(20,4:9),↙
SelExhTemp(20,4:9),'-or',SelPowerOutput(28,4:9),SelExhTemp(28,4:9),'-or',SelPowerOutput(28,9:↙
11),SelExhTemp(28,9:11),'-or',SelPowerOutput(29,9:11),SelExhTemp(29,9:11),'-or',↙
SelPowerOutput(27,9:11),SelExhTemp(27,9:11),'-or')
legend([p(1),h2(1), ng(1)], 'Performance data', 'GasTurb: hydrogen', 'GasTurb: natural gas')


title('Exhaust gas temperature for hydrogen and natural gas with IGV variable geometry')
xlabel('Power output [kW]')
ylabel('Temperature [K]')

figure(11)
hold on
p=plot(ShfPwrGiven,ThermalEffGiven,'-og');
h2=plot(SelPowerOutputH2(28,:),SelThermalEffH2(28,:),'-ob',SelPowerOutputH2(1,1:4),↙
SelThermalEffH2(1,1:4),'-ob',SelPowerOutputH2(24,4:9),SelThermalEffH2(24,4:9),'-ob',↙
SelPowerOutputH2(11,4:9),SelThermalEffH2(11,4:9),'-ob',SelPowerOutputH2(16,4:9),↙
SelThermalEffH2(16,4:9),'-ob',SelPowerOutputH2(20,4:9),SelThermalEffH2(20,4:9),'-ob',↙
SelPowerOutputH2(28,4:9),SelThermalEffH2(28,4:9),'-ob',SelPowerOutputH2(28,9:11),↙
SelThermalEffH2(28,9:11),'-ob',SelPowerOutputH2(29,9:11),SelThermalEffH2(29,9:11),'-ob',↙
SelPowerOutputH2(27,9:11),SelThermalEffH2(27,9:11),'-ob')
ng=plot(SelPowerOutput(28,:),SelThermalEff(28,:),'-or',SelPowerOutput(1,1:4),SelThermalEff↙
(1,1:4),'-or',SelPowerOutput(24,4:9),SelThermalEff(24,4:9),'-or',SelPowerOutput(11,4:9),↙
SelThermalEff(11,4:9),'-or',SelPowerOutput(16,4:9),SelThermalEff(16,4:9),'-or',SelPowerOutput↙
(20,4:9),SelThermalEff(20,4:9),'-or',SelPowerOutput(28,4:9),SelThermalEff(28,4:9),'-or',↙
SelPowerOutput(28,9:11),SelThermalEff(28,9:11),'-or',SelPowerOutput(29,9:11),SelThermalEff↙
(29,9:11),'-or',SelPowerOutput(27,9:11),SelThermalEff(27,9:11),'-or')
legend([p(1),h2(1), ng(1)], 'Performance data', 'GasTurb: hydrogen', 'GasTurb: natural gas')


title('Thermal efficiency for hydrogen and natural gas with IGV variable geometry')
xlabel('Power output [kW]')
ylabel('Thermal efficiency [-]')


figure(12)
hold on
p=plot(ShfPwrGiven,ExhflowGiven,'-og');
h2=plot(SelPowerOutputH2(28,:),SelExhMassH2(28,:),'-ob',SelPowerOutputH2(1,1:4),SelExhMassH2↙
(1,1:4),'-ob',SelPowerOutputH2(24,4:9),SelExhMassH2(24,4:9),'-ob',SelPowerOutputH2(11,4:9),↙
```

```
SelExhMassH2(11,4:9),'-ob',SelPowerOutputH2(16,4:9),SelExhMassH2(16,4:9),'-ob',↙
SelPowerOutputH2(20,4:9),SelExhMassH2(20,4:9),'-ob',SelPowerOutputH2(28,4:9),SelExhMassH2↙
(28,4:9),'-ob',SelPowerOutputH2(28,9:11),SelExhMassH2(28,9:11),'-ob',SelPowerOutputH2(29,9:↙
11),SelExhMassH2(29,9:11),'-ob',SelPowerOutputH2(27,9:11),SelExhMassH2(27,9:11),'-ob')
ng=plot(SelPowerOutput(28,:),SelExhMass(28,:),'-or',SelPowerOutput(1,1:4),SelExhMass(1,1:↙
4),'-or',SelPowerOutput(24,4:9),SelExhMass(24,4:9),'-or',SelPowerOutput(11,4:9),SelExhMass↙
(11,4:9),'-or',SelPowerOutput(16,4:9),SelExhMass(16,4:9),'-or',SelPowerOutput(20,4:9),↙
SelExhMass(20,4:9),'-or',SelPowerOutput(28,4:9),SelExhMass(28,4:9),'-or',SelPowerOutput(28,9:↙
11),SelExhMass(28,9:11),'-or',SelPowerOutput(29,9:11),SelExhMass(29,9:11),'-or',↙
SelPowerOutput(27,9:11),SelExhMass(27,9:11),'-or')
legend([p(1),h2(1), ng(1)], 'Performance data', 'GasTurb: hydrogen', 'GasTurb: natural gas')


title('Exhaust mass flow for hydrogen and natural gas with IGV variable geometry')
xlabel('Power output [kW]')
ylabel('Mass flow [kg/s]')
```

C Accommodating plots from GasTurb

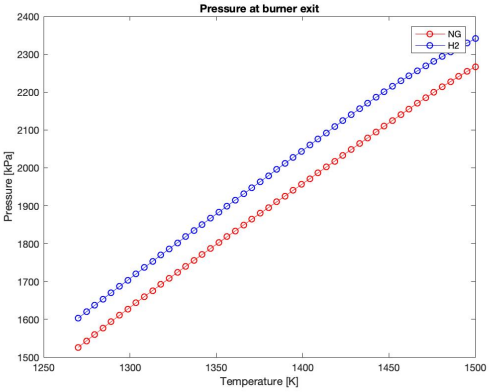

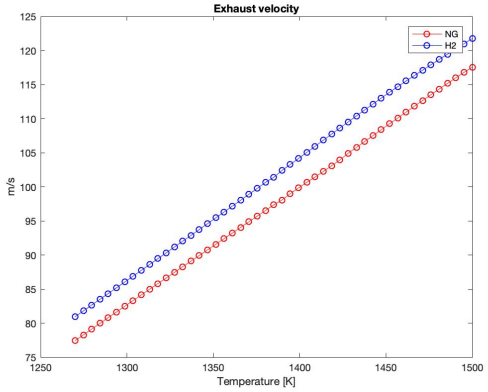

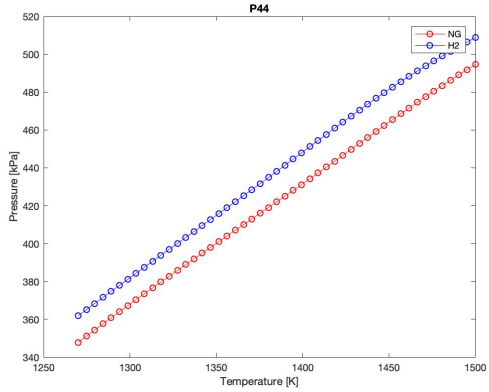

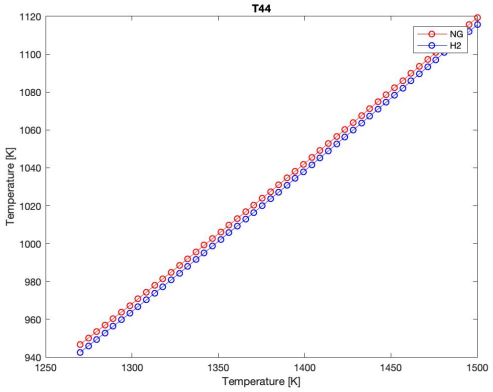

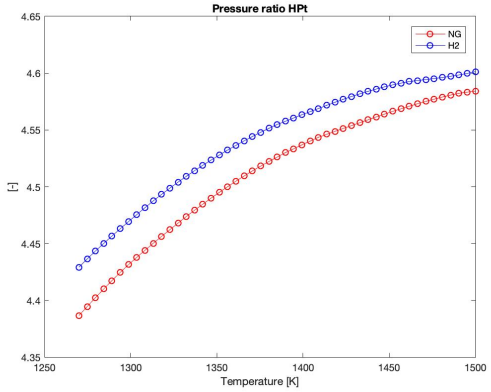

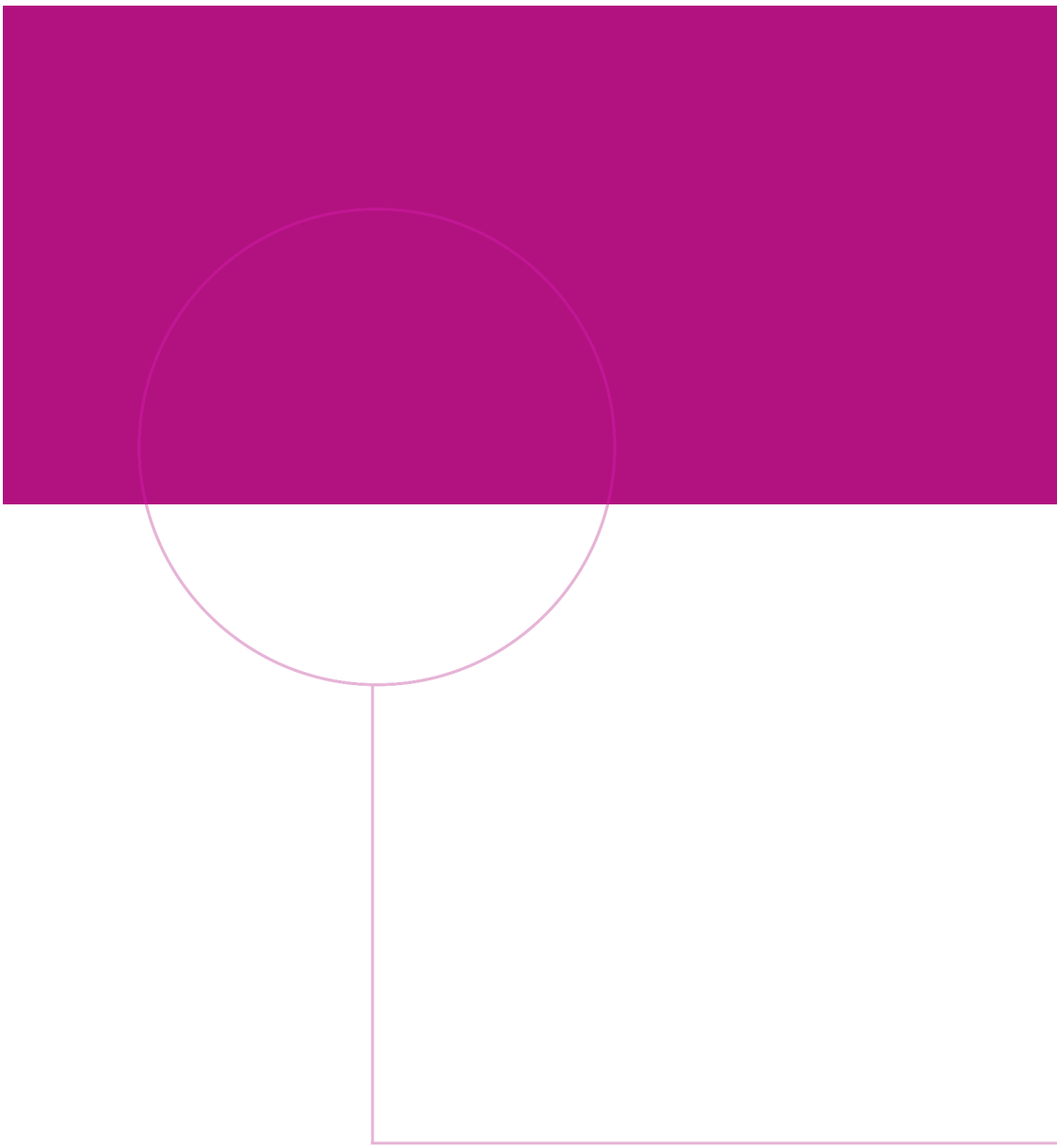

NTNU

Norwegian University of
Science and Technology